1-1-1980

Surface photometry of the Coma Cluster of galaxies.

John Spencer Sloan
University of Massachusetts Amherst

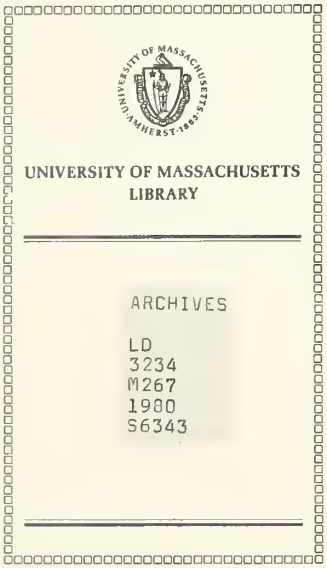
UNIVERSITY OF MASSACHUSETTS
LIBRARY
ARCHIVES
LD
3234
M267
1980
S6343

SURFACE PHOTOMETRY OF THE COMA CLUSTER OF GALAXIES

A Dissertation Presented

By

JOHN SPENCER SLOAN

Submitted to the Graduate School of the
University of Massachusetts in partial fulfillment
of the requirements for the degree of

DOCTOR OF PHILOSOPHY

February 1980

Astronomy

SURFACE PHOTOMETRY OF THE COMA CLUSTER

OF GALAXIES

A Dissertation Presented

By

John Spencer Sloan

Approved as to style and content by:

Tom R. Dennis

Tom R. Dennis, Chairman of Committee

Robert Krotkov

Robert Krotkov, Member

Nicholas Z. Scoville

Nicholas Z. Scoville, Member

Richard E. White

Richard E. White, Member

LeRoy F. Cook, Department Head
Department of Physics and Astronomy

February 1980

ACKNOWLEDGEMENTS

I especially wish to thank my advisor Tom Dennis and Dr. Ronald Zissell who have persevered through every imaginable problem I caused them. Thanks also to Kitt Peak National Observatory* for observing time and travel support.

Data processing was paid for by a grant from the University Computing Center of the University of Massachusetts. I wish to thank Mount Holyoke College Computing Center for the use of their facilities. This research and summer support for the author was funded in part by a Research Corporation grant.

Finally, I want to acknowledge the large debt I owe my aunts and uncles, the Palubniaks and Kundrats; my friends Linda McMahan, Judy Dietel and Dr. Bill and Robin Oegerle. Without their patient support this thesis would not have been completed.

This work is dedicated to my father, the late Kenneth T. Sloan, and to my parents, Mr. and Mrs. Joseph Velebir for their inspiration, encouragement and assistance through the years.

* Operated by the Association of Universities for Research in Astronomy, Inc., under contract with the National Science Foundation.

ABSTRACT

Surface Photometry of The Coma Cluster of Galaxies

(August 1979)

John Spencer Sloan, B.S., Fairleigh Dickinson University

Ph.D., University of Massachusetts
Directed by: Professor Tom Dennis

A large region ($\approx$ 8 square degrees) of the Coma Cluster has been studied using a new type of photometer which can discriminate against the light of foreground stars. While able to accurately correct for contaminating starlight, the overall photometric utility of the photometer is limited by night sky variations.

The total light distribution of the Coma Cluster at λ 7150Å and λ 8200Å is found to have an elliptical shape, the position angle of the major axis lying between 67° to 90°. The observed light distribution is found to correlate well with the galaxy distribution. Along the major axis of the Cluster, the luminosity can be traced out over two degrees from the Cluster center. At λ7150Å a mass-to-light ratio of 230 is found using a King model for the central region of the Cluster. Marginal evidence exists that at distances greater than 1.5° from the Cluster center along the major axis the Cluster is redder, indicating an integrated spectra of (K1V-K7V).

TABLE OF CONTENTS

TABLE OF CONTENTS

LIST OF TABLES

FIGURE CAPTIONS

FIGURE CAPTIONS

FIGURE CAPTIONS

C H A P T E R I

INTRODUCTION

Background

A large body of evidence has accumulated over the past few years which shows there is a severe problem if one tries to account for the well-known mass of the Coma Galaxy Cluster (number 1656 in Abell's (1958) catalogue) in terms of the visible galaxies which make up the cluster (Rood, Page, Kintner, and King 1972). As the prototypical example of a rich cluster of galaxies, the "missing mass" problem in the Coma Cluster has led a number of investigators to search for various forms of diffuse matter that might contribute significantly to the cluster's mass. A number of investigators, Zwicky (1951), deVaucouleurs (1960), deVaucouleurs and deVaucouleurs (1960), Welch and Sastry (1971, 1972), Kormendy and Bahcall (1974), Melnick, White and Hoessel (1977), Mattila (1977), and Thuan and Kormendy (1977) have studied and mapped the luminous matter in the cluster. It now seems probable that, based on any reasonable model for a diffuse gas or dust distribution that could supply the "missing mass", it would not have escaped detection by the variety of surveys completed to the present time. The possibility still exists that there might be a population of intergalactic stars with large mass-to-light ratios in sufficient numbers to stabilize the cluster.

Recent dynamical studies by White (1967a, 1976b, 1977) have shown that any unseen material in the Coma Cluster cannot be attached to individual galaxies in proportion to their luminosity, but must be distributed as a smooth intergalactic background. The theoretical treatment of the dynamics of spiral galaxies by Ostriker and Peebles (1973) indicates that these objects should be unstable against the formation of a bar unless the spiral arm region is embedded in an extensive diffuse mass distribution. Lecar (1975) has shown that if the Coma Cluster galaxies had formed with extended "Ostriker-Peebles" halos, the halos by now would have been disrupted to form a diffuse background of intergalactic stars.

The strongest evidence for these massive halos comes from 21 cm observations of spiral galaxies which show the rotation curves for these objects remain flat out to distances as much as 100 kpc (Roberts and Rots 1973, Hanschich and Burke 1975, Krum and Saltpeter 1977). Recent support for the existence of these halos comes from the work of Hegyi and Gerber (1977) who report the detection of an optical halo surrounding NGC4565 out to a distance of 34 kpc from the plane of the galaxy. In addition, their data shows the light emitted by the halo to be from stars later than K7. Thus, an intergalactic stellar component to the Coma Cluster composed of such late type stars might exist and contribute enough mass to resolve the "missing mass" problem.

Recently, the exact geometry of the Coma Cluster has come under much study. In the past, most investigators have treated the Coma Cluster as having spherical symmetry. However, inspection of a photograph of the Cluster e.g., field 160 of Zwicky and Herzog (1963), or Figure 11 in Shane and Wirtanen (1954) suggests that the Cluster is elongated. Whereas many authors (Abell (1962), Rood et al. (1972), Bahcall (1973), and others) have commented on this ellipticity, only recently have quantitative values for the ellipticity and position angle of the major axis ($\approx 67^{o}$) become available (Schippen and King (1978), Thompson and Gregory (1978).

Radial velocity observations (Rood et al. 1972) have shown that rotation, perhaps the most straightforward explanation for ellipticity in a dynamical system like the Coma Cluster, can be ruled out. Alternative mechanisms by which this ellipticity may have arisen in the Coma Cluster, have been discussed by Schipper and King (1978), Thompson and Gregory (1978), and Valtonen and Byrd (1979).

Purpose

Based on the preceding discussion, an investigation of the distribution of light within the Coma Cluster that would concentrate on the spectral region where the flux from these hypothetical intergalactic stars is maximum seems warranted. Such a program of surface photometry would be expected to

provide information not only on the existence of such an intergalactic stellar component, but also provide information on the mass-to-total light ratio. Observations made in a number of colors add additional information on the population make-up of the emitting stars. These observations would provide a direct measurement of the cluster light, without the need for galaxy counts and assumptions about the faint end of the galaxy luminosity function as has been done in the past.

Previous Work

As has been discussed by Thuan and Kormendy (1977) a reasonably consistent body of data now exists on the background light near the center of the Coma Cluster. Except for the photoelectric observations of deVaucouleurs and deVaucouleurs (1970) and Melnick, White and Hoessel (1977) this data has been compiled from observation made of the inner 14 arc minutes of the Cluster. DeVaucouleurs and deVaucouleurs scanned a strip 0.55 arc minutes North-South by 88 arc minutes East-West at the declination of the brighteos cluster member NGC4889, using a non-filtered 1P21 photomultipler tube. They found that the total light distribution differs little from the distribution of galactic light and calculated a total integrated magnitude and color index of m_{total} (B)=8.5, (B-V)=1.0 for the inner 100 arc minutes of the cluster.

The major observational difficulty encountered in the

measurement of small surface brightness difference over an extended object like the Coma Cluster, is the proper correction for temporal variations in the night sky level. In an effort to correct for this problem, Melnick, White and Hoessel (1977) have made use of a second telescope to monitor the sky during their observations. They observed a region 14 arc minutes wide by 78 arc minutes long, with its center at $\alpha = 12^h57^m21^s$, $\delta = 28\ 10'\ 16''(1950)$, in the g and r bands of Thuan and Gunn's (1976) photometric system. They find (as did deVaucouleurs and deVaucouleurs (1960) that the light distribution in the Coma Cluster follows the galaxy distribution, and that the total luminosity of the cluster is very close to the sum of the contributions from individual galaxies. They also report that the intergalactic medium needed to bind the cluster should have a mass-to-visual light ratio of at least 1000.

Method

In order to carry out the investigation described above, one needs an accurate value for the proper background level. As the conventional cluster radius is about 100 arc minutes, the actual base line may lie outside the region that has been studied by existing photometry. To complicate the determination of the base line, the Coma Cluster is known to have an elliptical shape (Schipper and King 1978, Thompson and Gregory 1978). The current investigation extends 1 degree North and

South of the cluster center and 2 degrees in the East-West direction.

The observations were made in two spectral bands centered on $\lambda 7150\text{Å}$ and $\lambda 8200\text{Å}$, with a band pass of 100Å. These bands were chosen because of the fortunate coincidence that, when the flux from these hypothetical M Stars is appropriately redshifted, relatively transparent regions in the M star's spectrum are put into regions devoid of OH emission from the earth's atmosphere (see Figure 1a, b). The third band was the standard blue photometric band to allow a comparison with previous work.

If this intergalactic stellar component is present and spread out in a more diffuse manner than the visible galaxies, the expected contribution to the light of the night sky from these stars is only a few parts in 1000. Thus, one needs the photometric accuracy that is obtained photoelectrically; but to get a good signal-to-noise ratio one must use a large scanning aperture. This large scanning aperture poses no problems as far as spatial resolution is concerned since the standard value for the Coma Cluster radius is 100 arc minutes; but it does mean there will be a significant number of foreground stars present in the field, whose light must be discriminated against. The "multiplexing night sky photometer" and the data reduction procedure that is described in chapter II should be able to work to a photometric

Fig. 1a, 1b. Spectrum of the night sky near λ 7150Å and λ8200Å, from Broadfoot and Kendall (1968). The superimposed solid line is the flux from a model atmosphere for a main-sequence star with an effective temperature of 3000 K and solar abundances, calculated by Mould (1976). The wavelength scale for the M-star flux has been redshifted by 7000 km/sec, as appropriate for the Coma Cluster; the scale of ordinates is arbitrary. It is a fortunate coincidence the redshift puts these relatively transparent regions in the M-star spectrum into regions devoid of OH emission from the earth's atmosphere.

FIG.1a.

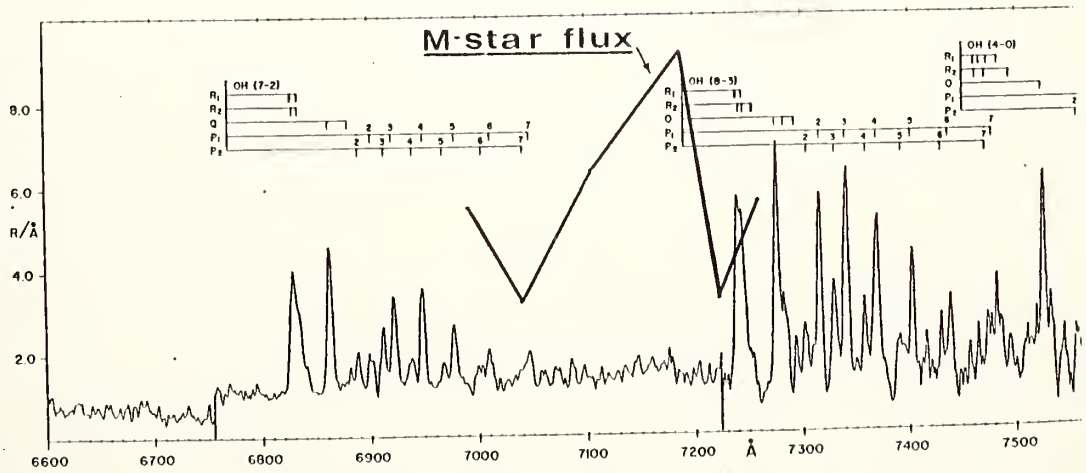
M-star flux
OH (7-2)
OH (8-5)
OH (4-0)
8.0
6.0
4.0
2.0
R/Å
6600
6700
6800
6900
7000
7100
7200
Å
7300
7400
7500
Wavelength

FIG. 1b.

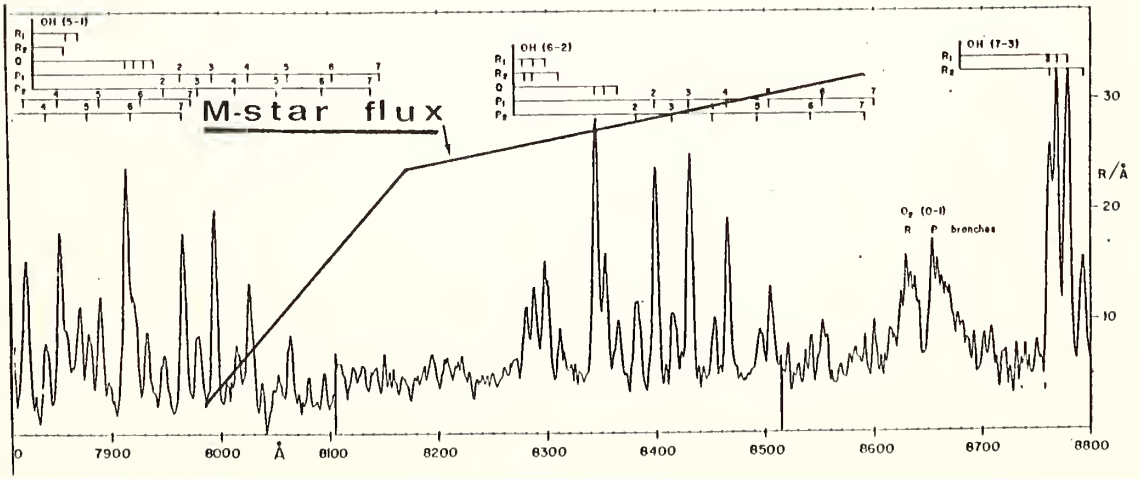
OH (5-1)
OH (6-2)
OH (7-3)
M-star flux
O_2 (0-1)
R P branches
R/Å
30
20
10
7900
8000
Å
8100
8200
8300
8400
8500
8600
8700
8800
Wavelength

accuracy the high signal-to-noise ratio of a large scanning aperture, while at the same time discriminating against the light of foreground stars.

C H A P T E R II

The Equipment

In our study of the Coma Cluster we are interested in detecting features which might stand out above the background sky level by only a few tenths of a percent. Roach and Gordon (1973) discuss the experimental difficulties encountered in the study of the Zodiacal Light, Airglow, galaxies and clusters of galaxies, and other diffuse objects. The primary experimental difficulties encountered are the accurate correction for foreground stars and separating out the various diffuse components from one another. The theory and design of a "multiplexing night sky photometer" with the ability to discriminate against foreground stars and carry out high precision measurements of the night sky, has been discussed by Dennis (1979). The "multiplexing night sky photometer" is a powerful tool for simultaneously solving both problems, of how to exploit the high-signal-to noise ratio of a large scanning aperture, while retaining information on the light from foreground stars. The use of the "multiplexing night sky photometer" and decoding procedures described in this section should help to alleviate the starlight correction problem whereas the disentanglement of the various diffuse components might still pose a fundamental limitation for the intended photometry of the Coma Cluster.

Star Correction

Even though the Coma Cluster is situated near the North Galactic Pole ($b=87.4^{\circ}$) starlight will still constitute some 14% of the total light of the night sky (Allen 1976). We wish to obtain an estimate of the number of stars in our 18.54′ aperture, whose light we will have to discriminate against to reach our intended goal of 0.1% photometry.

Dennis (1979) has prepared a number of "topographic maps" where the number of stars n(R,A), whose light must be discriminated against to reach an "index of photometric precision" R, with a scanning aperture of area A, are shown by contours in the R,A, plane. The index of photometric precision is defined as

$$R = \frac{\text{uncertainty due to stars fainter than } m_r}{\text{total sky brightness}} \qquad (1)$$

where it has been assumed that light from all stars brighter than m_r has been removed from the record. Dennis's "topographic map" for b=80 is reproduced in Figure 2; we find that in order to reach a goal of R=0.1% with a scanning aperture of area 0.075° we need to correct on the average for the light from 30 stars.

The Instrument

The photometer to be described in this section was de-

Fig. 2. Dennis's topographic map" for $b=80^{o}$, here the number of stars n(R,A) whose light must be discriminated against to reach an "index of photometric precision" R, with scanning aperture of area A, are shown by contours in the R,A, plane. For the current study, the region of interest falls in the lower right hand corner of the plot.

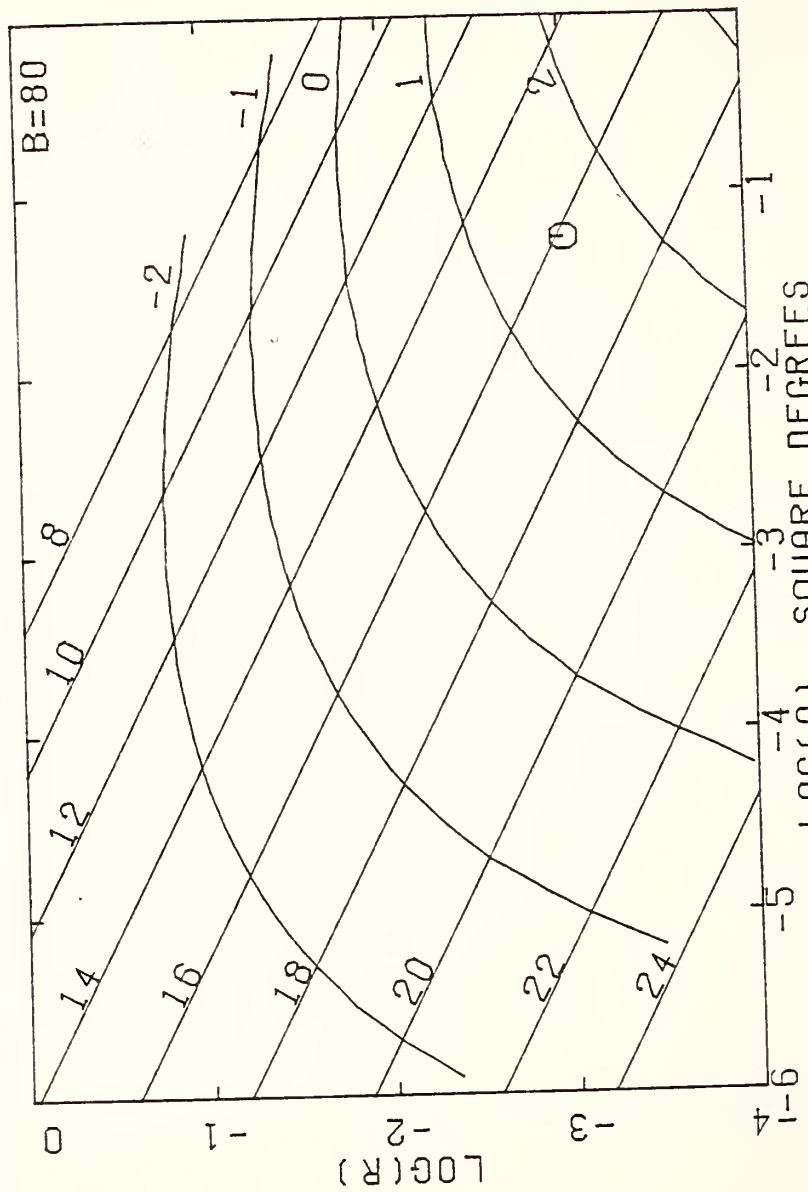
B=80
8
10
12
14
16
18
20
22
24
-2
-1
0
1
2
0
-1
-2
-3
-4
LOG(R)
-6
-5
-4
-3
-2
-1
LOG(A), SQUARE DEGREES

signed by Dr. T. Dennis and constructed by Dr. R. Zissell during the Spring of 1976. It is a "second generation" version of the device which was briefly described by Dennis (1974).

A schematic drawing of the device is given in Figure 3.

(a) The first element is a fine setting eyepiece. This is used to set the telescope on a guide star before initiating an observation; it is retracted for the actual observational process.

(b) A few thousandths of an inch before the true focal plane is the entrance aperture of the photometer; for the observation, a circular aperture 18.54 arc minutes in diameter was used.

(c) Following the entrance aperture, at the true focal plane, is a Ronchi ruling (see Figure 4) of 50 lines per inch (at the focal plane of the #4-0.4 meter telescope, a line pair corresponds to 14.5 arc seconds). This ruling is mounted in the central boring of a precision worm gear (165 teeth on a 7 inch pitch diameter) manufactured by the Edward Byers Company. The rotating assembly is held in place laterally and longitudinally by precision ball bearings (see Figure 5) in such a manner that lateral motion of the assembly will not exceed a few ten-thousandths of an inch, a few percent of the distance corresponding to one line pair.

(d) The next element in the system is a filter holder.

Fig. 3. Schematic diagram of the apparatus.

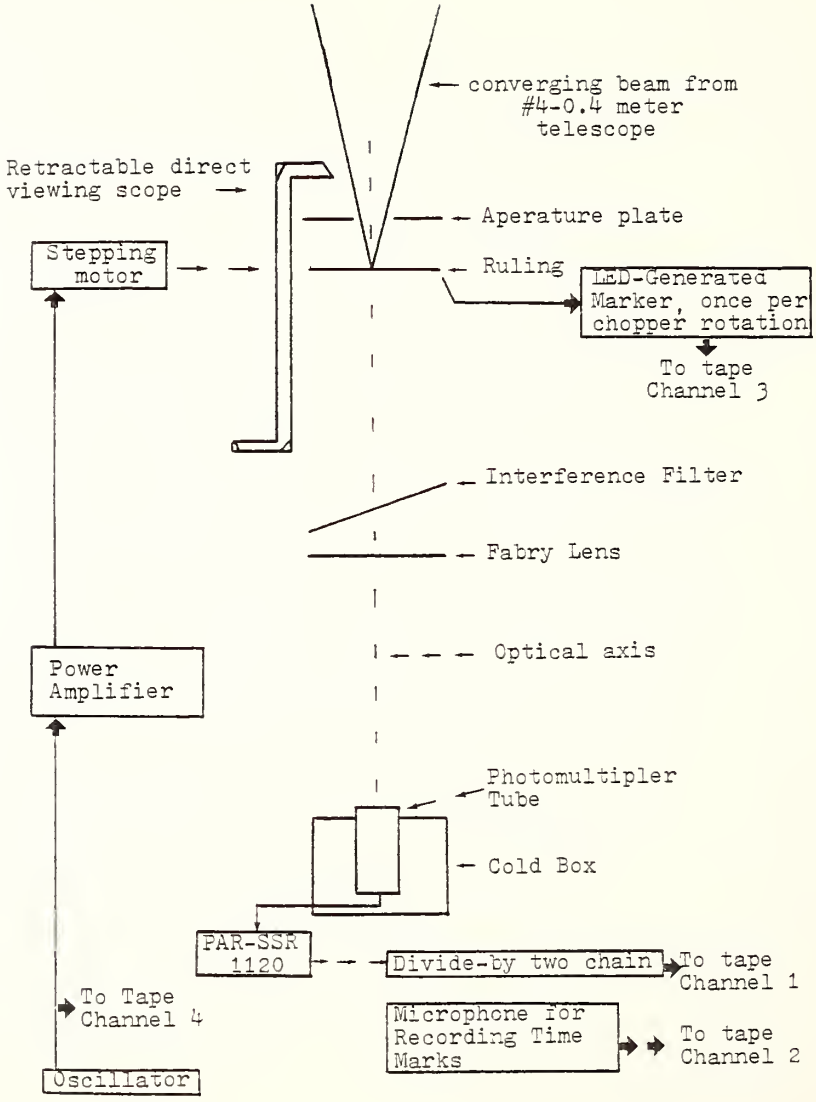
converging beam from
#4-0.4 meter
telescope
Retractable direct
viewing scope
Aperature plate
Stepping
motor
Ruling
LED-Generated
Marker, once per
chopper rotation
To tape
Channel 3
Interference Filter
Fabry Lens
Optical axis
Power
Amplifier
Photomultipler
Tube
Cold Box
PAR-SSR
1120
Divide-by two chain
To tape
Channel 1
To Tape
Channel 4
Microphone for
Recording Time
Marks
To tape
Channel 2
Oscillator

Fig. 4. Enlargement of the Ronchi ruling used for the Coma Cluster observations, the ruling has 50 lines per inch, a line pair thus corresponds to 14.5 arc seconds at the focal plane of the #4-0.4 meter telescope.

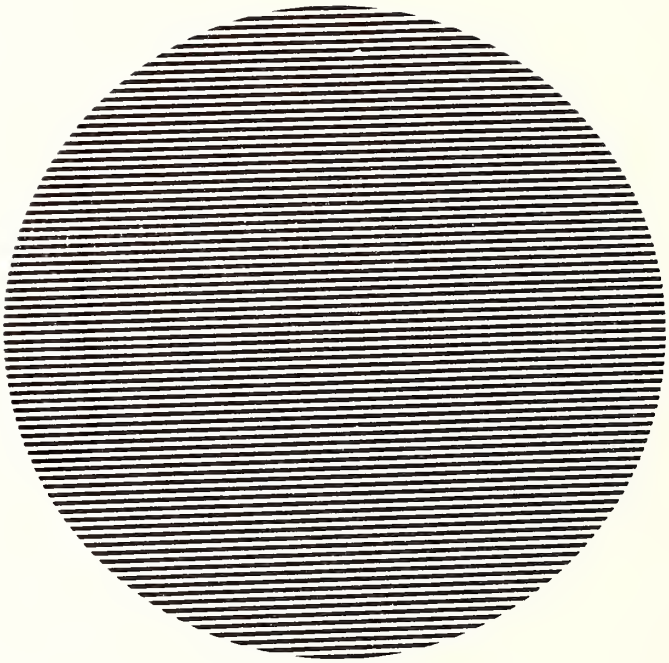

Fig. 5. Photograph of the photometer early in construction. The Byer worm and worm gear can be clearly seen as well as the system of ball-bearing supports. The Ronchi ruling fits against the groove which can be seen within the 4-inch central boring of the gear.

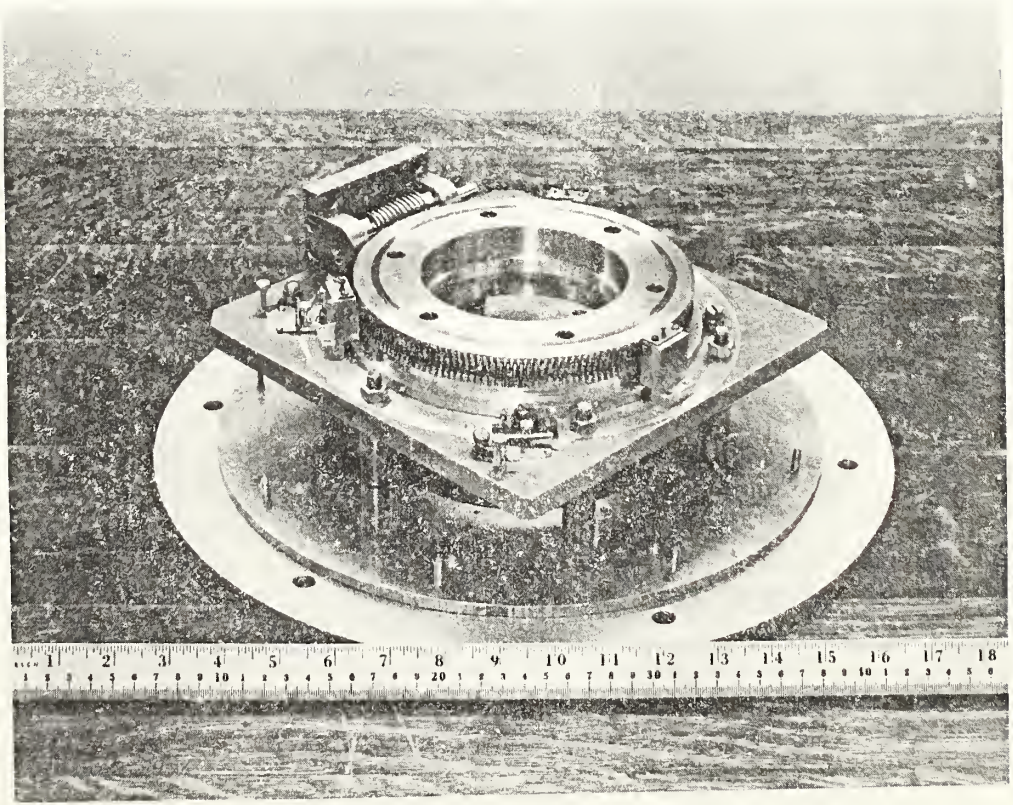

For the Coma Cluster observations the filters used were: two 150Å interference filter purchased from Baird-Atomic, for which transmission tracings are given in Figure 6 and a blue broad band (Fernie 1974) filter package consisting of a 4mm BG-12, 2mm BG-18, and 1mm GG-4 Schott glass filter, the response function of this filter package with the RCA 31034A tube used for the observation is given in Figure 7.

(e) Following the interference filter is a Fabry lens, which images the telescope objective onto the photocathode.

(f) The cold box is a thermo-electric device from Products for Research, Inc. It houses an RCA 31034A tube, a high efficiency tube with quantum efficiency above 20% out to λ8500Å.

In order to avoid scattered light and to keep internal reflections to a minimum, blackened cylindrical baffles were used within the photometer. To avoid vibration problems, the fan was removed from the cold box and mounted on the telescope pier, air was brought to the cold box via a flexible vacuum hose.

The electronics included the following. A crystal oscillator is used to derive a waveform which drives a stepping motor to provide rotation to the ruling (one rotation every 30 seconds). This waveform is also recorded on one track of a four track Sony tape recorder model #TC-277-4 to provide phase reference. The photo-multiplier pulses are amplified

Fig. 6. Transmission tracings of the two 150Å interference filters purchased from Baird-Atomic.

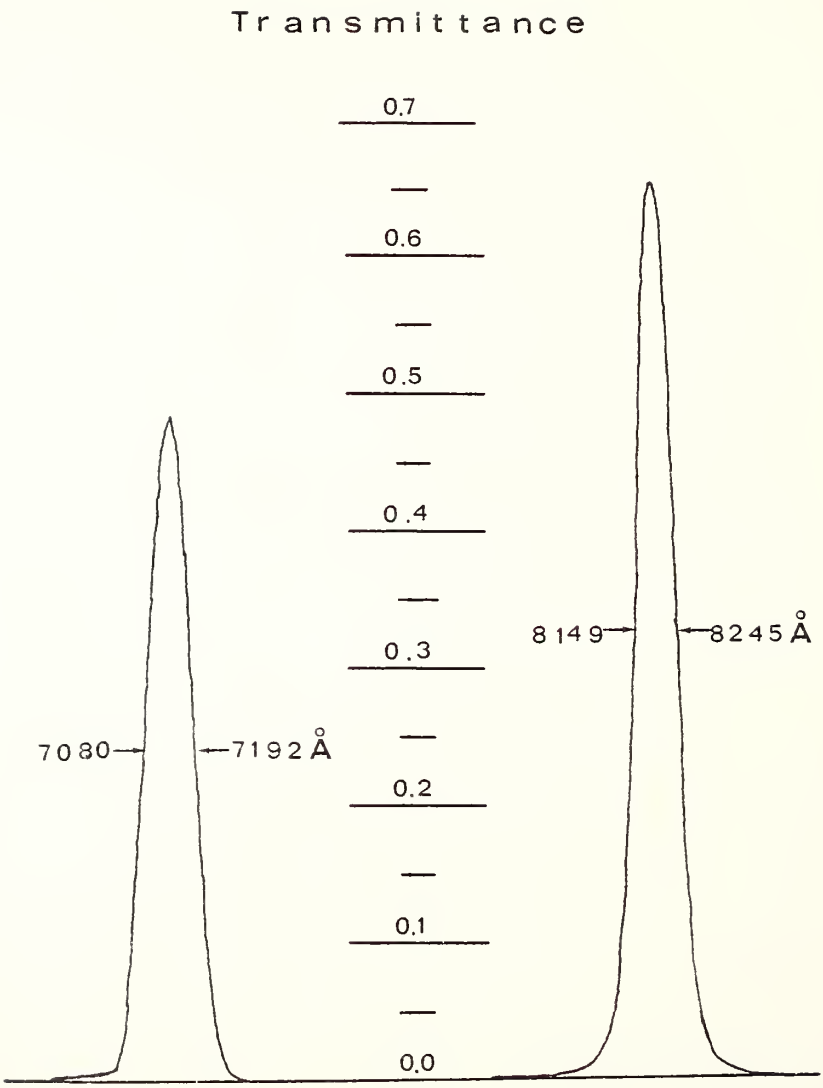
Transmittance
0.7
0.6
0.5
0.4
0.3
0.2
0.1
0.0
7080
7192 Å
8149
8245 Å

Fig. 7. Response function of the blue broad band filter package with the RCA 31034A tube used in these observations.

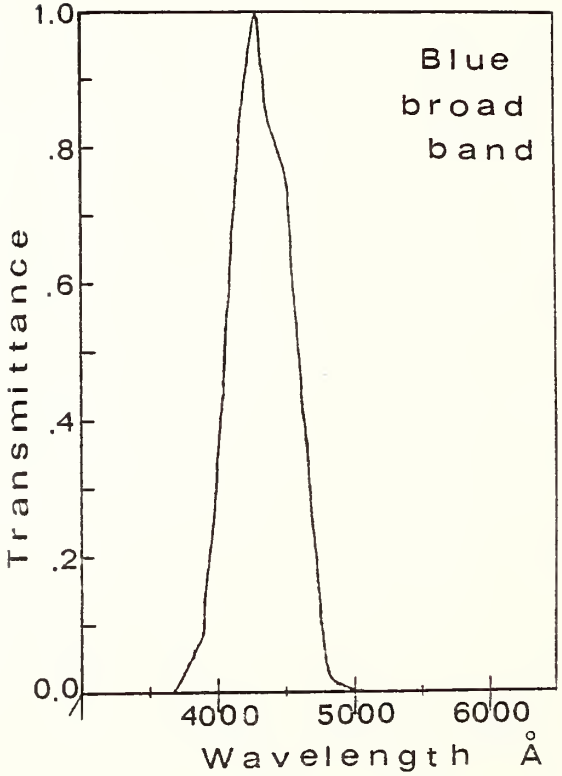
1.0
.8
.6
.4
.2
0.0
Transmittance
Blue
broad
band
4000
5000
6000
Wavelength Å

and shaped by a PARC model 1120 preamplifier (which has a dead time of 10^{-8} seconds), and then used to drive a chain of flip-flops producing at the output a square wave whose frequency is proportional to the count rate; this waveform is recorded on another channel of the tape recorder. For a typical frame of Coma Cluster data, the approximate frequency of the recorded signal was $\approx$400 Hz. Finally, there are infrared LED-phototransistor switches which monitor the rotation of the worm and worm gear to produce a sharp signal each time the worm gear completes a rotation (see Figure 8). Figures 9 and 10 show the photometer on the Mount Holyoke College 24" telescope.

The fourth tape channel was used for verbally recording scan identification information and sidereal time markers.

Processing of Audio Tapes

Before any subsequent data reductions can take place the audio frequency tapes must be transcribed into a readable form for the University of Massachusetts CDC 6800 computer. In practice the conversion has been carried out as follows. The audio tapes are first processed by a PDP-8/e computer, which (via the A-to-D converter input) counted oscillations on the signal against those on the reference channel to provide a digitized record, in which the photon counts have been put into bins of equal duration in time, as determined from the

Fig. 8. The partially assembled photometer. On the near side one can see the stepping motor and circuits for the LED generated reference markers attached to the worm block. Protruding from the photometer at the upper left hand corner of the picture is the mechanism for retracting the prism diagonal of the high magnification setting system. The cold box is held into place by the guide bars at the bottom center of the photograph. The velcro strips hold the light-tight enclosure in place.

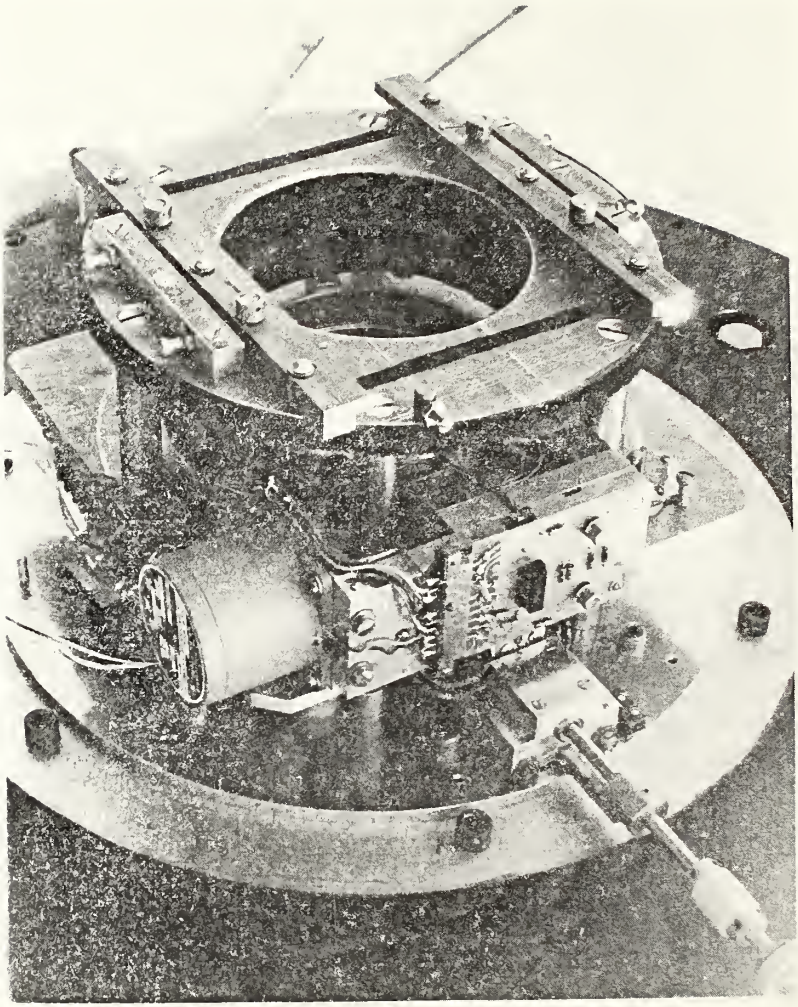

Fig. 9. Fully assembled photometer mounted on the 24-inch telescope. Here one sees the setting eyepiece and, just below it, the dark slide. The PARC model 1120 peramplifier-discriminator is attached to the cold box in this temporary fashion because it had arrived only days before the photograph was taken.

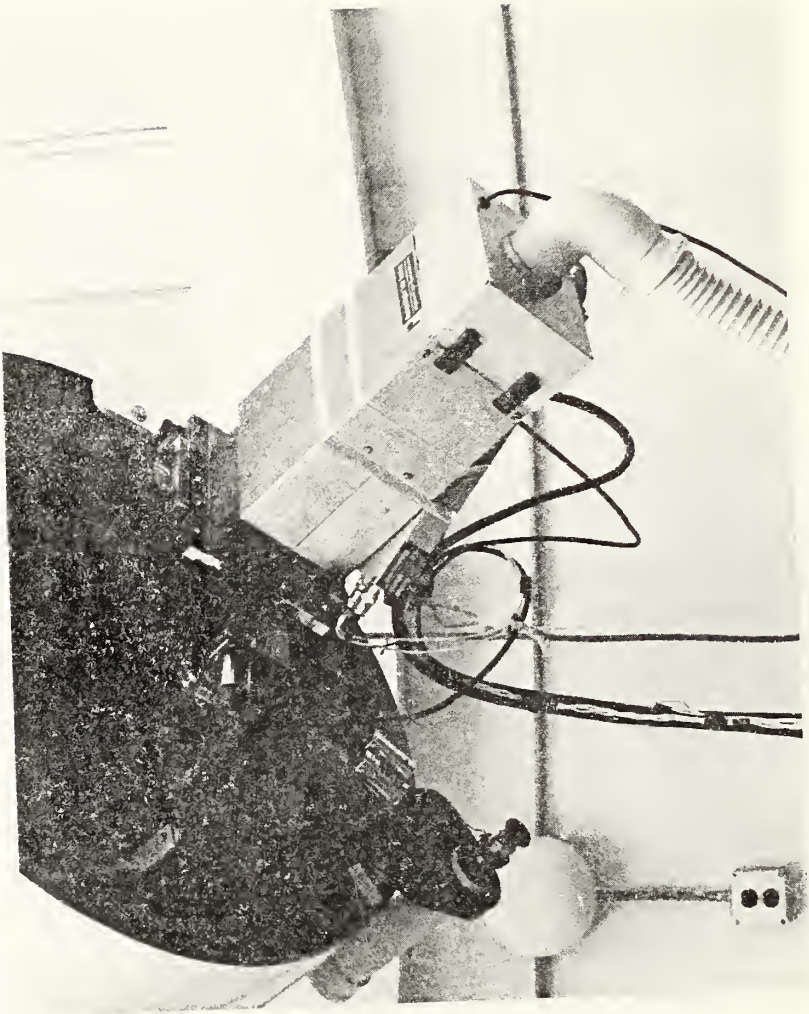

Fig. 10. Photometer in the 24-inch dome. The equipment rack holds, from top to bottom, the power supply for the stepping motor; high voltage source for the photomultiplier; panel container reference oscillator, divide-by circuits, "worm counter" and audio amplifier to drive the loudspeaker in the classic cigar-box enclosure; panel containing counter to monitor the reference oscillator and/or photometric signal and the power supply to the PARC counter; four channel Sony tape recorder; and at bottom the power supply for the Products for Research thermoelectric cold box.

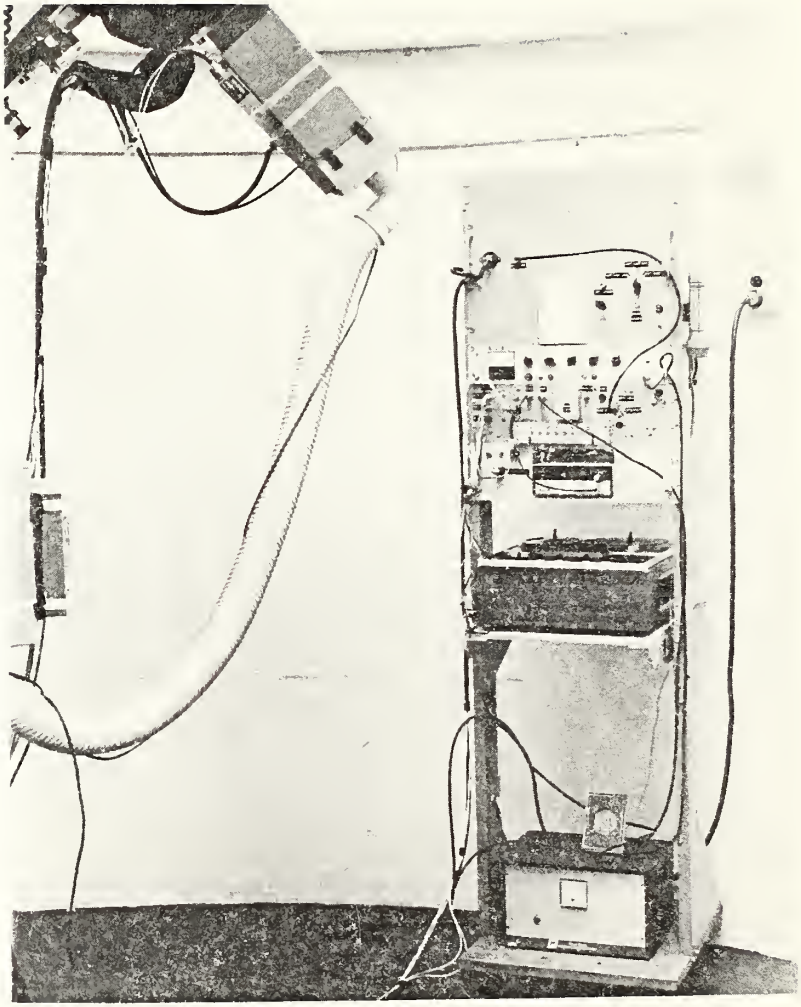

monitor channel.

Absolute phase synchronization for the digitization comes from the crystal oscillator generated wave form on the monitor channel. The digitization process was started by watching for the pulse generated by the worm gear monitor which had been recorded on one channel of the tape. For the Coma Cluster data one rotation of the ruling was divided into 600 bins, each bin corresponding to 110 reference oscillator pulses, or 0.05 seconds of time.

Because of the limited amount of core memory available on the PDP-8/e, a maximum of six rotations could be digitized at once. The digitized records were written onto DEC-TAPE. and when needed were transmitted to the University of Massachusetts computer (to be stored on disk) via a serial interface on the PDP-8/e.

Both before and during the actual transcription of scans, a number of different tests were used to check on the accuracy of the transcription processes. In almost all cases retranscription of the same frame produced the same record, a few frames noticeably those with very bright stars ($m < 9$) might have upon retranscription a checksum which differed by at most 0.05%. The transcription program also checked the number of reference counts present in the last bin of the last rotation to be transcribed; if this number differed from the expected

110 counts, the whole set of rotation was retranscribed.

Encoding and Decoding

The description of the encoding and decoding procedure, and the subsequent waveform calculation presented in this and the following section, follow that given by Dennis (1979, 1975).

From the construction of the photometer it is easy to visualize that as the Ronchi ruling is made to rotate (hereafter referred to as the chopper), the light from a star image or object whose spatial extent is smaller than the grating spacing will be alternately transmitted and blocked; an object whose spatial extent is greater than the grating spacing will not be modulated. The time record of the light transmitted by the chopper is referred to as the "signal waveform", and is the record upon which we perform the following analysis. A record of one complete rotation of the chopper is referred to as a frame of data.

A frame of data in the absence of noise may be represented as:

$$S(t) = \sum_{i}^{n} a_i s_i(t) + c \qquad (2)$$

where s(t) is the photometric signal, the a_i's are the amplitudes for each of the stars in the field and $s_i(t)$ their time dependence, n is the number of stars in the field and c is the contribution due to the unmodulated component. From a knowledge

of the geometry of the observational situation and a knowledge of coordinates for each of the stars in the field, one may compute (by the method described in the next section) $s_i(t)$ the "synthesis waveform" for each of the stars at any instant of time.

If one normalizes the "synthesis waveforms", $s_i(t)$ so that

$$0 \leq s_i(t) \leq 1 \tag{3}$$

it is possible to derive "detector waveforms"

$$d_i(t) = s_i(t) - \tfrac{1}{2}. \tag{4}$$

We have pictured a frame of data to be the sum of the contribution from n stars plus a continuous background, we are thus interested in solving for the n a_i's and c; to determine these n + 1 quantities we can find a set of n + 1 linear equations as follows. Upon multiplying equation 2 by each of the n detector waveforms in succession, and integrating over the entire observational record, one obtains a set of n equations

$$a_1\int s_1 d_j dt + a_2\int s_2 d_j dt + \ldots + a_i\int s_i d_j dt + \ldots + a_n\int s_n d_j dt + c\int d_j dt = \int S(t) d_j(t) dt \tag{5}$$

which is nearly diagonal because

$$\int s_i(t)d_j(t)dt \begin{cases} \approx 0, & i \neq j \\ = \text{some normalizing constant}, & i=j \end{cases} \tag{6}$$

The final equation, obtained by integrating equation 2 over the entire record is

$$a_1 \int s_1 dt + \ldots + a_n \int s_n dt + c \int dt = \int S(t)dt. \tag{7}$$

Waveform Calculation

The key to the data reduction problem is the accurate calculation of the set of "synthesis waveforms" $s_i(t)$. We start by defining on the chopper (the Ronchi ruling) a rectangular coordinate system (X,Y) with the origin near the center of rotation, and located on an opaque-transparent boundary (Figure 11). This turns out to be a left handed coordinate system with the X-axis parallel to the rulings when viewed from behind the telescope.

We can now define an "astrometrist's" coordinate system (x,y), with the center of rotation taken to coincide with the tangent point (Konig 1933).

$$x = F \frac{\cos\delta \sin\Delta\alpha}{\sin\delta \sin\delta_0 + \cos\delta \cos\delta_0 \cos\Delta\alpha} \tag{8}$$

$$y = F \frac{\sin\delta \cos\delta_o - \cos\delta \sin\delta_o \cos\Delta\alpha}{\sin\delta \sin\delta_o + \cos\delta \cos\delta_o \cos\Delta\alpha} \qquad (9)$$

Where F = focal length

δ_o = declination of the chopper axis

δ = star's declination

$\Delta\alpha$ = hour angle difference (star - chopper axis).

From the geometry presented in Figure 11, we may easily write transformation between the two coordinate system to be

$$Y = y \cos\theta + x \sin\theta + y_o ; \qquad (10)$$

With this transformation in hand, one may now define phase on the ruling to be

$$\rho = \frac{Y}{a} \qquad (11)$$

where a = ruling spacing, which can be used to calculate the "synthesis waveforms" $s_i(t)$.

A simple but informative example of the meaning of $s_i(t)$ can be seen in Figure 12 . Figure 12 is a plot of transmission versus phase calculated on the assumption that star images are point sources. In this trivial example $s_i(t)$ would be either 1 or 0 depending on whether the star is in the clear or being occulted. In reality stars are neither point source nor can their shape be represented in a simple manner.

Fig. 11. The coordinate system used in calculating the "synthesis waveforms", a = ruling spacing, theta zero (not shown on the diagram) is defined to be the initial angle of the ruling measured from the north-south direction.

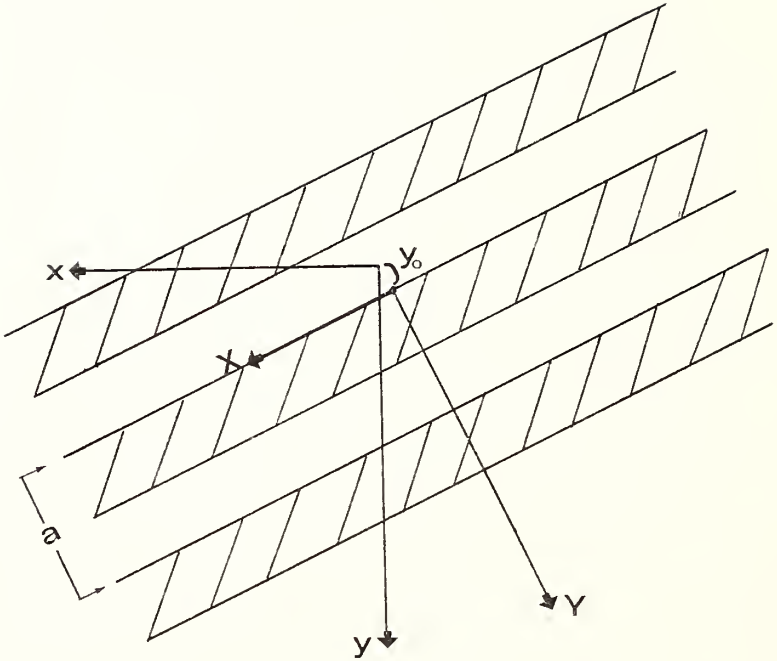
x
y_o
X
a
y
Y

Fig. 12. In the limit of representing a star image as a point source, the "synthesis waveform" reduces to that of a square wave.

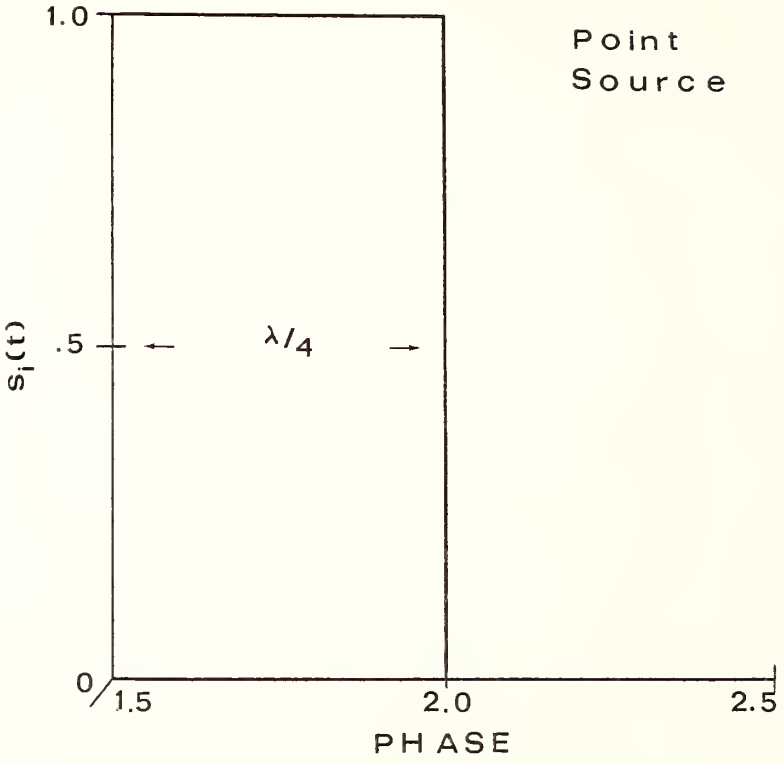
1.0
.5
0
$s_i(t)$
$\lambda/4$
1.5
2.0
2.5
PHASE
Point
Source

Form of Image

As mentioned in the previous section, the calculation of a "synthesis waveform" requires a knowledge of the actual image intensity distribution in the focal plane of the telescope. Theoretically, the necessary information can be found by convolving a model for the star's image with the chopper, taking into account both the rotation of the chopper and the diurnal motion of the star. Before carrying out this lengthy convolution, an attempt was made to find a suitable representation for $S_i(t)$ empirically. Data taken with the Mount Holyoke 24 inch showed that, to a good approximation, one could write the "synthesis waveforms" as

$$s_i(t) = \sin((\phi - 1)*\eta + 1)/2. \qquad (12)$$

Initial reductions of observations made at Kitt Peak showed that even though the set of geometrical parameters was well determined, the calculated waveform based on equation 12 didn't represent the observed waveform as well as expected. From Figure 13 one can see that the calculated waveform underestimates the sky level, and is too narrow near maximum but too broad near minimum transmission.

To gain further insight into the problem, the final ruling scans were studied. For these scans the telescope had been clamped in right ascension and declination; the ruling was not rotating and was aligned North-South. The

Fig. 13. Comparison between the observed and calculated waveform assuming a sinusoid as the synthesis waveform.

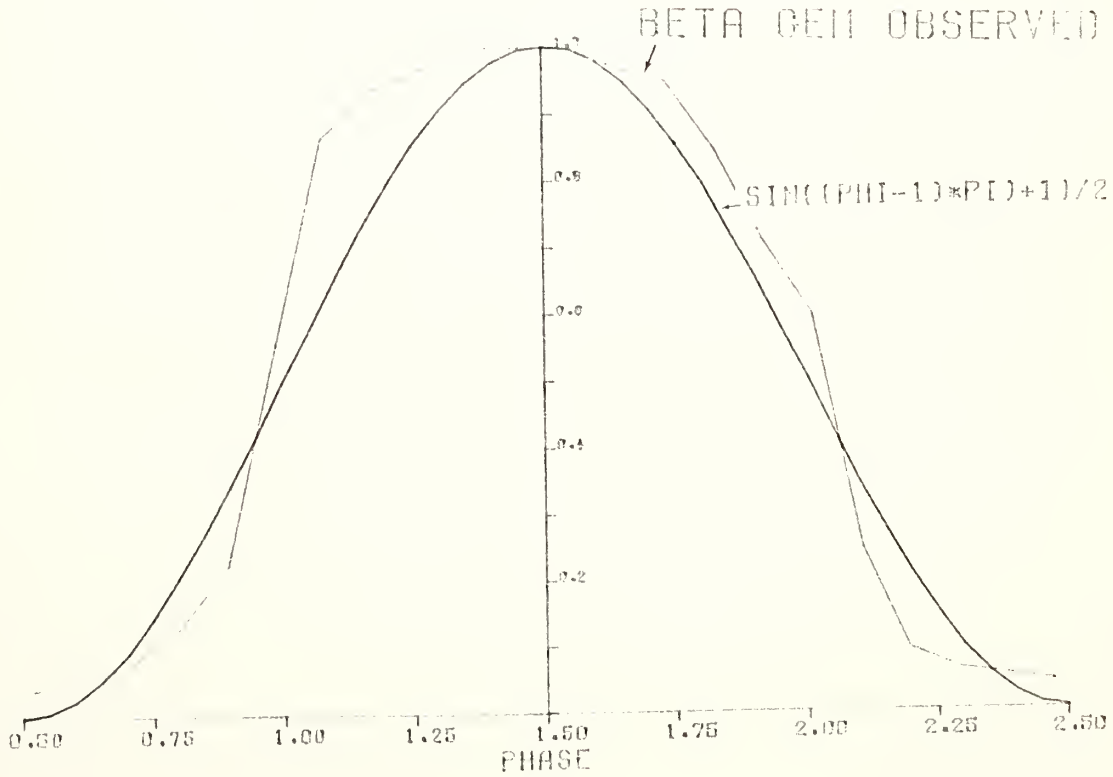
BETA GEN OBSERVED
SIN((PHI-1)*PI()+1)/2
0.8
0.6
0.4
0.2
0.50
0.75
1.00
1.25
1.50
1.75
2.00
2.25
2.50
PHASE

1.15 magnitude star β Geminorum drifted through the center of the actual image distribution with the fixed chopper. Figure 14 shows a comparison of the observed record with that predicted by a sinusoid. A diagram showing the position of the star image, with respect to the ruling as a function of phase can be found in Figure 15. From Figure 14 it was clear that the empirically determined synthesis waveform would not be suitable for use with the Kitt Peak data, so the actual convolution of a model image with the chopper needed to be carried out. The failure of the empirical relation for the "synthesis waveforms" is probably due to the better seeing encountered at Kitt Peak compared to that on an August night in South Hadley, Massachusetts.

To start a Gaussian intensity profile was assumed for the star image, when the convolution of this model image with the chopper is performed (Figure 16) one is left with the difference of Error Functions. In Figure 17 we compare the "synthesis waveform" generated by assuming a Gaussian star profile with the previous empirical Sinousoid. The result is encouraging, in that the top of the profile is broader and the bottom narrower than the empirical form, and by varying the size of the "seeing" disk one can better fit the observed profile (Figure 18). Though a better fit is obtained for the portion of the record in which the star is in the clear (phase 1.50), the calculated waveform misses badly

Fig. 14. Comparison between the "fixed ruling" scan of β Geminorum and the record predicted by a sinousoid representation of the "synthesis waveform".

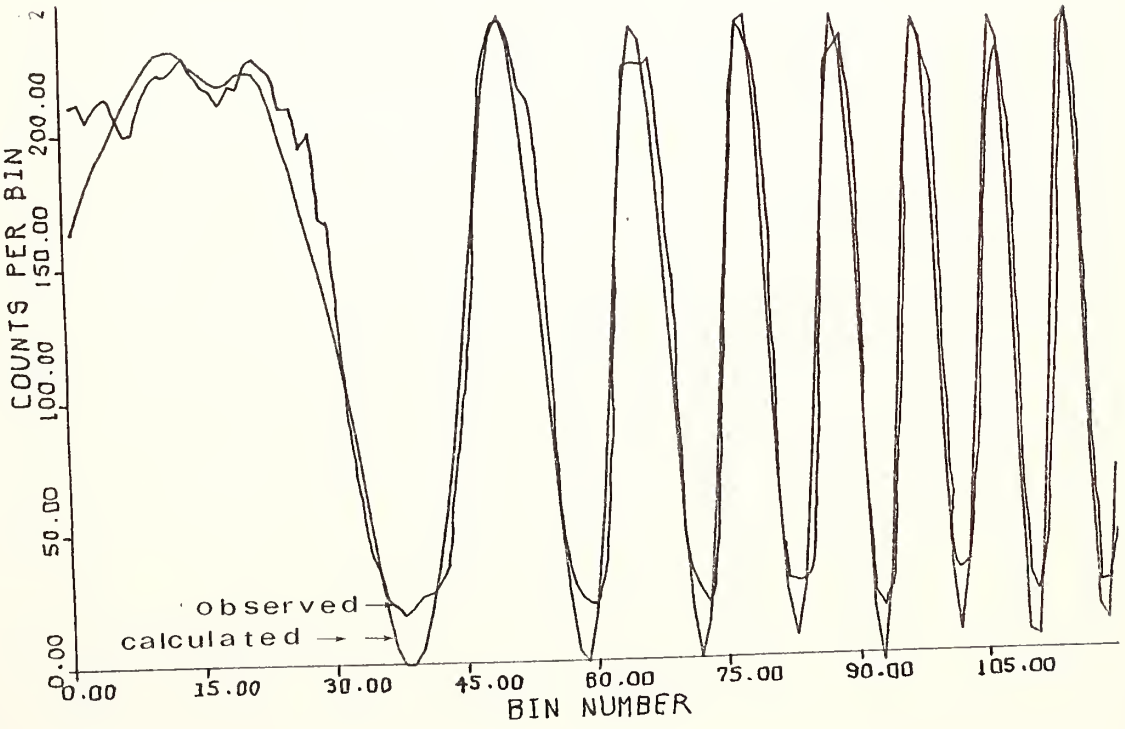
COUNTS PER BIN
0.00
50.00
100.00
150.00
200.00
observed
calculated
0.00
15.00
30.00
45.00
60.00
75.00
90.00
105.00
BIN NUMBER

Fig. 15. A diagram showing the position of a star with respect to the ruling as a function of phase.

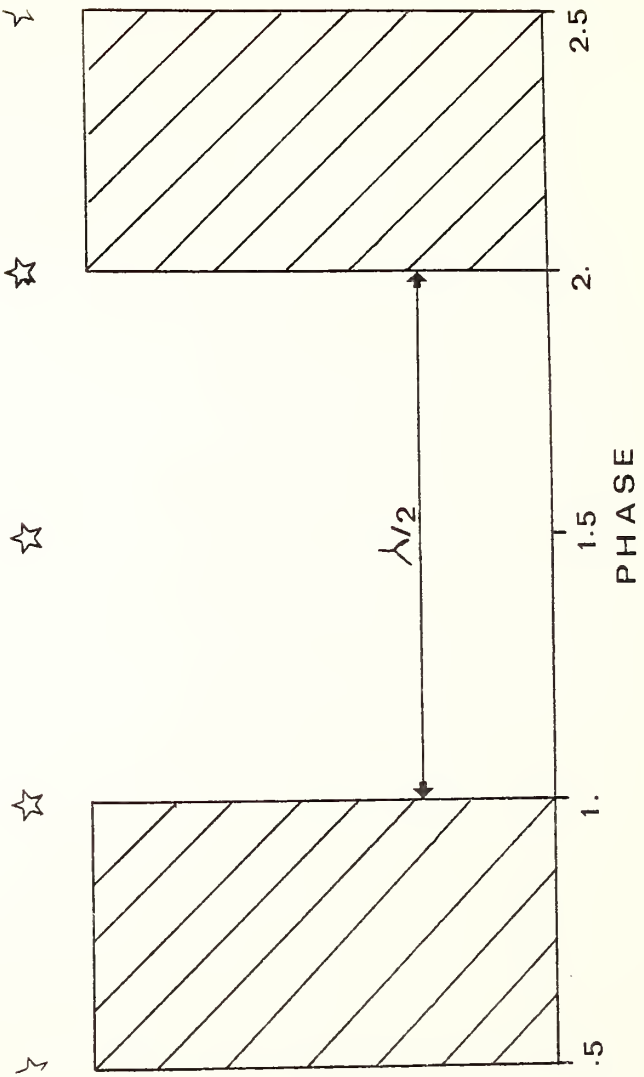
2.5
2.
1.5
1.
.5
PHASE
λ/2

Fig. 16. The "synthesis waveform" versus phase, calculated using a Gaussian profile for the star image.

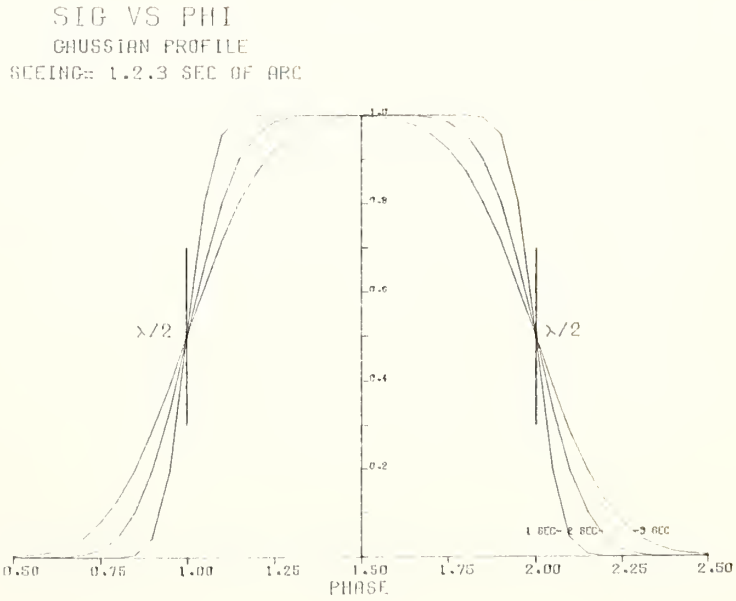
SIG VS PHI
GAUSSIAN PROFILE
SEEING= 1.2.3 SEC OF ARC
λ/2
λ/2
0.50
0.75
1.00
1.25
1.50
1.75
2.00
2.25
2.50
PHASE

Fig. 17. A comparison of the synthesis waveform calculated using a Gaussian star profile with that determined using the sinousoid representation.

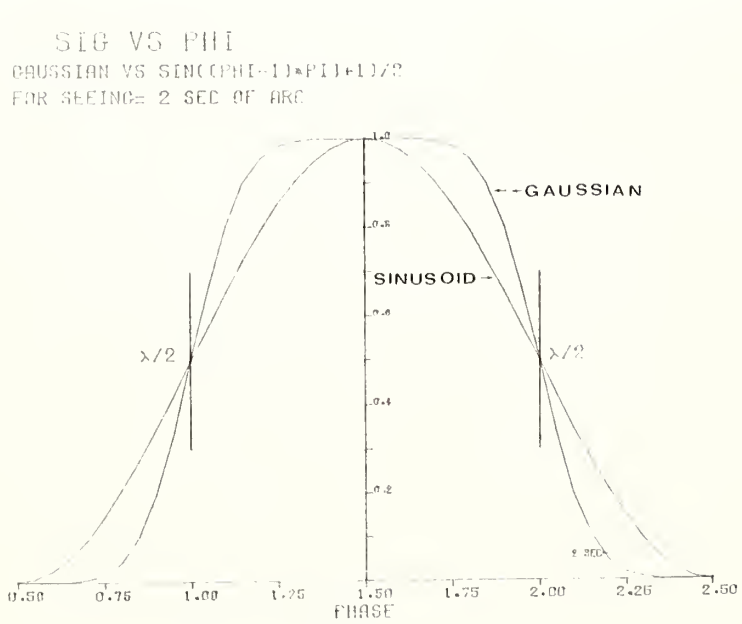
SIG VS PHI
GAUSSIAN VS SIN((PHI-1)*PI)+1)/2
FOR SEEING= 2 SEC OF ARC
GAUSSIAN
SINUSOID
λ/2
λ/2
2 SEC
0.50
0.75
1.00
1.25
1.50
1.75
2.00
2.25
2.50
PHASE

Fig. 18. Comparison between the "fixed ruling" scan of β Geminorum and the record predicted by assuming a Gaussian profile for the star image.

BETA GEM OBSERVED VS
GAUSSIAN PROFILE
FOR SEEING= 2 SEC OF ARC

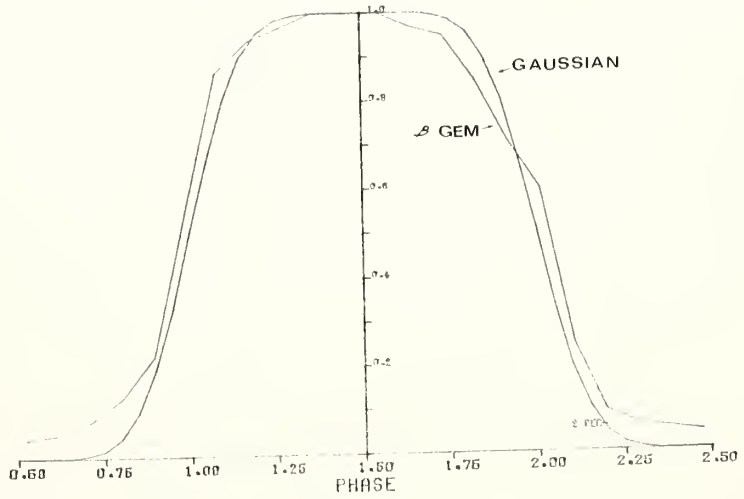

when the star is occulted. What is needed then is a profile that would have broader wings than the Gaussian, so as to distribute more light to the outer part of the image.

A similar problem has been encountered by Zissell (1973) in observations made with his "Oscillating Mirror Area-Scanner". After trying a number of different models he reports a suitable representation for the convolution of a star image with the single slit of his scanner to be

$$F(x) = A/(Y^{(2.0 + 0.5Y)} + 1), \qquad (13)$$

where A = maximum count rate

$$Y = \left| \frac{x - B}{H} \right|$$

B = the channel of axis of symmetry

H = the width at half amplitude

As this representation is already the convolution of a narrow slit with the actual image, it is not directly applicable to our case of a wide slit. As the de-convolution of equation 13 is difficult, the composite model of a star image formulated by King (1971) was tried instead.

The composite profile determined by King consists of a central core, an exponential drop, and an extended inverse-square aureole extending out some 5°. To carry out the convolution with the chopper a set of curves consisting of

(a) A Gaussian $r < 1.7"$, (b) a Gaussian plus an exponential $1.6" \leq r \leq 3"$, a set of exponentials $1.6" < r < 10"$, and (c) a power law index $n = -2$ for $10" < r < 3 \times 10^4$ was fitted to the data in Figure 1 of King's paper. The set of curves was combined and normalized so that

$$\int_0^{2\pi} \int_0^{3 \times 10^4} I(r)\, r\, dr\, d\theta = 1 \qquad (14)$$

The resulting approximation is shown in Figure 19. Integration of the fit to King's data showed that 4.6% of the star's light was contained in the inverse-square sureole, which is in good agreement with the value of about five percent stated by King.

The resulting intensity distribution for King's composite profile was then convolved with the chopper. The results of this somewhat lengthy numerical procedure are shown in Figure 20. If we now compare (Figure 21), these results with that of the simple Gaussian image we see that approximately 5% of the light has been distributed into the wings of the profile, whereas the shape of the central region has been unchanged. If we again compare our calculated waveform with the observed record for β Gemenorum Figure 22a, b, we see that though not quite perfect a substantial improvement has been made, especially when the star was being occulted (phase

Fig. 19. Approximation to King's star profile.

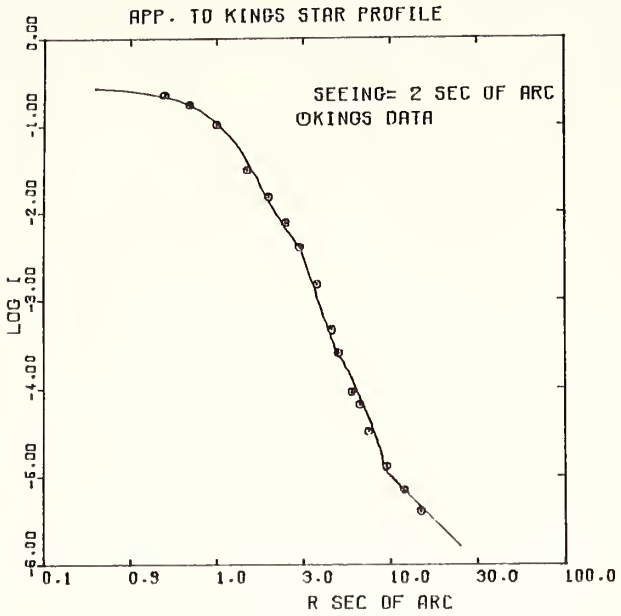
APP. TO KINGS STAR PROFILE
SEEING= 2 SEC OF ARC
⊙KINGS DATA
LOG I
0.00
-1.00
-2.00
-3.00
-4.00
-5.00
-6.00
0.1
0.9
1.0
3.0
10.0
30.0
100.0
R SEC OF ARC

PAUSE

Fig. 20. The "synthesis waveform" versus phase, calculated using an approximation to King's star profile.

CONVOLUTION OF KINGS PROFILE

FOR SEEING= 1.2.3 SEC OF ARC

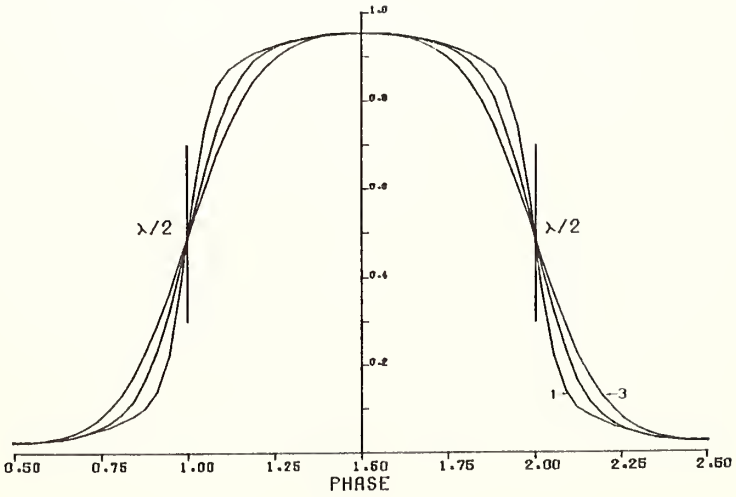

Fig. 21. A comparison of the "synthesis waveform" calculated using a Gaussian star profile with that determined using King's star profile.

PAUSE
?

GAUSSIAN PROFILE
VS KINGS PROFILE
FOR SEEING= 2 SEC OF ARC

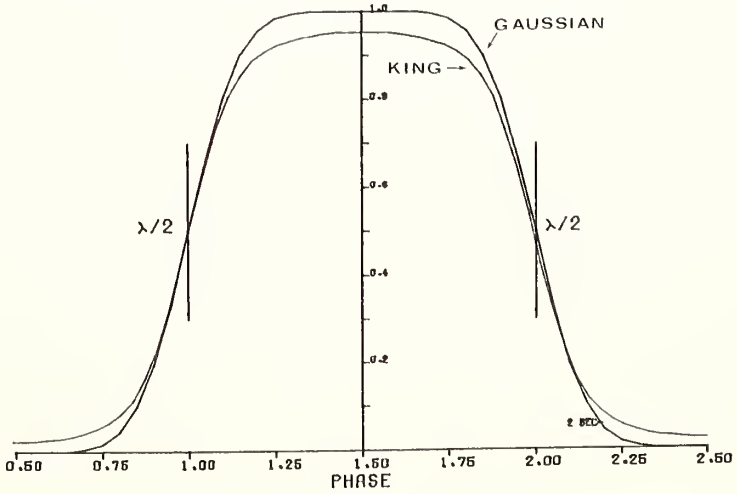

Figs. 22a, 22b. Comparison between the "fixed ruling" scan of β Geminorum and the record predicted by assuming a King star profile, for different values of the seeing disk.

PAUSE
?

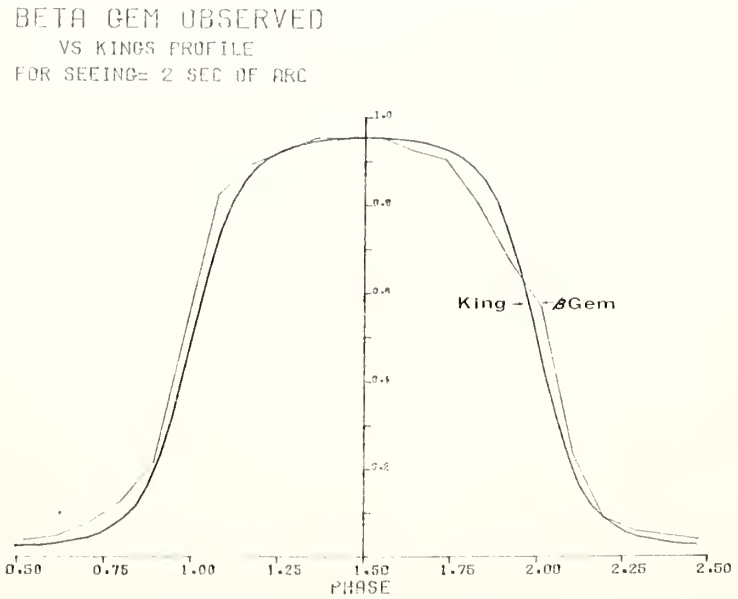
BETA GEM OBSERVED
VS KINGS PROFILE
FOR SEEING= 2 SEC OF ARC
King
βGem
0.50
0.75
1.00
1.25
1.50
1.75
2.00
2.25
2.50
PHASE

PAUSE
?

BETA GEM OBSERVED
VS KINGS PROFILE
FOR SEEING= 3 SEC OF ARC

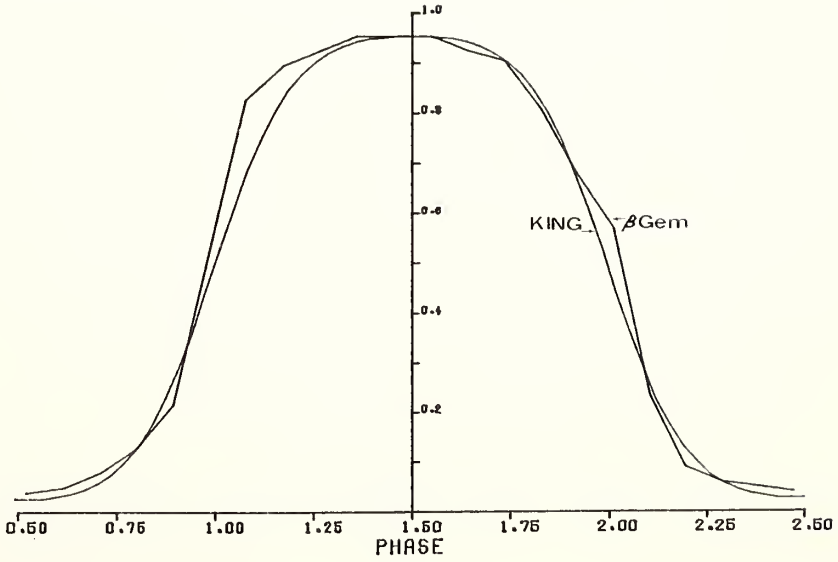

Fig. 23. Comparison between observed and calculated waveform assuming King's profile for a star image, as discussed in the text.

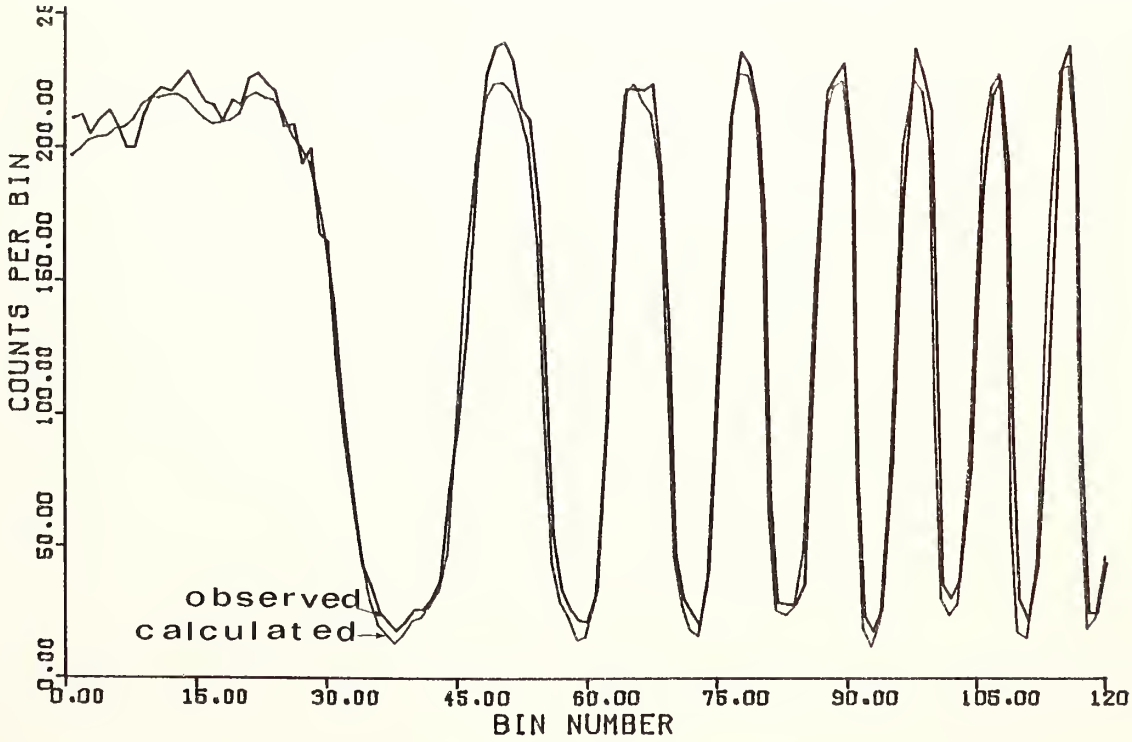
COUNTS PER BIN
0.00
50.00
100.00
150.00
200.00
0.00
15.00
30.00
45.00
60.00
75.00
90.00
105.00
120
BIN NUMBER
observed
calculated

0.5). The main data reduction program was modified to calculate the "synthesis waveforms" based on the approximation to King's composite model presented above, Figure 23, showing the improved fit obtained for the same record shown in Figure 13. The composite star profile of King was used for all subsequent reductions of Coma Cluster scans.

As has been discussed by Zissel (1973) the image formed by a Cassegrain telescope will not be radially symmetric, there being diffraction spikes with the same pattern as the secondary mirror supports. As the #4-0.4 meter telescope has four equally spaced supports, the recorded profile should be symmetric without regard to the direction of scanning, and pose no special problem.

CHAPTER III

OBSERVATIONS

Initial testing of the instrumentation was carried out during the summer of 1976 on the Mount Holyoke 24-inch telescope.

The present observations were taken with the Kitt Peak #4-0.4 meter telescope on nine consecutive nights, from February 9th to February 17th, 1977, using the photometer described in chapter II. The observations consisted of drift scans through the cluster at various declinations north and south of the cluster center. The origins and lengths of the scans can be seen in Figure 24.

The cluster was observed through a circular entrance aperture 18.54 arc minutes in diameter, and the diurnal motion with the telescope drive stopped provided a drift rate of 6.63 arc minutes per frame of data (one rotation of the chopper). Data were collected during 24 hours covering the spectral region at λ 7150Å, and λ8200Å (λ100Å bandwidth), and blue (broad band). To supply information on the uniformity of the field response, drift scans at various declinations through the field were made using the bright stars β Leonis m = 2.14, and β Geminorum.

The observing procedure consisted of the sequence-reference region-scan north of the cluster center-reference

Fig. 24. The origins and lengths of the scans of the Coma Cluster.

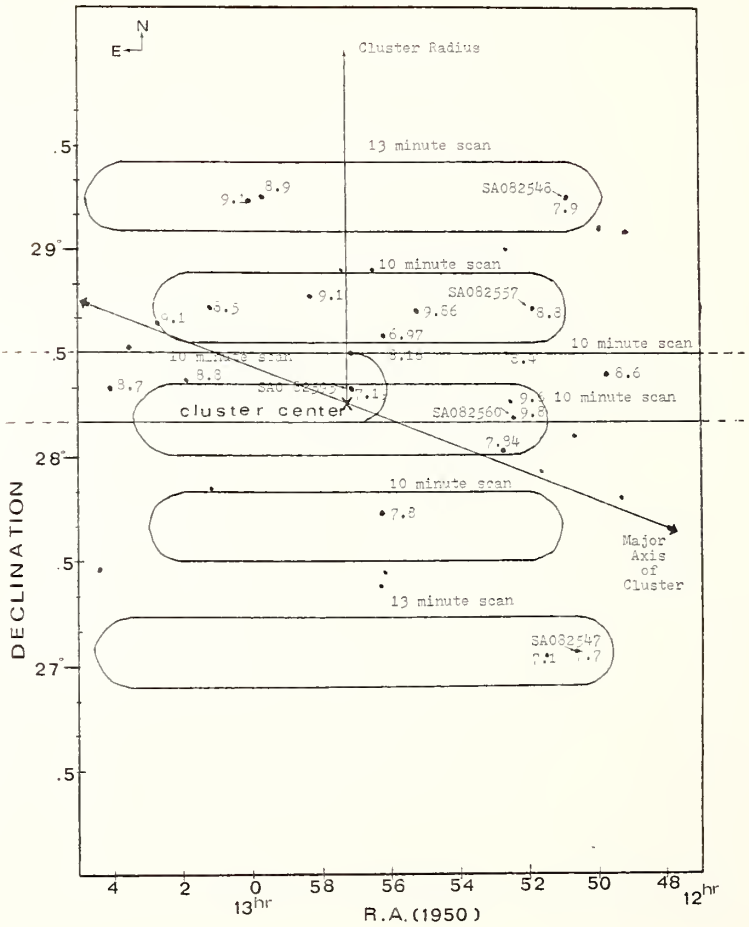
N
E
Cluster Radius
13 minute scan
SA082546
7.9
10 minute scan
SA082557
9.56
8.3
6.97
10 minute scan
8.6
cluster center
SA082560
9.8
10 minute scan
7.84
10 minute scan
7.8
Major Axis of Cluster
13 minute scan
SA082547
7.7
DECLINATION
29°
28°
27°
.5
4
2
0
58
56
54
52
50
48
13hr
12hr
R.A.(1950)

region-corresponding scan south of the Cluster center - reference region-drift scan north etc. Table I gives the identification of the "set up" stars, the numbers of scans made of each region, and the sequence used in scanning them, for those nights from which data were later reduced. The convention used for identification of scan regions is: X, meaning the scan was North on South of the Cluster center by X minutes of an arc. As an example, the northern most scan is designated N61, meaning that region scanned was 61 arc minutes north of the Cluster center.

The data were taken as follows: the telescope was moved to the "set up" star (SAO 82595) for the "Reference Region scan", after the star had been centered in the fine setting eyepiece, the guide scope was retracted, and the telescope drive was switched off 2.7 seconds before the start of a scan. This last step was to ensure that the telescope would have a chance to settle down before the start of a scan. Subsequent data reductions have shown that telescope motion had continued into rotation one of each scan (Figure 25). Because of this problem the first frame of data was not reduced. Following the reference region scan, the telescope was then moved to begin the sequence of scanning given in Table I.

A complete sequence of reference region-long scan ref-

TABLE 1

OBSERVING LOG

SCAN IDENTIFICATION	SET UP STAR	TIMES SCANNED λ7150 Å	TIMES SCANNED λ8200 Å	LENGTH OF SCAN
	NIGHTS OF FEBRUARY 13-14, 14-15, 15-16, 1977			
Reference Region	SAO 82595			1 minute
S4	SAO 82560	7	3	10 minutes
Reference Region				1 minute
N61	SAO 82548	3	2	13 minutes
Reference Region				1 minute
S71	SAO 82547	3	2	13 minutes
Reference Region				1 minute
N25	SAO 82557	3	2	10 minutes
Reference Region				1 minute
S37	Off Set	3	1	10 minutes
Reference Region				1 minute
N5	SAO 82595	3	2	10 minutes
Reference Region				1 minute
N5	Off Set to RA = $12^{hr}_{48}{}^{min}$	3	2	10 minutes
	NIGHT OF FEBRUARY 12-13, 1977			
Reference Region	SAO 82595			1 minute
S4	SAO 82560			10 minutes
Reference Region				1 minute
N15	SAO 82564			10 minutes
Reference Region				1 minute
S13	SAO 82565			10 minutes
Reference Region				1 minute

Fig. 25. A comparison of the observed and calculated waveform, shows that the telescope was still drifting for the first 100 bins of frame one.

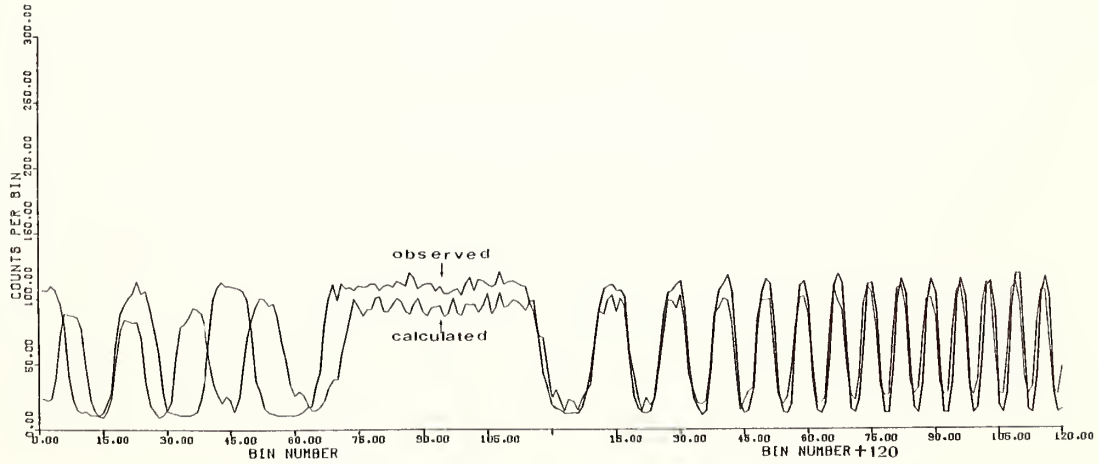
COUNTS PER BIN
0.00
50.00
100.00
150.00
200.00
250.00
300.00
observed
calculated
0.00
15.00
30.00
45.00
60.00
75.00
90.00
105.00
BIN NUMBER
15.00
30.00
45.00
60.00
75.00
90.00
105.00
120.00
BIN NUMBER+120

erence region took on the average 14 or 17 minutes depending on whether it was a 10 or 13 minute scan. Subsequent data reductions have shown that overlap in the starting positions of each scan has been maintained on the average to ± 1.2 arc seconds in declination and 1.5 seconds in right ascension.

All scans were carried out when the cluster was within 3 hours of the meridian, a maximum of 1.3 air-masses being encountered for a few scans. Data collection continued on most nights until the beginning of astronomical twilight, though only those scans taken before moonrise on a given night were later reduced. Appendix 1 contains a listing of and relevant data for those scans later reduced. Plots of the variation in the reference region for the nights of interest are given in Appendix 2.

Data taken at Kitt Peak was recorded on TDK "AUDUA L-1800" recording tape, a low noise, high output tape at 3/34 ips. Typical minimum sky counts through the λ7150Å interference filter were 100,000 counts per 30 secs. The dark count ($\approx$ 60 counts) was negligible. As a typical frame of data has $\approx 10^5$ counts, photon noise will limit our sensitivity to $\approx$ 0.3% of the night sky level, though averaging of scans at best should lower this limit to 0.17% (0.3%/(3(average number of scans per region))$^{\frac{1}{2}}$).

As outlined in chapter II, in order to reduce the data,

one requires the accurate positions for all the stars present in the field of view down to some limiting magnitude ($\approx$16 for the present case). The necessary positions were obtained by measuring a 48 inch Schmidt plate (loaned from Dr. J. Kormendy) on the two axis Grant measuring engine at Kitt Peak National observatory. In all, the positions of over 4000 objects were obtained. These coordinates were then compiled to form a star catalogue which was checked for duplicate measurement and systematic shifts between measuring sessions. The compiled catalogue has a limiting magnitude ($m \approx 16.5$) obtained by measuring approximate blue magnitudes from a Palomar Sky Survey Print (King and Raff 1977) that is somewhat fainter than required.

C H A P T E R IV

Performance of the Photometer

In this section I wish to discuss in some detail the performance of the "multiplexing night sky photometer" and decoding procedures described in chapter II. During the period in which observations were taken at Kitt Peak the photometer's electronics and hardware functioned almost flawlessly, with the exceptions that the last night of observing was lost, due to a cracked bearing in the chopper assembly. The original RCA 31034A tube taken to Kitt Peak failed on the second night of observing and had to be replaced. As the moon's position had already made the early part of the observing run unfavorable, this failure resulted in no lost observations of the Cluster.

Geometrical Parameters

The calculation of the synthesis waveform outlined in chapter II requires positional information for the chopper axis and stars in the field, in addition, the accurate determination of the three geometrical parameters, the focal length of the telescope, Y_o, and Θ_o (defined in Figure 11) are also required.

A trial value for the focal length is obtained by using the fixed ruling scans. In these scans the ruling is aligned North-South, is not rotating, and a bright star is allowed

to drift through the field. As the declination of the star and chopper axis are known, this information along with the ruling spacing and observed record can be combined to obtain a value for the focal length. An initial value for Y_o and Θ_o were obtained from direct measurements of the photometer.

These initial values were then used to reduce frames of data with the ruling rotating and a bright star drifting through the field at varying declinations. Small pertabulations were made on the parameter set to obtain a consistant set of values that matched data taken at all declinations. These improved parameters were then used to reduce data taken on various nights, and were found to produce equally good results. The parameter set of focal length = 7252 mm, Y_o = 0.1770 mm, and Θ_o = -1.72493 radians was adopted for all further data reduction.

Field Efficiency

The first scans studied in detail were those taken to supply a check on the uniformity of the field efficiency. A short segment of one such scan made through the λ 150Å filter is shown in Figure 26. Figure 27 presents the maximum amplitude observed versus the number of wavelengths from the center of the field for scans made through the λ150Å interference filter. As can be seen from this plot, the field efficiency is anything but uniform. To further complicate

Fig. 26. A short segment of a "fixed ruling scan"; the star is β Leonis, and the number of counts observed divided by 112 vs. bin number is plotted.

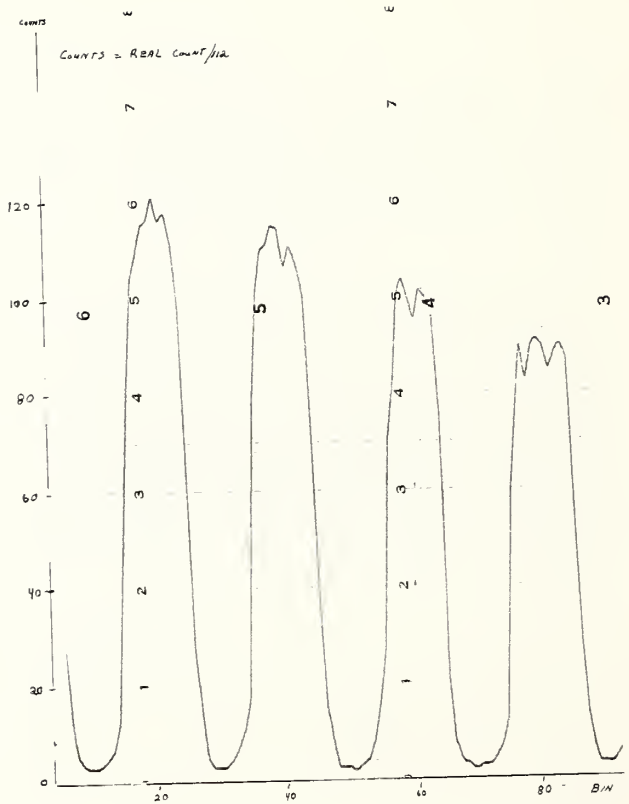
COUNTS
COUNTS = REAL COUNT/12
120
100
80
60
40
20
0
20
40
60
80
BIN
6
5
4
3

Fig. 27. Maximum amplitude observed vs. wavelengths from the center of the field, for a fixed ruling scan taken at λ7150Å.

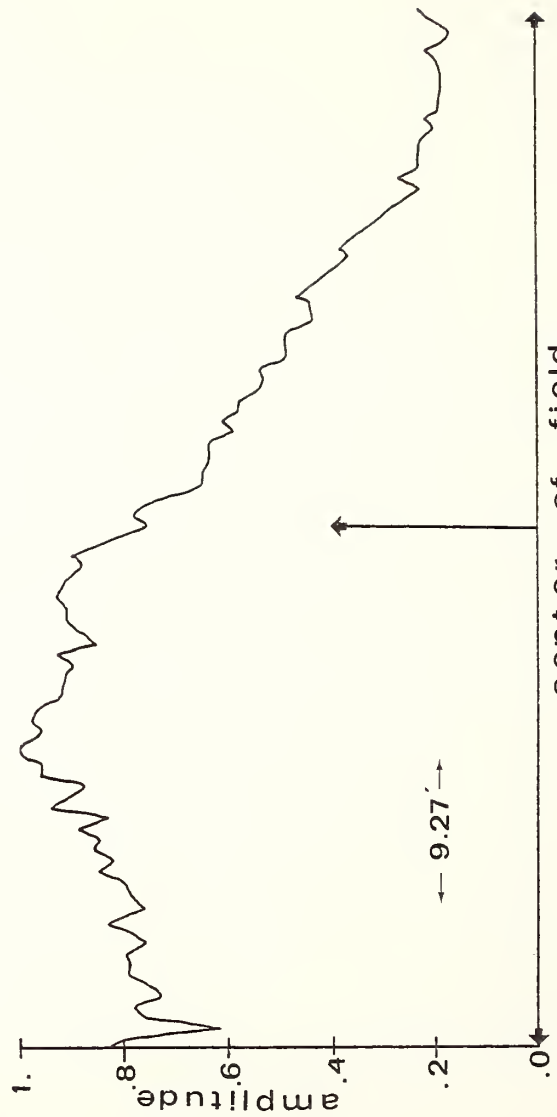
7150 Å
amplitude
1.
.8
.6
.4
.2
.0
9.27'
center of field

the situation, transcription of additional scans showed that the shape of the curve varied slightly from night to night and with the particular filter being used. There is also some indication that the shape of the curve varies slightly near the northern edge of the field. Though the shape of the curve may vary, the efficiency over the majority of the field was found to be very constant in the North-South direction (Figure 28).

What produced this nonuniform response? The first thought that comes to mind is vignetting. Whereas some vignetting is certainly present, the great asymmetry of the plot and the extent of the effect, combined with ray tracings of the system rule vignetting out as the major problem. Though the cause is still uncertain, it is possible that since the RCA 31034A has a slanted photocathode as well as a very narrow entrance window, and with the current apparatus, the beam was just filling the photo cathode, any small misalignment in the optical system might be the main cause of the problem.

The nonuniformity poses no major computational problem. In fact it had been assumed that a small correction would be necessary. The correction is made by supplying a table of efficiency versus position in the field to the main data reduction program. The net effect is that equation 2 now reads:

Fig. 28. Maximum amplitude observed vs distance from the center of the field in the North-South direction. For this scan, the ruling had been aligned East-West and the star β Leonis was driven through the field, South to North.

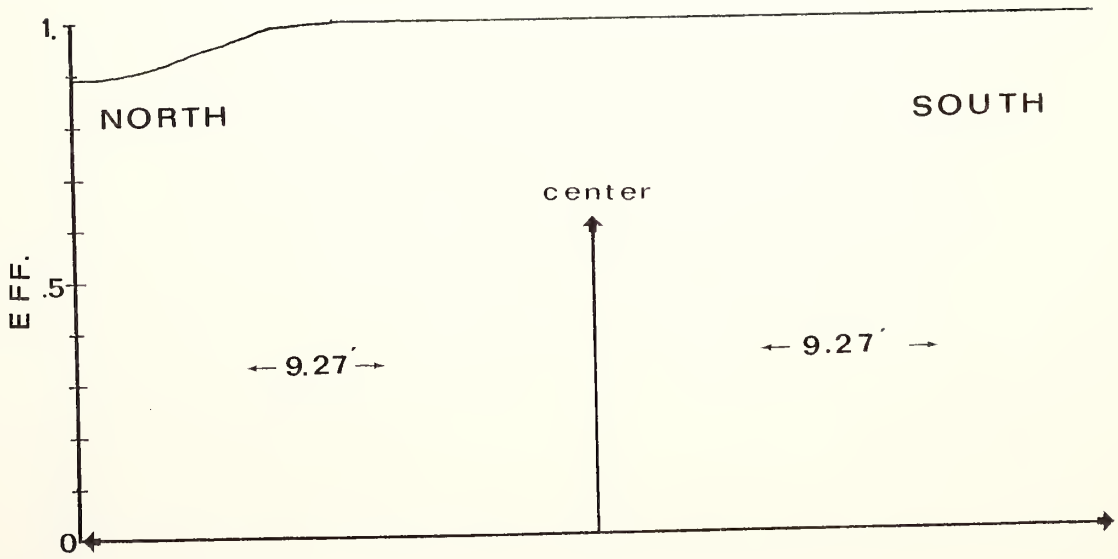
1.
NORTH
SOUTH
center
EFF.
.5
9.27'
9.27'
0

$$S(t) = \Sigma_i \, a_i \, \varepsilon_i(t) s_i(t) + c \qquad (15)$$

where $\varepsilon_i(t)$ is the field efficiency. For the Coma Cluster data, this table is hard to produce as one needs bright stars passing at various declinations through the field. Very few data of this type exist, as pains were taken to avoid fields containing bright stars. Nevertheless, the necessary tables have been prepared, and are presented in Figure 29. A separate table was not prepared for scans made through the λ8200Å filter as the very limited data available showed no marked deviation from the λ7150Å data.

Decoding Procedures

The data recording and transcription procedures described in chapter II worked quite satisfactorily. The only drawback was that, on the average $\approx$40 minutes was required to convert a ten minute scan from audio tape to final storage on disk.

With the transcribed data, field efficiency tables, star catalogue, and geometrical parameters available, the only remaining information needed, before a scan can be reduced, is the starting right ascension and declination for the chopper.

To obtain this information, a search was made in right

ascension and declination using the "set up" stars right ascension and declination as the starting point. Until an accurate value for the offset in the "fine setting" telescope was determined, this procedure consumed many hours at the teletype. Even with this offset known, the inaccuracy in the starting right ascension for a scan (± 1.5 seconds), caused by slight variations in when the telescope drive was turned off, made the search lengthy.

With starting parameter in hand, the actual reduction of a ten minute scan required some 40 seconds of central processor time on the University of Massachusetts CDC 6800.

A Single Scan

To demonstrate the system's ability to carry out the "star subtraction" process I discuss a representative scan of the Coma Cluster made through the λ7150Å filter. This S71 scan taken on the night of February 13, 14. 1977, while otherwise representative, is <u>atypical</u> in the range of stellar magnitudes encountered. As some of the frame can cover a dynamic range of approximately 4000 this scan represents an unusually difficult test for the system.

The observed data record for this scan, along with its calculated "star corrected" record are shown in Figure 30. Even if one had corrected for the foreground stars exactly,

Fig. 29. The measured mean field efficiency as a function of position in the field is presented; for data taken through the blue broad band filter and at $\lambda = 7150\text{Å}$.

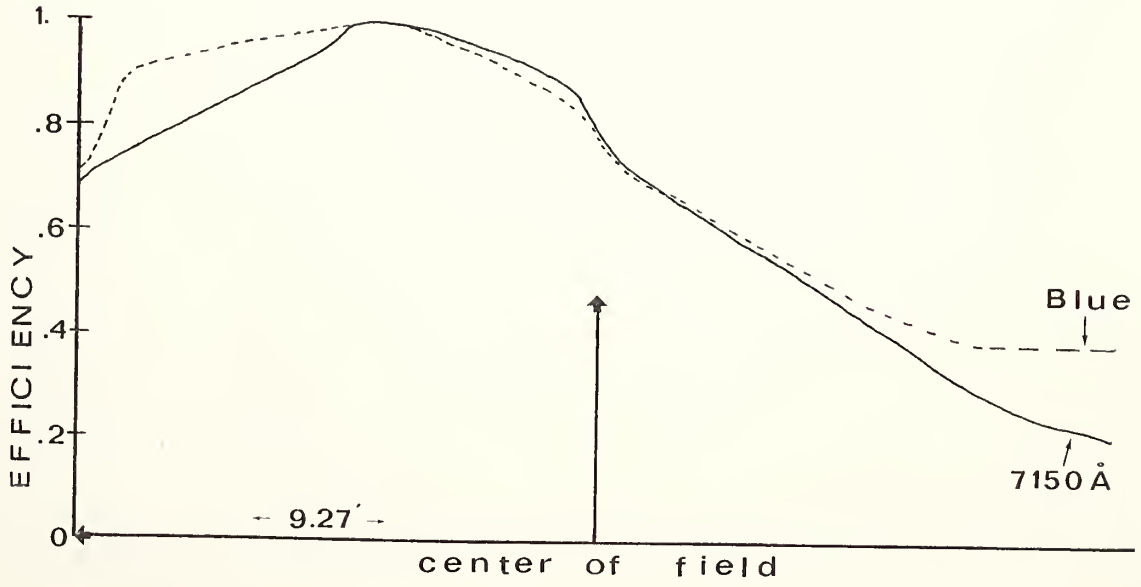
1.
.8
.6
.4
.2
0
EFFICIENCY
Blue
7150 Å
9.27′
center of field

Fig. 30. The observed data record (upper curve) along with its calculated "star corrected" record (middle curve), are shown for the S71 scan discussed in the text. The lower curve shows a typical 13 minute segment of the variation of the night sky observed through the λ7150Å filter. The blank sky curve has been shifted downward for simplicity.

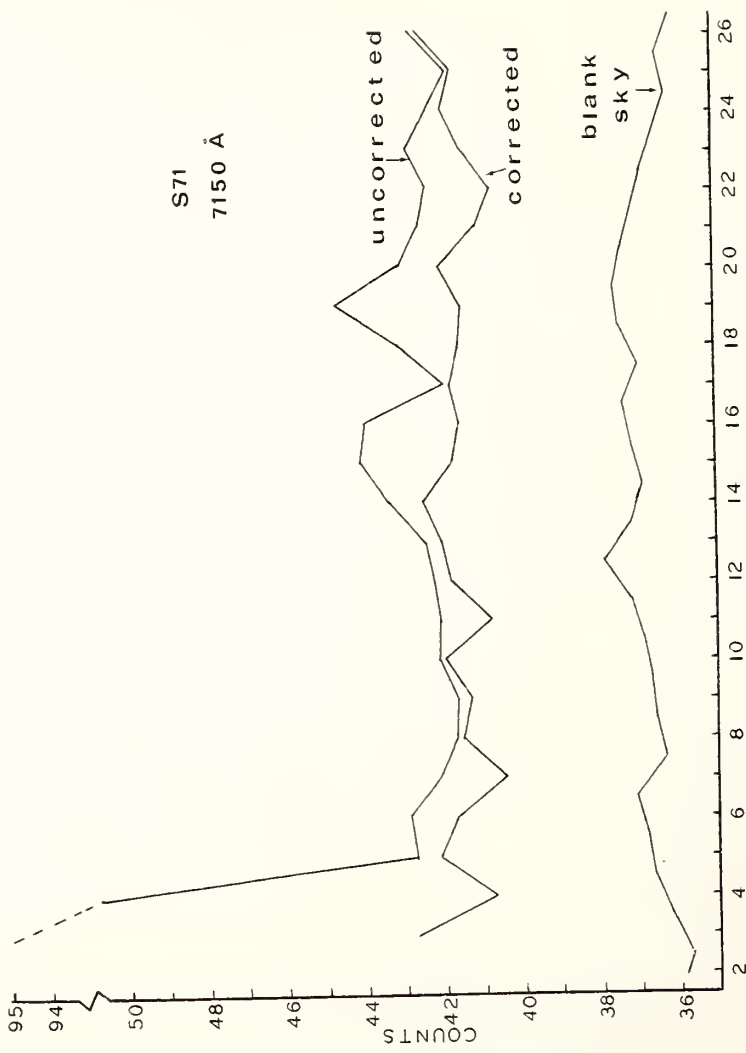
S71
7150 Å
uncorrected
corrected
blank
sky
COUNTS
FRAME NUMBER
95
94
50
48
46
44
42
40
38
36
2
4
6
8
10
12
14
16
18
20
22
24
26

the calculated record will still show the variations due to the night sky. The third curve plotted in Figure 30 shows a typical 13 minute segment of the variation of the night sky observed through the λ7150 Å filter. This curve does not represent the actual variation of the sky during this particular scan, but is shown only to give some idea of the typical variation encountered.

From Figure 30 one can see that the "star subtraction" process has worked exceedingly well. Consider frame three, in which the presence of the 6.9 magnitude star SA082554 has more than doubled the count rate. Whereas in the "star corrected" record the calculated amplitude for the sky, may at most be a percent or two higher than the value suggested by neighboring frames. Reduction of the Coma Cluster data suggests that on the average the "star subtraction" processes was accurate to 1.7 percent of the sky level predicted by adjacent frames. A partial explanation for the error in "star subtraction" can be found in Figure 20. From this figure we see that by using the composite star profile discussed in chapter II we are likely to underestimate the sky level by $\approx$1.5 percent. A second source of error could be inaccurate coordinates for one or more of the stars in the field. Figure 31 shows the percent change in the calculated sky amplitude for frame three, produced by introducing errors into the coordinates for SA082554. Where as the measured coordinates for stars in the field should be accurate to 0.4 arc seconds,

Fig. 31. The resulting error in the calculated mean sky level, produced by introducing errors into the coordinates of one of the stars in the field.

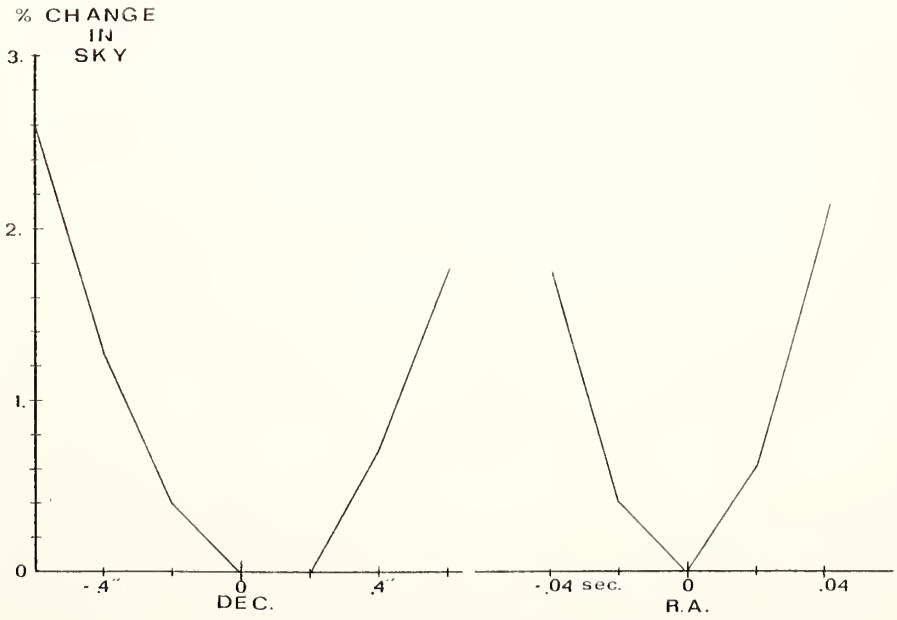
% CHANGE
IN
SKY
3.
2.
1.
0
-.4"
0
DEC.
.4"
-.04 sec.
0
R.A.
.04

it is difficult to say what fraction of the "star subtraction" error might in practice be due to inaccurate coordinates. Considering the photocathode problem discussed above and the inherent limitations placed on the star subtraction process by photon noise and scintillation, the results of rotation three are most encouraging.

The remaining frames of this scan are representative of the majority of Coma Cluster data in the magnitude range present in each frame. Again as can be seen in rotations 14 to 20, for those frames in which bright stars are present the star subtraction process has performed well. Frames 7 to 14 and 21 to 26 probably contain no stars brighter than magnitude 13, as judged from a cursory scan of a Palomar Sky Survey photograph of the region. As to be discussed later in this section the "star correction" for these frames should range from zero to a few percent, which is consistant with the calculated record.

Comparison of the calculated record with the observed night sky variation, shows the calculated record to be somewhat more "jagged". This "jaggedness" shows up primarily in frames where a bright star is in the field for only a short fraction of the time. As the star is in the field for less than one rotation of the chopper, little information has been gained on which to base a solution for the star's amplitude, and hence a poorer solution.

Whereas the "star subtraction" capabilities of the photometer can be discussed using any of the Coma Cluster scans, evaluation of its photometric accuracy requires a scan taken through the blue (broad band) filter.

Whereas the $\lambda 7150\text{Å}$ and $\lambda 8200\text{Å}$ data could be used for this test, the lack of R,I photometry for the area studied makes the use of the blue broad band data preferable.

For scans of the Coma Cluster taken in the blue, the number of stars with catalog UBV photometry is small. While at Kitt Peak observations were made of the Pleiades Cluster for a separate project. As these Pleiades scans have a number of stars with catalog UBV photometry in every frame, they are ideal for discussing the photometer's ability.

Figures 13 and 23 already discussed in chapter II are from one such 10 minute scan, taken through the blue broad band filter. Taking Figure 23 as an example, there were six stars brighter than 10th magnitude with known photoelectric B magnitude in the field. The solution for this ten minute scan showed that for the brighter stars in the field, the average error from the known photoelectric magnitudes was ≈ 0.1 magnitude. (The calculated magnitudes were obtained by normalizing to one of the stars in the field and are thus not corrected for any color terms). In frames where the

magnitude range was small and there are no bright stars (mag $\approx$ 6) present, the average error was 0.05 m. In frames where the magnitude range was as great as eight magnitudes, the solution for the fainter stars was very poor, the faintest stars even at times being given negative amplitudes in the solution.

Reduction of the Coma Cluster scans taken in the blue have shown that for the SAO stars, the calculated magnitude (the normalization now derived from the Pleiades data) came within $\approx$ 0.08 magnitude of their true photoelectric values. Here again, for the faintest stars (m = 16), the computed solutions attributed negative amplitudes to some of those stars. For the faint stars, the solution shows $\approx$ 50% positive and 50% negative amplitudes. This effect can be understood in terms of the observed count ratio as follows.

A typical frame of data taken at Kitt Peak has $\simeq 10^5$ counts, which means that photon noise limits us to $\simeq$0.3% photometry, or that stars contributing less than 300 counts per frame are lost to the noise. Scaling from the bright stars where photoelectric data is available, a 10th magnitude star would contribute $\approx 4 \times 10^3$ counts per frame, whereas a star fainter than 15th magnitude would contribute less than the 300 counts needed to be detected. Thus, the aforementioned problem of negative amplitudes in the solution for the faint stars seems to be understood. The average of $\approx$10

scans should then give us our goal of 0.1% photometry.

While the calculated and catalog B magnitudes show on the average agreement to a tenth of a magnitude, which is satisfactory for the present project, it is still quite poor when compared to standard photometric techniques. For example, the set up star for the reference scans SA082595 is calculated to have a magnitude of 7.69 compared to its catalog value of 7.61 (Blanco et al.), an error of 0.08 magnitude. An error of only 0.02 magnitude would be expected from Poisson noise alone. Whereas some of the error is most certainly due to the inaccurate transformation of the catalog magnitudes to the scale appropriate to the photometer, errors in the photocathode map and image shape will also contribute, the exact evaluation of the relative contributions being difficult to judge. Dennis (1979) has discussed the possibility of doing stellar photometry with this system. He finds there is actually a net disadvantage to multiplexing the stars onto the background, except for possibly the most crowded fields, if one is interested in only obtaining stellar magnitudes.

C H A P T E R V

RESULTS AND DISCUSSION

Reduced Scans

The actual data analysis was carried out in two parts. First the "star subtraction" procedure described in chapter II, and evaluated in chapter IV, was performed in those scans listed in Appendix I. Then, a correction for the variation in the sky level during the observation was applied to each "star corrected" scan.

Linear interpolation in time between the "reference region" sky levels before and after each scan was used to estimate the correction for each frame of data. Though this particular correction will remove slow variations in the sky level, shorter period variations must still be averaged out. These short period variations were found to be of the order of 0.7% of the mean sky level during one scan.

The scans of the nights of February 12-13, February 13-14, and February 15-16 were then averaged and filtered (using a three frame running mean) to produce one curve for each declination region. Before averaging, a careful check was made to see if the scans from any one night differed systematically from those of the other nights; no such effect was found.

The full set of reduced scans is presented in Figures 32 to 47. Each point on the plot represents a region 18.54 arc minutes (North-South) by 25.17 arc minutes (East-West). Scans are presented in order of decreasing declination.

The error bars shown for each observation, represent the standard error calculated from the internal consistancy of the three data points averaged together. The average uncertainty in the reduced scans is found to be 0.6%.

The uncertainty in the sky amplitude arises from two sources, counting statistics and uncorrected night sky variations. The uncertainty due to counting statistics is given by Dennis (1979) as,

$$a_o = (T(1+n/4))^{\frac{1}{2}} \qquad (16)$$

where T = total number of counts in the record and n the number of stars in the field. For a typical frame a_o = 0.65%. To this must be added quadratically 0.7% for the typical uncorrected night sky variations (see chapter IV, page 63), to give an estimated uncertainty of 0.96%, in a single frame of data. Finally the uncertainty should be reduced to 0.56% by averaging three scans. This is in excellent agreement with the actual observed value of 0.6%.

Individual Scans

Baseline

The baseline, at a distance of about one degree north

Fig. 32 to 47. The full set of reduced scans are presented in order of decreasing declination. For each scan, the sky amplitude as a function of right ascension (frame number) is plotted. The horizontal axis has been shifted to account for the differences in starting right ascension. The right ascension corresponding to the center of the Coma Cluster (RA=$12^{hr}57.4^{min}$DEC=$28^{o}15'$, 1950) is indicated on each plot by an arrow. In addition the number of stars corrected for (n), the photoelectric magnitudes (if known) for stars in the field and the number of bins the star was in the field are given at the top of each plot.

COUNTS
36
38
40
42
44
7150 Å
2
4
6
8
10
12
14
16
18
20
22
24
FRAME NUMBER
N61
n=19 8.02/246 10.20/304
n=17 10.78/400 10.20/600
n=15 10.78/600 10.20/600 11.09/558
n=17 10.78/600 10.20/157 11.09/600 10.77/311
n=16 11.09/364 10.77/600
n=19 9.86/516 10.77/172
n=20 9.86/70 10.25/402
n=21 10.25/600
n=16 10.25/600
n=20
n=24
n=24
n=21
n=15
n=12
n=12 8.93/480
n=16 8.93/600 11.21/591
n=19 8.93/600 11.21/600
n=13 11.21/463
n= 9
n=11
n=16
n=16

FIGURE 32

COUNTS
64
62
60
58
56
8200 Å
N61
FRAME NUMBER
2
4
6
8
10
12
14
16
18
20
22
24
26
n=19 8.02/246 10.20/304
n=17 10.78/400 10.20/600
n=15 10.78/600 10.20/600 11.09/558
n=17 10.78/600 10.20/157 11.09/600 10.77/311
n=16 11.09/364 10.77/600
n=19 9.86/516 10.77/172
n=20 9.86/70 10.25/402
n=21 10.25/600
n=16 10.25/600
n=20
n=24
n=24
n=21
n=15
n=12
n=12 8.93/480
n=16 8.93/600 11.21/591
n=19 8.93/600 11.21/600
n=13 11.21/463
n=9
n=11
n=16
n=16

FIGURE 33

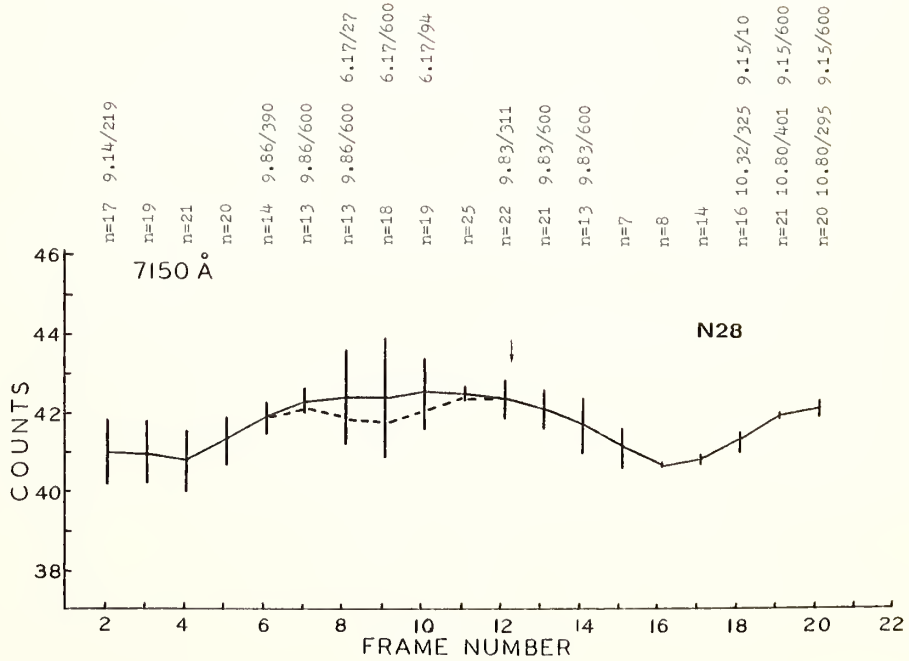
n=17 9.14/219
n=19
n=21
n=20
n=14 9.86/390
n=13 9.86/600
n=13 9.86/600 6.17/27
n=18 6.17/600
n=19 6.17/94
n=25
n=22 9.83/311
n=21 9.83/600
n=13 9.83/600
n=7
n=8
n=14
n=16 10.32/325 9.15/10
n=21 10.80/401 9.15/600
n=20 10.80/295 9.15/600
7150 Å
N28
COUNTS
46
44
42
40
38
2
4
6
8
10
12
14
16
18
20
22
FRAME NUMBER

FIGURE 34

64
62
60
58
COUNTS
8200 Å
N28
2
4
6
8
10
12
14
16
18
20
FRAME NUMBER
n=17 9.14/219
n=19
n=21
n=20
n=14 9.86/390
n=13 9.86/600
n=13 9.86/600 6.17/27
n=18 6.17/600
n=19 6.17/94
n=25
n=22 9.83/311
n=21 9.83/600
n=13 9.83/600
n=7
n=8
n=14
n=16 10.32/325 9.15/10
n=21 10.80/401 9.15/600
n=20 10.80/295 9.15/600

FIGURE 35

7150 Å
N15
COUNTS
FRAME NUMBER
46
44
42
40
38
2
4
6
8
10
12
14
16
18
20
n=27 8.41/190 11.32/216
n=28 11.32/574
n=16
n=12
n=15 6.97/179
n=23 6.97/600
n=25 6.97/600 8.16/318
n=25 6.97/ 54 8.16/600
n=21 8.16/600
n=22 8.16/158
n=18
n=16
n=19
n=18
n=23
n=27 10.71/473
n=28 10.71/600 9.34/236
n=27 10.71/ 25 9.34/600
n=20 9.34/ 3 9.89/34

FIGURE 36

n=27 11.16/192 9.88/218
n=26 11.68/503
n=18 11.68/600 10.29/598
n=14 11.68/337 10.29/515
n=10
n=13
n=15 12.70/365
n=12 12.70/600
n=15 7.62/439 12.70/301
n=21
n=26
n=27
n=23 11.90/313
n=23 11.90/600
n=20 11.90/308
n=18
n=17
n=16
n=9
S4
7150 Å
COUNTS
FRAME NUMBER
46
44
42
40
38
2
4
6
8
10
12
14
16
18
20

FIGURE 37

COUNTS
66
64
62
60
58
56
2
4
6
8
10
12
14
16
18
20
FRAME NUMBER
8200 Å
S4
n=27 11.16/192 9.88/218
n=26 11.68/503
n=18 11.68/600 10.29/592
n=14 11.68/337 10.29/515
n=10
n=13
n=15 12.70/365
n=12 12.70/600
n=15 7.62/439 12.70/301
n=21
n=26
n=27
n=23 11.90/313
n=23 11.90/600
n=20 11.90/308
n=18
n=17
n=16
n=9

FIGURE 38

n=27 11.16/192 9.88/218
n=26 11.68/503
n=18 11.68/600 10.29/592
n=14 11.68/337 10.29/515
n=10
n=13
n=15 12.70/365
n=12 12.70/600
n=15 7.62/439 12.70/301
n=21
n=26
n=27
n=23 11.90/313
n=23 11.90/600
n=20 11.90/308
n=18
n=17
n=16
n=9
BLUE
S4
COUNTS
58
56
54
52
2
4
6
8
10
12
14
16
18
20
FRAME NUMBER

FIGURE 39

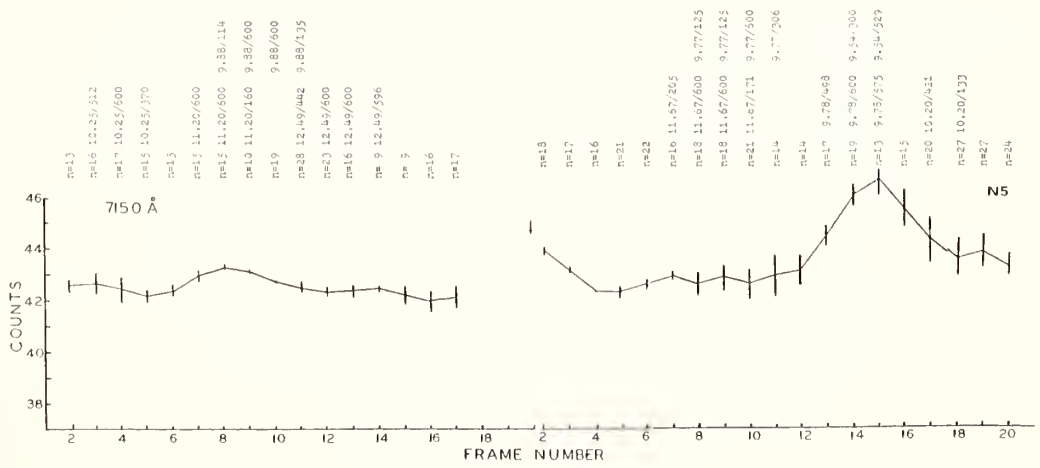

FIGURE 40

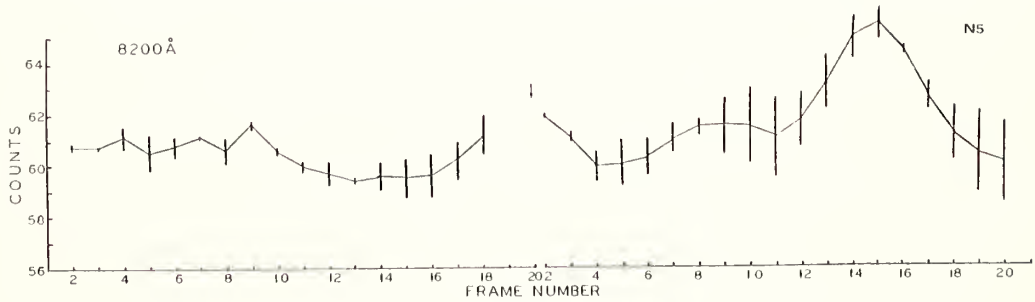
n=13
n=16 10.25/512
n=17 10.25/600
n=15 10.25/370
n=15
n=15 11.20/600
n=15 11.20/600 9.88/114
n=10 11.20/150 9.88/600
n=19 9.88/600
n=28 12.49/442 9.88/435
n=23 12.49/600
n=16 12.49/600
n= 9 12.49/596
n= 9
n=16
n=17
n=12
n=17
n=16
n=21
n=22
n=16 11.67/205
n=18 11.67/600 9.77/125
n=18 11.67/600 9.77/600
n=21 11.67/471 9.77/600
n=14 9.77/306
n=14
n=17 9.78/498
n=19 9.78/600 9.54/300
n=13 9.78/575 9.54/529
n=15
n=20 10.20/421
n=27 10.20/133
n=27
n=24
8200Å
N5
COUNTS
64
62
60
50
56
2
4
6
8
10
12
14
16
18
20
2
4
6
8
10
12
14
16
18
20
FRAME NUMBER

FIGURE 41

FIGURE 42

S13
7150 Å
COUNTS
FRAME NUMBER
46
44
42
40
38
2
4
6
8
10
12
14
16
18
20
n=26 7.84/176 9.71/14
n=16 9.71/600
n=15 9.71/600
n=13 9.71/462
n=14
n=14
n=14
n=12
n=5
n=13
n=16
n=18 11.33/197
n=11 11.33/600
n=15 11.33/600
n=19 11.33/268
n=18
n=17
n=16

FIGURE 43

S37
7150 Å
COUNTS
FRAME NUMBER
38
40
42
44
2
4
6
8
10
12
14
16
18
20
n=16
n=16
n=20
n=23
n=23
n=10
n=14 10.21/89
n=20 10.21/600 7.98/356
n=21 10.21/199 7.98/72
n=15 10.33/255
n=17 10.33/600
n=15 10.33/397
n=15 10.63/500 10.70/90
n=19 10.63/181 10.70/600
n=20 10.70/600
n=25 10.70/331
n=12
n=15
n=15

FIGURE 44

COUNTS
64
62
60
58
56
2
4
6
8
10
12
14
16
18
20
FRAME NUMBER
S37
8200 Å
n=16
n=16
n=20
n=23
n=23
n=23
n=10
n=14 10.21/89
n=20 10.21/600 7.98/356
n=21 10.21/199 7.98/72
n=15 10.33/255
n=17 10.33/600
n=15 10.33/397
n=15 10.63/500 10.70/90
n=19 10.63/181 10.70/600
n=20 10.70/600
n=25 10.70/331
n=12
n=15
n=15

FIGURE 45

COUNTS
FRAME NUMBER
7150 Å
S71
n=18 7.68/261 6.92/600
n=18 6.92/600
n=15 6.92/121
n=16 10.51/316
n=23 10.51/600
n=29
n=17
n=17
n=10
n= 9
n=10
n=14
n=22 10.70/415
n=18 10.70/600
n=17 10.70/600
n=14 10.36/17
n=18 11.33/567 10.36/600
n=21 11.33/600 10.36/600
n=17 11.33/484 10.36/241
n=12
n=21
n=18
n=13
n=14
n=19

FIGURE 46

COUNTS
64
62
60
58
8200 Å
2
4
6
8
10
12
14
16
18
20
22
24
26
FRAME NUMBER
S71
n=18 7.68/261 6.92/600
n=18 6.92/600
n=15 6.92/121
n=16 10.51/316
n=23 10.51/600
n=29
n=17
n=17
n=10
n= 9
n=10
n=14
n=22 10.70/415
n=18 10.70/600
n=17 10.70/588
n=14 10.36/17
n=18 11.33/567 10.36/600
n=21 11.33/600 10.36/600
n=17 11.33/484 10.36/241
n=12
n=21
n=18
n=13
n=14
n=19

FIGURE 47

or south of the Cluster center, is found to be the same. Figure 48 presents a comparison of the northernmost scan N61 with the southermost scan S71, for λ7150Å and λ8200Å respectively. As can be seen from Figure 48 the magnitude and spatial distribution of the surface brightness for a given color is very similar at distances of about one degree North and South of the Cluster center.

It is striking that the brightness gradient in the first nine frames of the λ8200Å data is so much steeper than the rest of the record, and is absent in the λ7150Å data. As the same stars are present in these frames for both colors, and the effect is not seen at λ7150Å, the surface brightness increase seen at λ8200Å can not be due to the star subtraction process. As will be discussed later this brightness gradient is found to coincide with the increase in brightness of the major axis of the Cluster at longer wavelengths.

Using King's (Rood et al., 1972) model for the Coma Cluster and parameters appropriate to this photometer, Cronin (1978) has calculated that at a distance of one degree from the Cluster center, the Cluster should contribute 0.16% of the night sky level. This value should fall to 0.10% at a radius of 78 arc minutes from the Cluster center. Thus it is expected that these particular scans should give an accurate indication of the baseline, the Cluster now having dropped below our level of detectability.

Fig. 48. A comparison of N61 with S71, for λ=7150A and λ8200A.

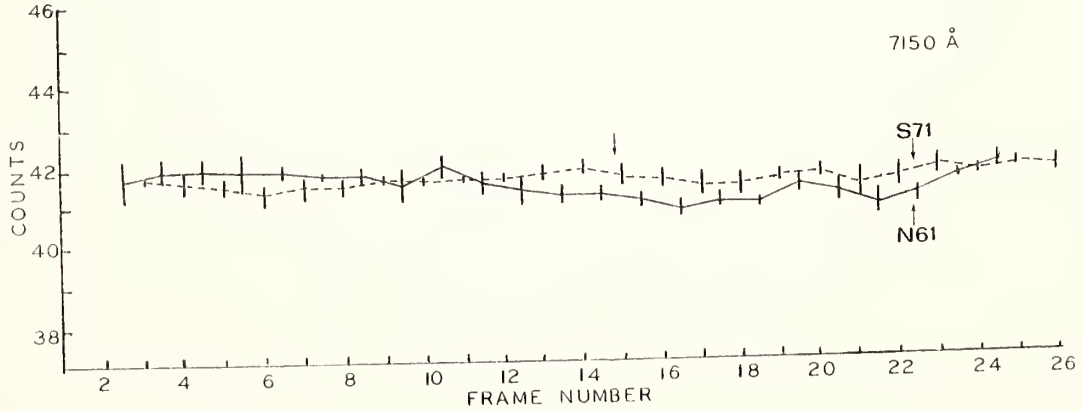
7150 Å
S71
N61
COUNTS
FRAME NUMBER
46
44
42
40
38
2
4
6
8
10
12
14
16
18
20
22
24
26

FIGURE 48

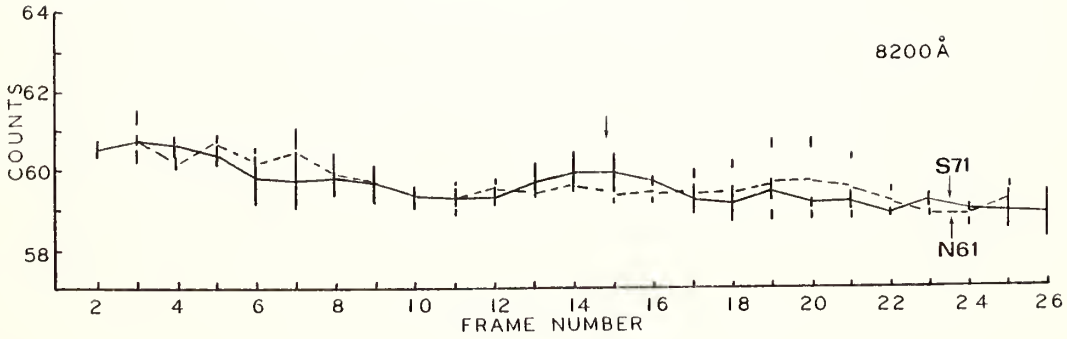
64
62
60
58
COUNTS
8200Å
S71
N61
2
4
6
8
10
12
14
16
18
20
22
24
26
FRAME NUMBER

FIGURE 48

Excess Surface Brightness

At a distance of 37 arc minutes south of the Cluster center, the Cluster is still not detectable, whereas at 28 arc minutes north of the center the Cluster is detected at a level two to three times the value predicted by Cronin (1978).

Closer to the Cluster center by about 0.5 degrees are the S37 and N28 scans. Figure 49 presents a comparison of S37 with S71, for each color. As can be seen from Figure 49 there is now a steep brightness gradient over at least the first seven frames of data, in both colors. Frame eleven marks the point of closest approach to the Cluster center, 37 arc minutes. At this distance the Cluster should contribute only 0.4% of the night sky level, and thus be undetectable.

At a distance of 28 arc minutes from the Cluster center, corresponding to frame twelve of the N28 scan, the Cluster is expected to appear at an amplitude 0.8% of the night sky level. Figure 50 presents a comparison of the N28, with the N61 scan for both colors. As can be seen from Figure 50, the surface brightness distribution is markedly different from south of the Cluster center (see Figure 49). Although frames six to twelve are contaminated by the presence of SA092589 (m_v=6.97, A5) and SA082596 (13.16' south of the center of the

Fig. 49. A comparison of S37 with S71 for both colors.

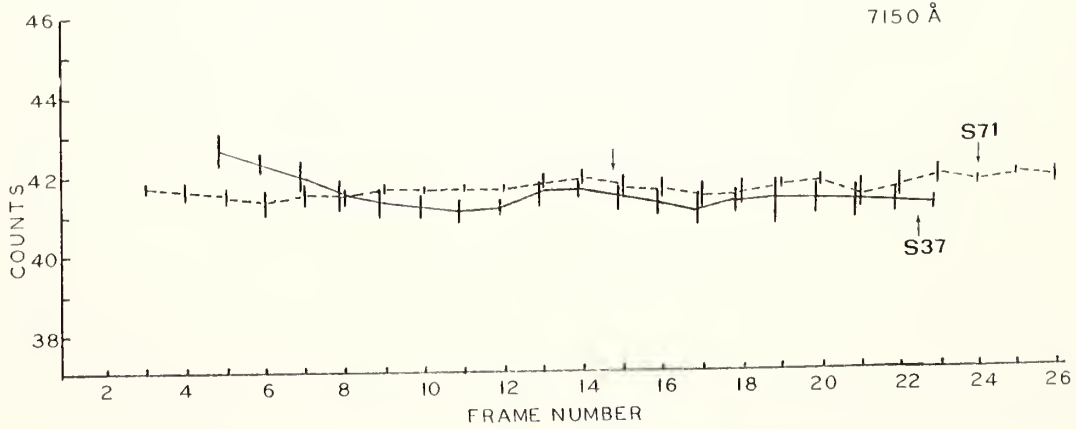
7150 Å
S71
S37
COUNTS
FRAME NUMBER
46
44
42
40
38
2
4
6
8
10
12
14
16
18
20
22
24
26

FIGURE 49

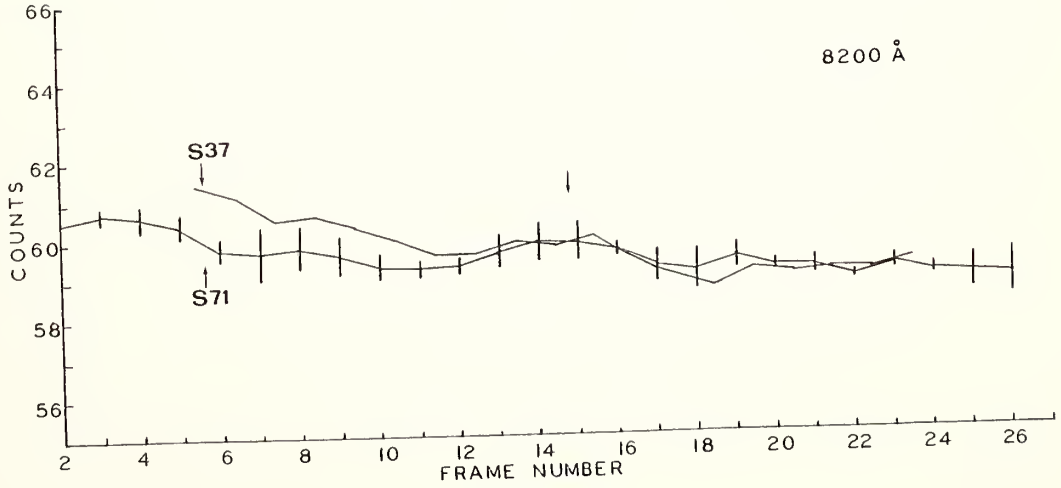
8200 Å
S37
S71
COUNTS
66
64
62
60
58
56
2
4
6
8
10
12
14
16
18
20
22
24
26
FRAME NUMBER

FIGURE 49

Fig. 50. A comparison of N28 with N61, for both colors.

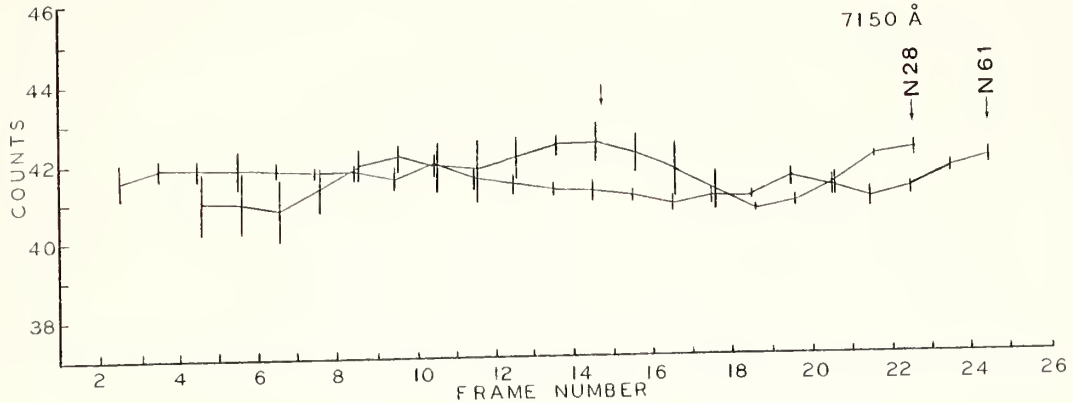
7150 Å
N28
N61
COUNTS
46
44
42
40
38
2
4
6
8
10
12
14
16
18
20
22
24
26
FRAME NUMBER

FIGURE 50

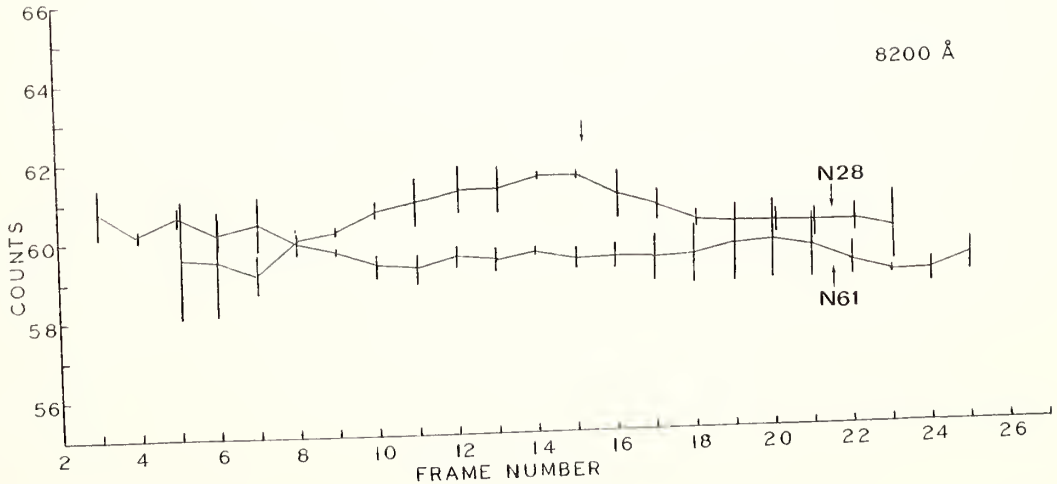
8200 Å
N28
N61
COUNTS
FRAME NUMBER
66
64
62
60
58
56
2
4
6
8
10
12
14
16
18
20
22
24
26

FIGURE 50

field, m_v=8.16 F5), calculations show that even in the worst possible cases, the entire increase in surface brightness cannot be due to contaminating starlight. The dashed line in Figure 50 shows the corrected record for this "worst case" calculation. As the surface brightness reaches a maximum during frames eleven and twelve, which correspond to the closest approach to the Cluster center, all of the increase is due to the Cluster. The measured amplitude is found to be some two to three times the predicted value (Cronin 1978). In the next section the validity of this somewhat unexpected result will be discussed in terms of the measured overall light distribution.

Major Axis

The steep brightness gradient observed in the first few frames of scans south of the Cluster center and the last few frames of scans north of the center, coincides with the major axis of the cluster.

As has been discussed earlier, the first few frames of the S37 show a steep brightness gradient, from Figure 50 one can see this effect is now showing up in the last few frames of N28. In Figure 51, S37 has been reflected through the origin and plotted with N28. As can be seen from this plot, both the baseline and the surface brightness gradient are almost equal, but are orientated in the opposite sense.

Fig. 51. A comparison of S37 after reflection through the origin with N28. A similar comparison for the λ8200Å data is not presented due to lack of data at S37.

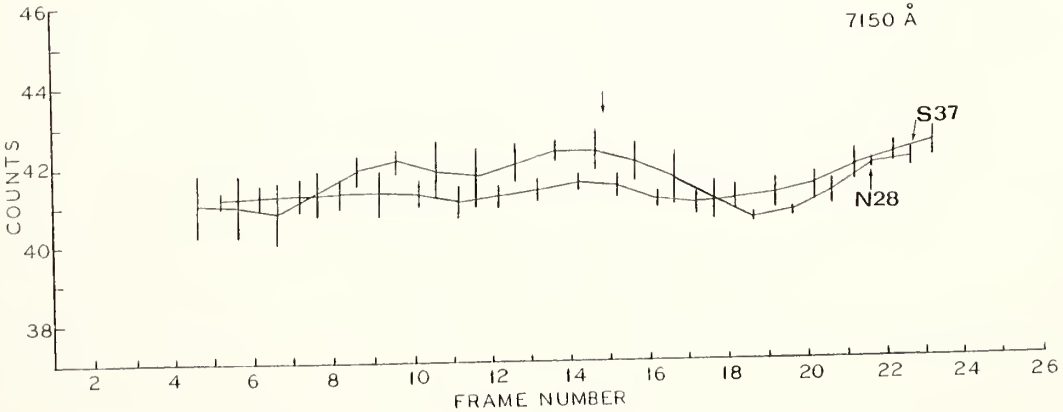
7150 Å
S37
N28
COUNTS
46
44
42
40
38
2
4
6
8
10
12
14
16
18
20
22
24
26
FRAME NUMBER

FIGURE 51

The orientation of the surface brightness gradient turns out to coincide with the major axis of the Cluster (Thompson and Gregory 1978), and will be taken up again in the next section.

Asymmetry in Central Scan

The scans taken closest to the cluster center are found to be asymmetric. An explanation for the asymmetry is given in terms of the elliptical shape of the Cluster.

Figure 52 a,b presents a comparison of the scan taken closest to the Cluster center with the northern and southern-most scan S71, N67 . It is immediately apparent that to the east of the Cluster the light distribution in the center scan has not yet dropped to the level of the baseline, whereas to the west of the Cluster, by frame two, the surface brightness has blended into the baseline suggested by N61 and S71. Though the baseline has not yet been reached east of the Cluster, the last few frames of N61 seem to indicate that the baseline, to the north-east of the Cluster is rising and approaching the level of the scan. This north-east, south-west asymmetry is consistent with scanning across the major axis of the Cluster.

It is interesting to consider whether the apparent asymmetry can be due to the star subtraction process. Four considerations rule out this possibility. First, the number and brightness of the stars in the field does not correlate with

Fig. 52a, b. A comparison of the S4 scan with both N61 and S71 for data taken at λ7150Å and λ8200Å.

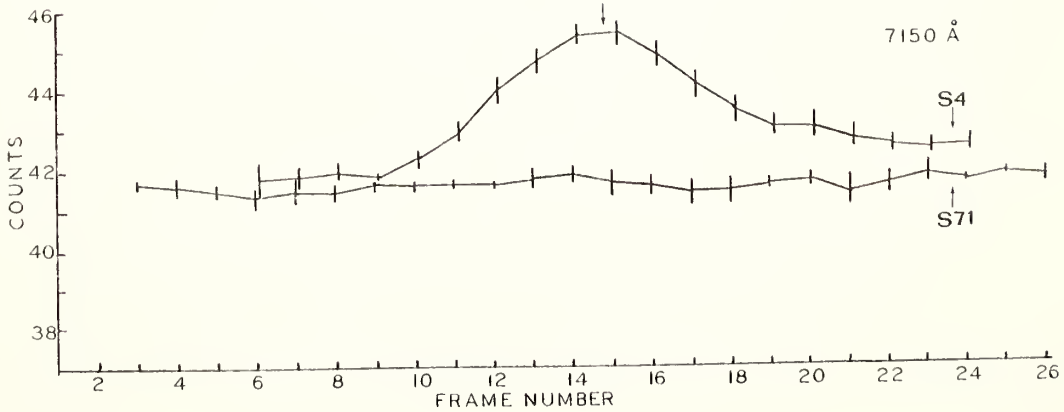
7150 Å
S4
S71
COUNTS
FRAME NUMBER
46
44
42
40
38
2
4
6
8
10
12
14
16
18
20
22
24
26

FIGURE 52a

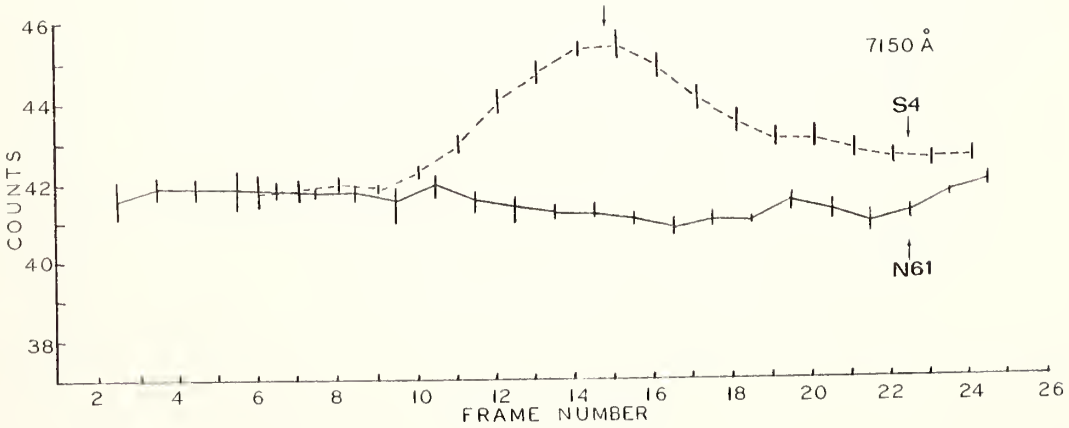
7150 Å
S4
N61
COUNTS
46
44
42
40
38
2
4
6
8
10
12
14
16
18
20
22
24
26
FRAME NUMBER

FIGURE 52a

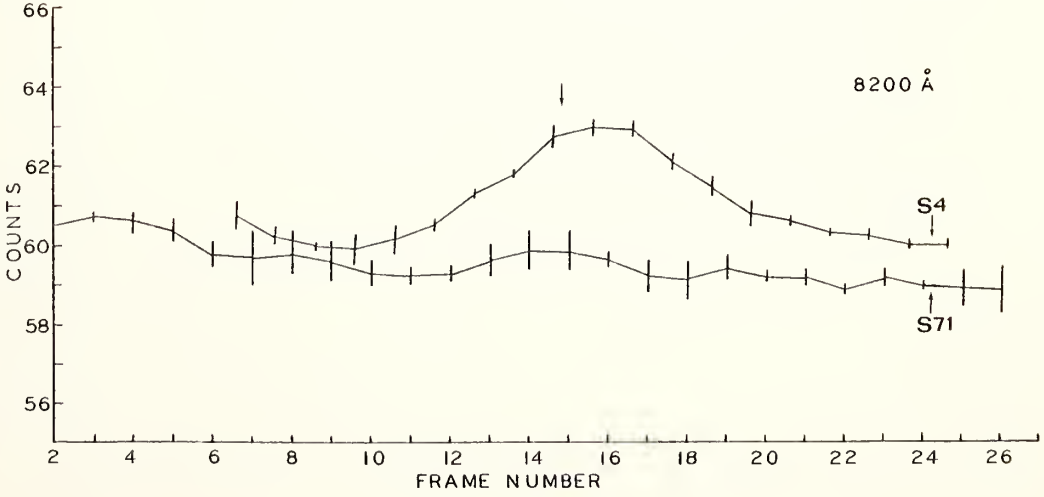
66
64
62
60
58
56
COUNTS
8200 Å
S4
S71
2
4
6
8
10
12
14
16
18
20
22
24
26
FRAME NUMBER

FIGURE 52b

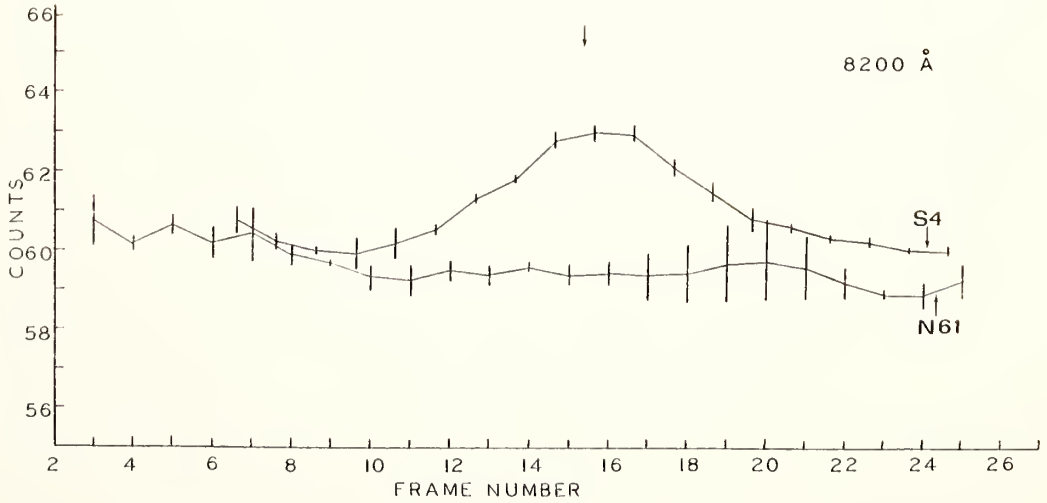
8200 Å
S4
N61
COUNTS
FRAME NUMBER
66
64
62
60
58
56
2
4
6
8
10
12
14
16
18
20
22
24
26

FIGURE 52b

the effect; second, as the effect is present in the early frames of the S37 scans and the latter frames of the N28 scans this rules out a systematic effect in the reduction procedure; third, the shape and magnitude of the gradient is about equal north and south of the Cluster, in data collected on a number of different nights; fourth, the effect correlates with the position angle of the major axis of the cluster; there is no doubt that the effect is real and is not an artifact of the star subtraction process.

Baseline East-West

The baseline in the east-west direction is higher than at the same distance north and south of the Cluster. This effect can be understood in terms of the major axis of the cluster being orientated almost east-west.

The long scans extending some two degrees from the cluster center, had been expected to supply information on the baseline in the east-west direction. However, as can be seen in Figures 37 to 39, the observed light distribution does not return to the "blank sky" level estimated from the N61 and S71 scans, but instead is found to be increasing away from the Cluster center. To the east of the Cluster center, contaminating starlight (estimated by the dashed curve) from SAO 82648 and SAO 82659 is certainly responsible for part of the increase, whereas to the west, no such contamination is

present. Again, this effect correlates with the major axis of the Cluster and will be discussed in the following section.

Blue Data

In the above discussion no mention has been made of the data taken through the blue filter. The detailed type of comparison made above is not possible for this data, as equipment failure prevented full coverage of the region.

Where data is available in all three colors, the general agreement is good. The only apparent difference is that, to the west of the Cluster center, the brightness distribution of the center blue scan blends into the background sooner than at λ7150Å and λ8200Å.

A similar effect can be seen in the baseline of deVaucouleurs and deVaucouleurs observations (1970, Figure 4). In Figure 53, a line of equivalent slope to that in deVauccouleurs' observation is plotted with the blue center region scan. As can be seen from Figure 53 both the direction and magnitude of the slope are about equal. When the difference in observing conditions are taken into account (location, telescope, relations to meridian and sunrise), the agreement in Figure 53 leaves little doubt that the feature is real.

The absence of extended data in the blue makes it impossible to say exactly how the overall light distribution differs between the blue and λ7150Å and λ8200Å. The differ-

Fig. 53. A line of equivalent slope to that in deVaucouleurs' observations is plotted with the blue center region scan.

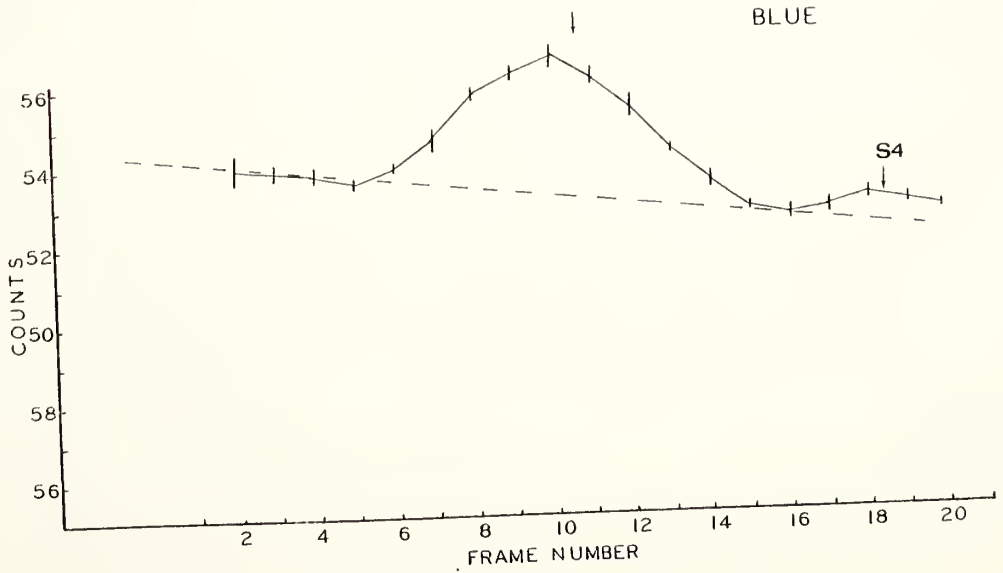
BLUE
S4
56
54
52
50
58
56
COUNTS
2
4
6
8
10
12
14
16
18
20
FRAME NUMBER

FIGURE 53

ences in the observing conditions mentioned above rule out the Zodical Light or scattered moonlight as the cause, but high galactic latitude reflection nebulosity can not be ruled out. The absence of the effect at λ7150 Å and λ8200 Å is consistant with reflection nebulosity being the cause, though more observations are needed to be sure.

Overall Light Distribution

The individual scans discussed in the previous section were combined to produce the "pin" maps presented in Figures 54 to 56. Before discussing these maps it is important to state that they measure the total light, and are at such low spatial resolution that direct comparison with previous work is not possible. The shaded region of Figure 54 marks the region investigated photoelectrically by Melnick, White and Hoessel (1977); all previous photometric work on the Cluster within this region.

The most obvious feature of the light distribution is its orientation from north-east to south-west. Bahcall (1973), Schipper and King (1973), and Thompson and Gregory (1978) have discussed a similar asymmetry found in galaxy counts of the Coma Cluster. Within a radial distance of 0.5° from the center of the Cluster, the position angle of the major axis (measured north through east) is found to lie almost east-west, but decreases to 67° for the interval of 1.5° to 3° from the Cluster center (Table 1, Thompson and Gregory (1978).

Fig. 54. The shaded region marks the region investigated photoelectrically by Melnick, White and Hoessel (1977).

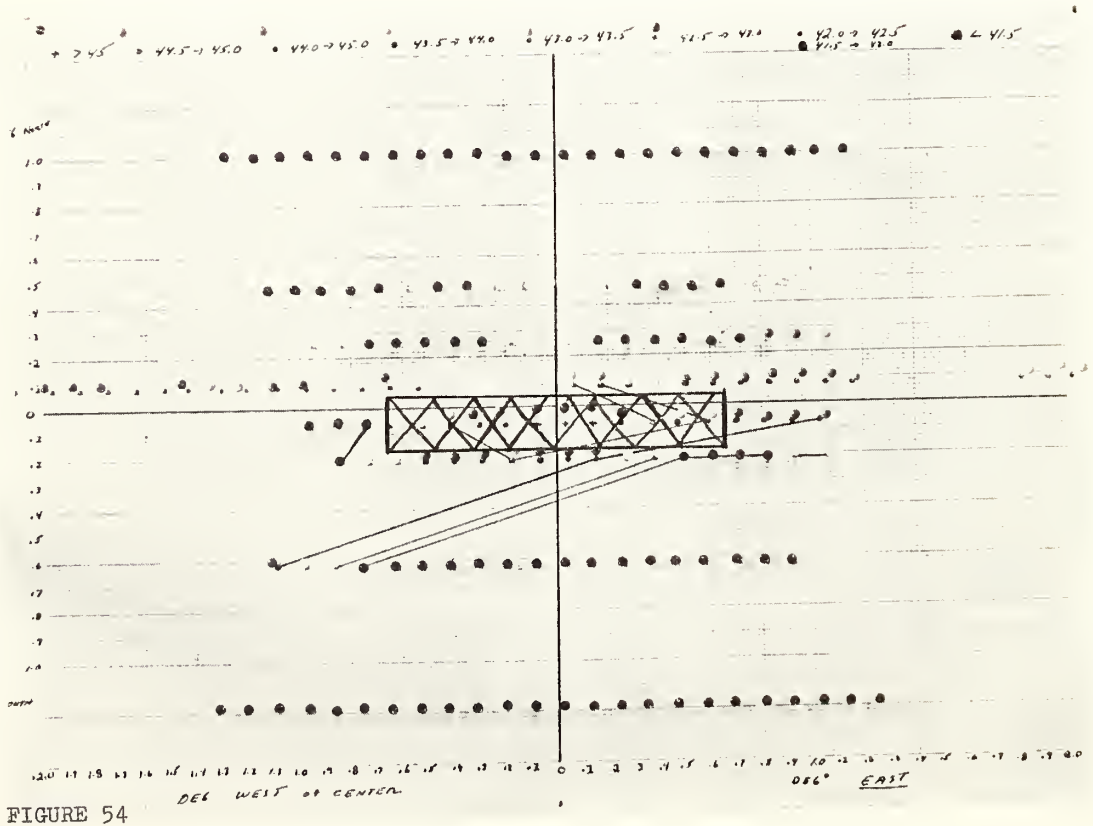

FIGURE 54

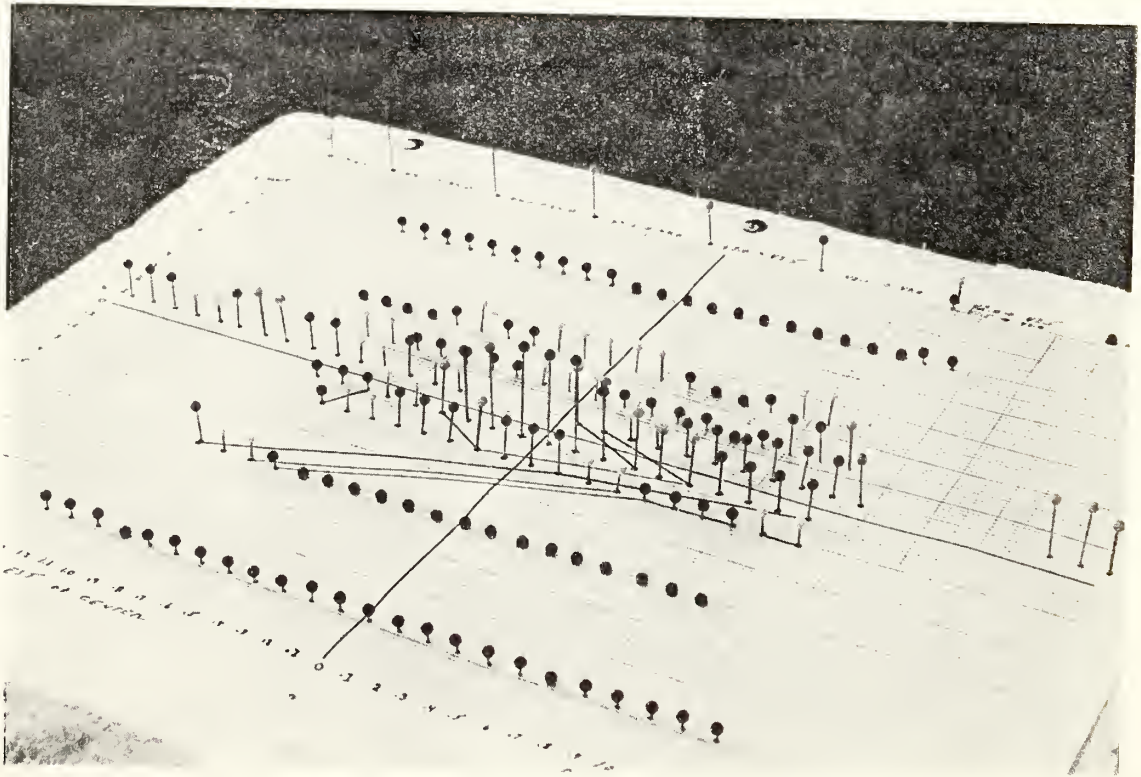

FIGURE 55

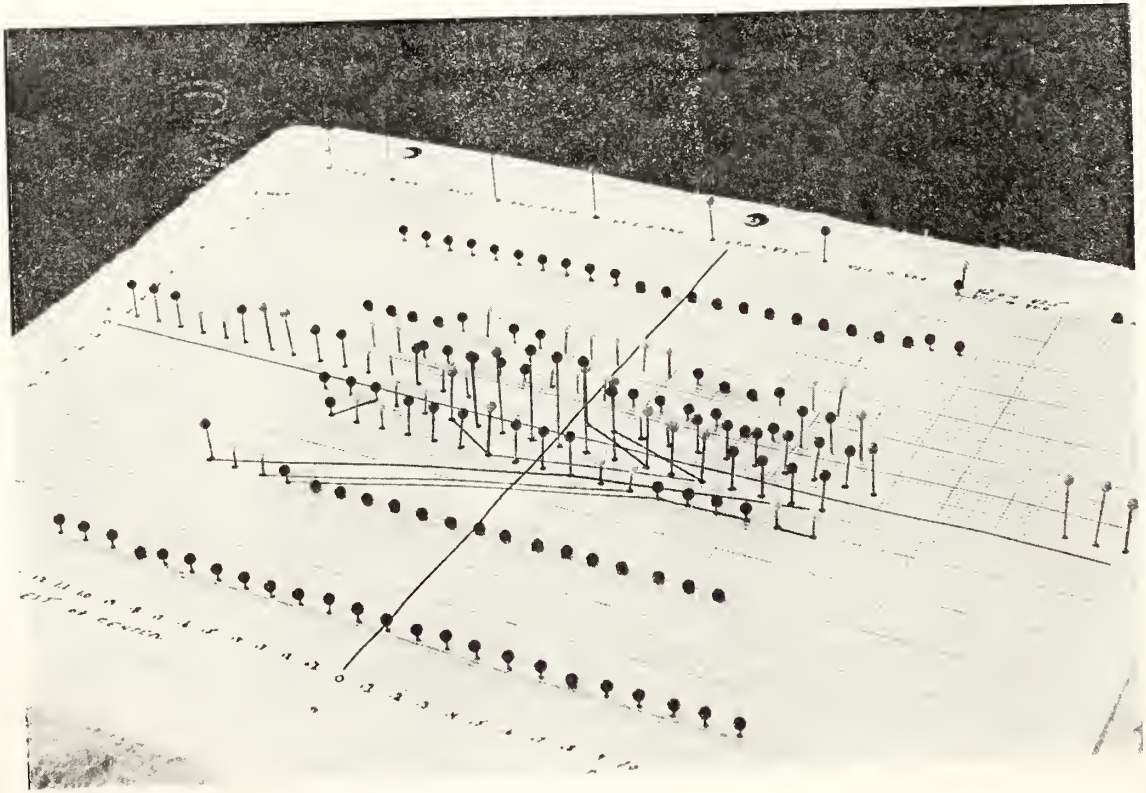

FIGURE 55

Fig. 56. A view along the major axis of the light distribution at λ7150Å (i.e. looking southwest-northeast).

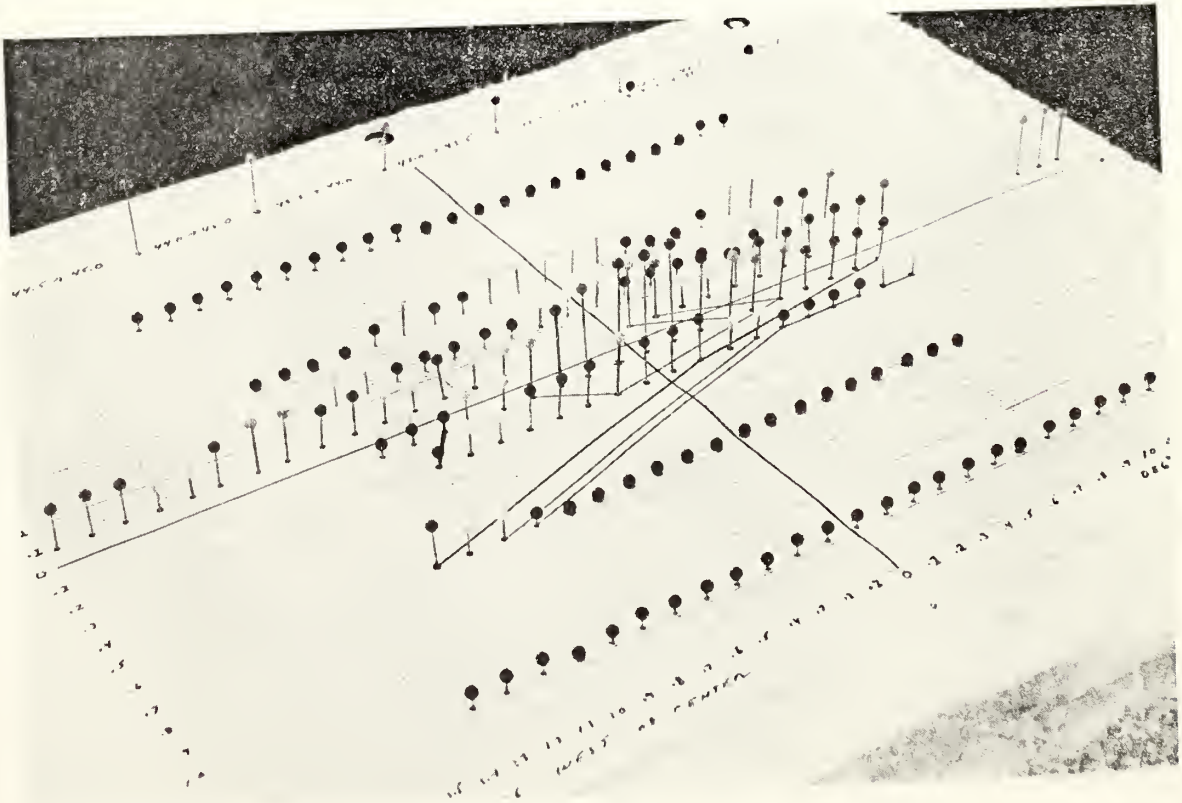

FIGURE 56

Fig. 57. A view looking southeast-northwest of the λ8200Å model.

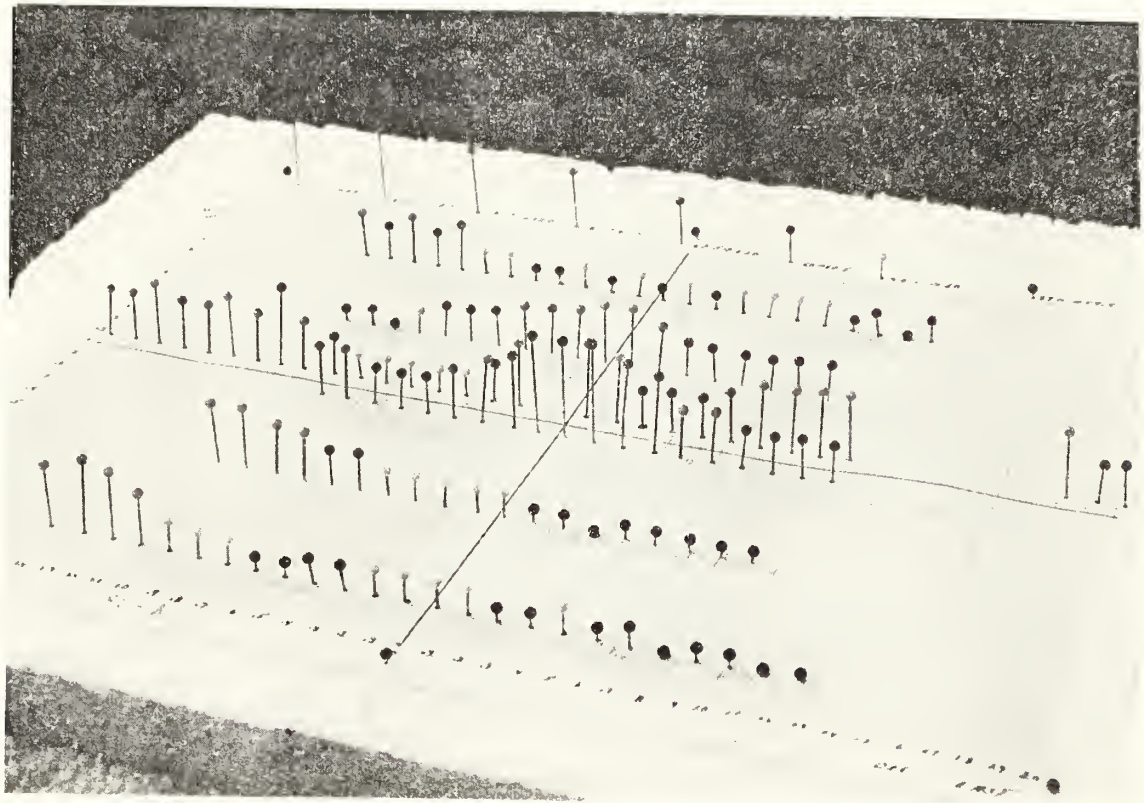

FIGURE 57

Fig. 58. A view along the major axis of the light distribution (i.e. looking southwest-northeast).

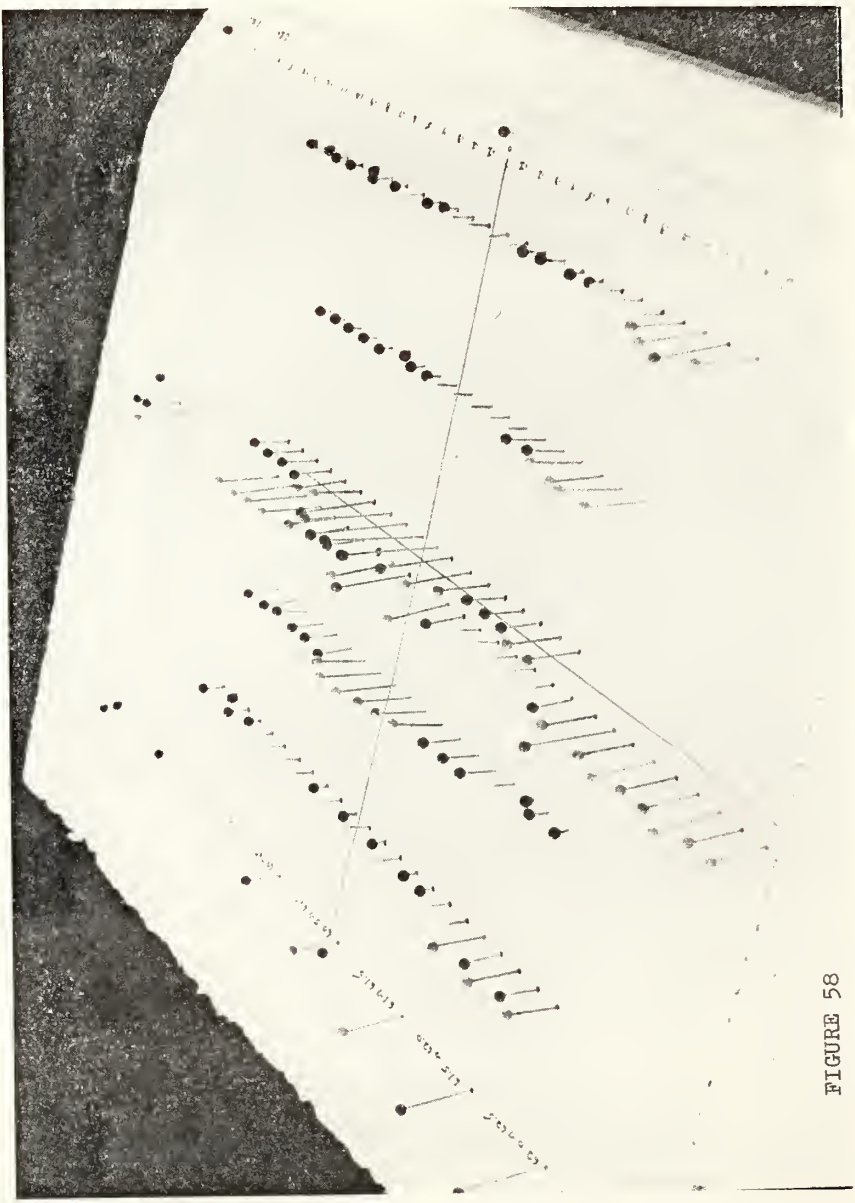

FIGURE 58

Fig. 59. A view looking southeast-northwest of the blue broad band model.

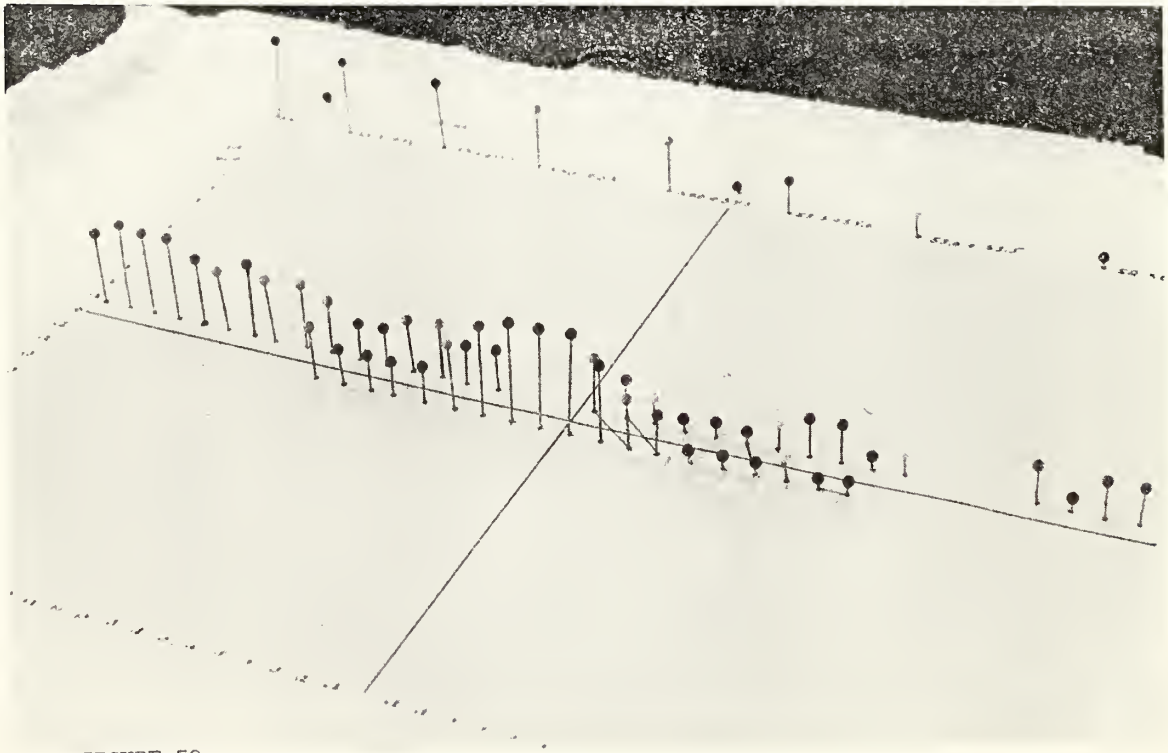

FIGURE 59

Similarly, the axis ratio decreases from approximately 0.84 to 0.55 over this range, indicating that at lower isoplets the distribution is more elliptical.

Overlaid on Figures 54 and 56 is a dashed line corresponding to a position angle of 67 degrees. Inspection of Figures 54 and 56 suggest that indeed the major axis of the light distribution is consistent with a position angle of 76 to 90 degrees, and that the overall light distribution is elliptical in shape.

To perform a quantitative test for ellipticity (Schipper and King 1978) on the data presented in Figures 54 to 56 is not possible. The absence of data over parts of the record, especially along the probable major axis, would make interpretation of any such test questionable.

A number of other features associated with the Cluster show an elliptical distribution. Gorenstein, Fabrieant, Topka and Harndin (1979) have reported a marginal detection of ellipticity in the Soft X-ray structure of the Cluster. They find that, over the region 10' to 25' from the Cluster center, the position angle of the major axis is approximately east-west and has an axial ratio of 0.83. An extension of the intergalactic surface brightness to the south-west of the Cluster center has been reported by Welch and Sastry (1971) and Kormendy and Bahcall (1974); Melnick, White, and Hoessel

(1977) report that this feature is somewhat redder than the Cluster center. Whereas this feature is present on a much smaller scale than the total light distribution presented in Figures 54 to 59, it is interesting to note that this feature lies along the same axis. To the extent that galaxy counts can be used to trace the total gravitational potential of the Cluster, it is not surprising that the total light distribution presented in Figures 54 to 56, as well as the intergalactic surface brightness, and the Soft X-ray structure, all follow the galaxy distribution and in turn reflects its ellipticity.

What is surprising is that the surface brightness along the major axis can be traced out so far and is so constant at large distances from the Cluster center. A comparison of Figures 54 and 55 shows that at 7150 Å the south-west extension of the major axis is no longer visible at the distance corresponding to the S71 scans, while at 8200 Å the feature is clearly visible and broader. Based on the limited data available, it would thus seem, as one moves to greater radii, that the light distribution is redder, i.e. at longer wavelengths it is broader.

As discussed in the previous section, it is doubtful that the observed light distribution is an artifact of the star subtraction process. We can rule out the Zodiacal Light and high galactic latitude reflection nebulosity as the source of

the effect by the following argument. The measured (R-I) of 0.47 magnitude along the east-west extension of the light distribution is redder than that of the sun (R-I) = 0.29 (Allen 1976), the Zodiacal Light which should have an (R-I) index bluer than the sun can be ruled out as producing the effect. Regions of reflection nebulosity at high galactic latitudes have been reported by Sandage (1976). An inspection of the Palomar Print of this area shows no apparent nebulosity, and no mention of reflection nebulosity in the region can be found in the literature. Here again the observed (R-I) index appears to be too red to be produced by reflection nebulosity illuminated by light from the galactic plane. Light from such nebulosities would be expected to be bluer than the illuminating light of the galactic plane, about spectral class (A0), (Arny 1979) and hence is already bluer than the Zodiacal Light previously ruled out hence.

Comparison with the Galaxy Distribution

A comparison of the overall light distribution with galaxy counts for the cluster shows good agreement.

Figure 60 is a contour map of galaxy counts in the region of the Coma Cluster, this figure is reproduced from Figure Shane and Wirtannen (1954). Comparing this figure with Figures 54 and 55, one can see that the overall agreement of the measured light distribution and galaxy counts is quite close. From the galaxy counts presented in Figure 60 there

Fig. 60. Contour map of galaxy counts from Shane and Wirtannen (1954).

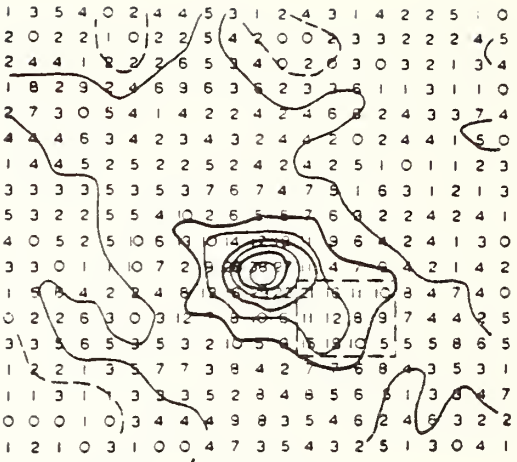

FIGURE 60

Reproduced from Shane and Wirtanen(1954)

is apparently a local increase in the number of galaxies about 0.5 degrees north of the Cluster center. This local increase in the number of galaxies coincides with the excess light present in frames twelve to sixteen of the N28 scans and probably accounts for the difference between the calculation herein described and the one based on Rood's model.

The Cluster Luminosity and Mass-to-Light Ratio

The determination of a total cluster luminosity and mass-to-light ratio depends critically on the mean sky level subtracted from the observations. In the present investigation we have searched systematically away from the Cluster center, to determine this baseline. As discussed in the previous section, the observed light distribution was found to have an elliptical shape, and along the major axis, the measured surface brightness has not yet dropped to a consistant baseline. In Table II, values for the total night sky brightness, adopted for the baseline are given. The values presented in this table for λ7150 Å and λ8200 Å are based on a straight mean of sky value taken from scans N61, S71, N28, and S37. Only those frames which were at least one degree away from the Cluster center, and at the same time away from the major axis of the Cluster, were considered (regions used are indicated on the scans presented earlier in the chapter). The standard error for each sky amplitude is given in Table II.

TABLE II

The surface brightness unit is one 10^m star per square degree (= S_{10}) or μ in mag/arc sec^2

COLOR	ADOPTED BASELINE		
	Amplitude	S_{10}	μ
Blue	52.63 ± 0.24	126	22.53
λ7150 Å	41.00 ± 0.28	413	21.24
λ8200 Å	58.99 ± 0.23	737	20.61

The minimum surface brightness of 22.53 magnitude arc seconds^{-2} for the blue observations is in excellent agreement with deVaucouleurs and deVaucouleurs (1970) value of 22.29 magnitude arc seconds^{-2}. Whereas this agreement must be in part fortuitous, the airglow component being so variable, it does serve as a check on the calibration procedure. As discussed in the previous section, both the S4 and the N5 scans lie along the major axis of the light distribution. Thus, the adopted baseline for the blue data is too high if the light distribution in the blue mimics the ones at 7150 Å and 8200 Å.

Table III presents the measured total luminosity within varying radii of the cluster center. These values are based on a Hubble constant H = 75 km/sec/Mpc (this value being chosen to ensure easy comparison with the work of Rood et al. 1976) and a mean radial velocity for the Coma Cluster of 6888 km/sec. (Rood et al. 1972). For these parameters the distance to the Coma Cluster is 92 Mpc (m - M = 34.8), and one arc minute corresponds to 26.7 Kpc. In addition we have taken M_V = 4.83, (B - V) = 0.65, (V - R) = 0.52 and (V - I) = 0.81 for the sun, when necessary in the calculations. The ellipticity of the Cluster has been taken into account, in calculating the last two entries in Table III. Where appropriate, a range of magnitudes and luminosities (calculated using maximum and minimum values for the surface brightness at large distances along the major axis) are given.

TABLE III

TOTAL LUMINOSITY

RADIUS	λ7150 Å		λ8200 Å		Blue	
	MT	L(L⊙)	MT	L(L⊙)	MT	L(L⊙)
9'	9.3	8.4×10^{11}	9.2	7.0×10^{11}	11.4	4×10^{11}
30'	6.8	8.6×10^{12}	6.62	7.4×10^{12}	8.7	4.38×10^{12}
60' x 36'	5.7	2.3×10^{13}	5.8-5.5	$1.6\text{-}2.1 \times 10^{13}$		
100' x 36'	5.5-5.3	$2.7\text{-}3.2 \times 10^{13}$	5.4-5.0	$3.3\text{-}2.3 \times 10^{13}$		

Note: The luminosities presented in this table were calculated by assuming an ellipse of uniform surface brightness for the outer region of the Cluster (where appropriate) adding on a graphic determination of the luminosity for the center region. The calibration for conversion from counts on the photometer system to standard magnitude is supplied by the stars in the field (see chapter IV).

Following the method described by Rood et al. (1972), a mass-to-light ratio for the Coma Cluster can be obtained from the data presented in Table III. Using the parameters given by Rood et al., (1972) for a King model of the Coma Cluster, and the measured luminosity within 9 arc minutes of the cluster center given in Table III, a mass-to-light ratio $(M/L)\lambda 7150=230$, $(M/L)\lambda 8200 = 307$ is calculated. These values are consistent with those of Abell (1977) (when corrected to this Hubble Constant) and Rood et al. (1972). To date, calculations of the mass-to-light ratio of the Coma Cluster have assumed spherical symmetry for the virial mass determination of the Cluster. While a determination of a mass-to-light ratio based on a virial mass determined by using the observed ellipticity of the cluster, and the luminosity presented in Table III is desirable, such a virial mass determination would be a separate project in itself as no values exist in the literature.

What is interesting is that the luminosity at $\lambda 7150$ Å and $\lambda 8200$ Å presented in Table III for an elliptical area (100' x 36') is 3 to 4 times the visual luminosity given by Rood et al., (1972) for a circular area of radius 100'. Thus the observed luminosity is in the right direction to lower the mass-to-light ratio of the cluster, though the exact amount will depending on a new calculation of the virial mass taking into account the Cluster ellipticity.

Table IV gives measured (R-I) indices as a function of position along the major axis to the south-west of the Cluster center. While exact error bars are difficult to determine, there does seem to be an increase in (R-I) index beyond $\simeq 1.5^{\circ}$ from the Cluster center. As mentioned earlier this effect can also be seen, by comparing the extent and magnitude of brightness gradient in the S71 and S37 scans. This effect, indicates that at greater distances from the Cluster center, the light distribution is redder and the integrated spectral class is closer to (K1V-K7V) than the G2V or later (R-I) = 0.29 indicated by the total measured light distribution.

A secondary maximum in the galaxy distribution of the Coma Cluster has been reported by Omer, Page, and Wilson (1965), and Thompson and Gregory (1978). This secondary maximum occurs at a distance of about 1.4 degrees from the Cluster center, which would correlate with the increase in the (R-I) index discussed above. A possible explanation for the secondary maximum in the galaxy distribution in terms of a remnant shell of galaxies has been given by Valtonen and Byrd (1979). It would thus seem that the change in the color index of the Cluster at $r = 1.5^{\circ}$ is correlated with a change in the overall dynamics of the cluster.

TABLE IV

(R-I) vs DISTANCE ALONG THE MAJOR AXIS

RADIUS	(R-I)
$.5^0$	0.12
1.0	0.23
1.5	0.56
2.0	0.47

C H A P T E R VI

CONCLUSIONS

Photoelectric observations of the Coma Cluster, extending some two degrees from the Cluster center, have been carried out using the "multiplexing night sky photometer". While able to accurately correct for contaminating starlight, the overall photometric utility of the photometer is limited by night sky variations.

The total light distribution of the Coma Cluster at $\lambda 7150$ Å and $\lambda 8200$ Å is found to have an elliptical shape, the position angle of the major axis lying between 67° to 90°. The observed light distribution is found to correlate well with the galaxy distribution. Along the major axis of the Cluster, the luminosity can be traced out over two degrees from the Cluster center. A mass-to-light ratio of $(230)_{7150}$, $(307)_{8200}$ is found using a King model for the central region of the cluster. Marginal evidence exists that at distances greater than 1.5° from the Cluster center along the major axis, the cluster is redder, indicating an integrated spectra of (K1V - K7V).

BIBLIOGRAPHY

Abell, G.O. 1958, Ap. J. Suppl. 3, 211.

_____. 1962, in Problems of Extra-Galactic Research, ed. G.C. McVittie (New York: Macmillan Co.), p. 213.

_____. 1977, Ap. J. 213, 327.

Allen, C.W. 1976, Astrophysical Quantities (The Athlone Press, University of London, London, England).

Arny, T. 1979, Private Communication.

Bahcall, N. 1973, Ap. J. 183, 783.

Broadfoot, A.L., and Kendall, K.R. 1978, JGR, Sp, 73, 426.

Blanco, V.M., Demers, S., Douglass, G.G. and Fitzgerald, M.P., PHOTOELECTRIC CATALOGUE (United States Naval Observatory, second series, Vol XXI.

Cronin, P. (unpublished).

Dennis, T.R. 1974, BAAS 6, 451.

_____. 1975, (unpublished).

_____. 1979, (in press).

Fernie, J.D. 1974, PASP 86, 836.

Gorrenstein, P., Fabricant, D., Topka, K., and Harnden, F.R., Jr. 1977, Ap. J. (Letter), 216, L95.

Gunn, J.E., Melnick 1975, BAAS 1, 412.

Haschick, A.D., and Burke, B.F. 1975, Ap. J. (Letters) 200, L137.

Heygi, D.J. and Gerber, G.L. 1977, Ap. J. (Letters) 218, L7.

Kormendy, J., and Bahcall, J.N. 1974, A.J. 79, 671.

King, I.R. 1971, PASP 89, 120.

King, I.R., and Raff, M.I. 1977, PASP 89, 120.

Konig, A. 1933, Handbruck der Astrophysik, Part 1, Vol. 1 Chapter 6.

Krum, N., and Saltpeter, E.E. 1977, Astr. and Ap. 56, 465.

Lecar, M. 1975 "Dynamical Friction in the Coma Cluster", in IAU Symposium No. 69, Dynamics of Stellar Systems, A. Hayli, ed., p. 161.

Mattila, K. 1977, Astr. and Ap. 60, 425.

Melnick, J., White, S.D.M., and Hoessel, J. 1977, MNRAS 180, 207.

Mould, J.R. 1976, Astr. and Ap. 48, 443.

Omer, G.C., Jr., Page, T.L., and Wilson, A.G. 1965, A.J. 70, 440.

Ostriker, J.O., and Peebles, P.J. 1973, Ap. J. 186, 467.

Roach, R.E., and Gordon, J.L. 1973, The Light of the night Sky (D. Reidel Publishing Company, Holland).

Roberts, M.S., and Rots, A.H. 1973, Astr. and Ap. 26, 483.

Rood, H.J., Page, T.L., Kintner, E.C., and King, I.R. 1972, Ap. J. 175, 627.

Sandage, A. 1976, A.J. 81, 954.

Schipper, L., and King, I.R. 1978, Ap. J. 220, 798.

Shane, C.D. and Wirtanen, C.A. 1954, A.J. 59, 285.

Thompson, L.A. and Gregory, S.A. 1978, Ap. J. 220, 809.

Thuan, T.X., Kormendy, J. 1977, PASP 89, 466.

Thuan, T.X., Gunn, J.E. 1976, PASP 88, 528.

Valtonen, M.J., and Byrd, G.G. 1979, Ap. J. 230, 655.

Vaucouleurs, G. de 1960, Ap. J. 131, 585.

Vaucouleurs, G. de, and Vaucouleurs, A. de 1970, Ap. J. (Letters) 5, 219.

Welch, G.A., and Sastry, G.N. 1971, Ap. J. (Letters) 169, L3.

_____. 1972, Ibid. 171, L81.

White, S.D.M. 1976A, MNRAS 174, 19.

_____.1976 B, MNRAS 177, 717.

_____.1977, MNRAS 179, 33.

Zissel, R.E. 1973, Ph.D. dissertation (University of Virginia).

Zwicky, F. 1951, PASP 63, 61.

Zwicky, F., and Herzog, E. 1963, Catalogue of Galaxies and Clusters of Galaxies, Vol. 2 (Pasadena: California Institute of Technology), p. 318.

APPENDIX 1

OBSERVING LOGS

O B S E R V I N G L O G

7150 Å DATA

FEBRUARY 12, 13, 1977

SCAN	COUNTS IN REFERENCE REGION	Δ C	% CHANGE	LOCAL	SIDERAL	TIME
REF-1	23054	3152	.158	10 hours	07 minutes	12 seconds
S4				10 hours	13 minutes	
REF-2	22382	2480	.125	10 hours	27 minutes	30 seconds
N15				10 hours	30 minutes	
REF-3	22232	2330	.117	10 hours	43 minutes	53 seconds
S13				10 hours	48 minutes	20 seconds
REF-4	21919	2017	.101	11 hours	0 minutes	5 seconds
S4				11 hours	4 minutes	35 seconds
REF-5	20718	816	.041	11 hours	18 minutes	16 seconds
N15				11 hours	22 minutes	12.6 seconds
REF-6	21044	1142	.057	11 hours	34 minutes	39 seconds
S13				11 hours	41 minutes	
REF-7	19902	—	—	11 hours	54 minutes	12 seconds
S 4						
REF-8	20152	250	.013	12 hours	9 minutes	48 seconds
N15				12 hours	13 minutes	17.8 seconds
REF-9	21110	1208	.061	12 hours	25 minutes	41 seconds
S13				12 hours	27 minutes	25 seconds
REF-10	22112	2210	.111	12 hours	45 minutes	30 seconds
S4				12 hours	49 minutes	31 seconds
REF-11	23596	3694	.185	13 hours	1 minute	49 seconds
N15				13 hours	14 minutes	30 seconds
REF-12	24690	4788	.241	13 hours	18 minutes	30 seconds
S13						
REF-13	26232	6330	.318	13 hours	37 minutes	

OBSERVING LOG

$\overset{\circ}{7150}$ A DATA

FEBRUARY 13, 14, 1977

COUNTS IN REFERENCE REGION	ΔC	%CHANGE	LOCAL	SIDERAL	TIME
22984	5040	.281	9 hours	50 minutes	30 seconds
			9 hours	56 minutes	24 seconds
22525	4581	.255	10 hours	8 minutes	26 seconds
			10 hours	12 minutes	11 seconds
21336	3392	.189	10 hours	27 minutes	24 seconds
			10 hours	30 minutes	50 seconds
21366	3422	.191	10 hours	47 minutes	1 second
			10 hours	51 minutes	53 seconds
20078	2134	.119	11 hours	10 minutes	30 seconds
			11 hours	13 minutes	28 seconds
19509	1565	.087	11 hours	26 minutes	14 seconds
19427	1483	.083	11 hours	38 minutes	16 seconds
			11 hours	40 minutes	42 seconds
18952	1008	.056	11 hours	52 minutes	30 seconds
			11 hours	56 minutes	0 seconds
17944	0		12 hours	07 minutes	57 seconds
19230	1286	.072	12 hours	55 minutes	0 seconds
			12 hours	58 minutes	1 second
19275	1331	.074	13 hours	13 minutes	41 seconds
			13 hours	18 minutes	12 seconds
19836	1892	.105	13 hours	33 minutes	11 seconds
			13 hours	36 minutes	37 seconds
19885	1941	.108	13 hours	48 minutes	46 seconds
			13 hours	51 minutes	18 seconds
20128	2184	.122	14 hours	2 minutes	54 seconds
20418	2474	.138	14 hours	17 minutes	0 seconds
			14 hours	21 minutes	30 seconds
21187	3243	.181	14 hours	33 minutes	57 seconds
			14 hours	37 minutes	57 seconds
22125	4181	.233	14 hours	51 minutes	0 seconds
24084	6140	.342	15 hours	05 minutes	15 seconds

OBSERVING LOG

λ7150 Å DATA

FEBRUARY 14, 15, 1977

SCAN	COUNTS IN REFERENCE REGION	ΔC	% CHANGE	LOCAL	SIDERAL	TIME
REF-33	20776	2404	13.1	9 hours	45 minutes	15 seconds
S4				9 hours	48 minutes	12 seconds
REF-34	20652	2280	12.4	10 hours	3 minutes	24.25 seconds
REF-35	20352	1980	10.8	10 hours	18 minutes	18 seconds
S71				rolling dies		
REF-36	20180	1808	9.8	10 hours	59 minutes	0 seconds
S71				11 hours	2 minutes	1 second
REF-37	19246	874	4.8	11 hours	17 minutes	2.2 seconds
S28				11 hours	20 minutes	1 second
REF-38	18946	574	3.1	11 hours	31 minutes	21 seconds
S37				11 hours	33 minutes	16 seconds
REF-39	19072	700	3.8	11 hours	45 minutes	01 seconds
REF-40	18894	522	2.8	11 hours	56 minutes	49 seconds
S5				11 hours	58 minutes	45 seconds
REF-41	18372	—	—	12 hours	10 minutes	2 seconds

O B S E R V I N G L O G

BLUE BROAD BAND

SCAN	COUNTS IN REFERENCE REGION	ΔC	% Change	LOCAL	SIDERAL	TIME
REF-1	22870	0	0	12 hours	38 minutes	57 seconds
S4				12 hours	42 minutes	
REF-2	23100	230	1.01	12 hours	53 minutes	22.57 seconds
S4				12 hours	55 minutes	45.90 seconds
REF-3	23148	278	1.22	13 hours	7 minutes	48.00 seconds
S4				13 hours	10 minutes	39.43 seconds
N5	23496	626	2.74	13 hours	23 minutes	21.80 seconds
REF-4	23444	574	2.51	13 hours	34 minutes	35.27 seconds
N5				13 hours	36 minutes	26.80 seconds
N5	23864	994	4.35	13 hours	45 minutes	50.66 seconds
Missed						
N5				13 hours	58 minutes	32.32 seconds
N5	24281	1411	6.17	14 hours	15 minutes	15 seconds
REF-5	24632	1762	7.70	14 hours	27 minutes	45 seconds
N5				14 hours	29 minutes	45 seconds
REF-6	24866	1996	8.73	Last Rotation		

O B S E R V I N G L O G
o
8200 A DATA

FEBRUARY 15-16, 1977

SCAN	AMPLITUDE OF REFERENCE REGION	Δ C	% CHANGE	LOCAL	SIDEREAL	TIME
REF-9	68.13	5.19	8.25	9 hours	55 minutes	30 seconds
S4				rolling dies		
REF-10	66.69	3.75	5.96	10 hours	23 minutes	0 seconds
S4				10 hours	25 minutes	38 seconds
REF-11	66.15	3.21	5.10	10 hours	38 minutes	9 seconds
N61				10 hours	41 minutes	37 seconds
REF-12	65.88	2.94	4.67	10 hours	56 minutes	53 seconds
S71				10 hours	59 minutes	53 seconds
REF-13	66.77	3.83	6.09	11 hours	14 minutes	41 seconds
N28				11 hours	17 minutes	37 seconds
REF-14	67.04	4.06	6.46	11 hours	29 minutes	24 seconds
S37				11 hours	31 minutes	24 seconds
REF-15	67.73	4.79	7.61	11 hours	48 minutes	0 seconds
REF-16	70.07	7.13	11.33	11 hours	59 minutes	43 seconds
N5				12 hours	1 minute	10 seconds
REF-17	70.63	7.69	12.22	12 hours	12 minutes	40 seconds
S4				12 hours	15 minutes	7 seconds
REF-18	70.87	7.93	12.60	12 hours	27 minutes	8 seconds
N61				12 hours	30 minutes	0 seconds
REF-19	69.71	6.77	10.76	12 hours	44 minutes	23 seconds
S71				12 hours	47 minutes	19 seconds
REF-20	68.94	6.00	9.53	13 hours	4 minutes	4 seconds
N28				13 hours	7 minutes	0 seconds
REF-21	67.54	4.60	7.31	13 hours	21 minutes	30 seconds
S 37				13 hours	23 minutes	31 seconds
REF-22	65.55	2.61	4.15	13 hours	35 minutes	29 seconds
REF-23	65.61	2.67	4.24	13 hours	47 minutes	11 seconds
N5				13 hours	48 minutes	48 seconds
S4				14 hours	01 minutes	2 seconds
REF-24	64.43	1.49	2.37	14 hours	12 minutes	21 seconds
N61				14 hours	15 minutes	12.9 seconds
REF-25	62.94	0	0	14 hours	30 minutes	3.7 seconds
S71				Gear dies		
REF-26	63.08	.14	.20	14 hours	47 minutes	30 seconds
S4				14 hours	51 minutes	
REF-27	64.29	1.35	2.19	15 hours	5 minutes	15 seconds

APPENDIX 2

VARIATIONS IN REFERENCE REGIONS

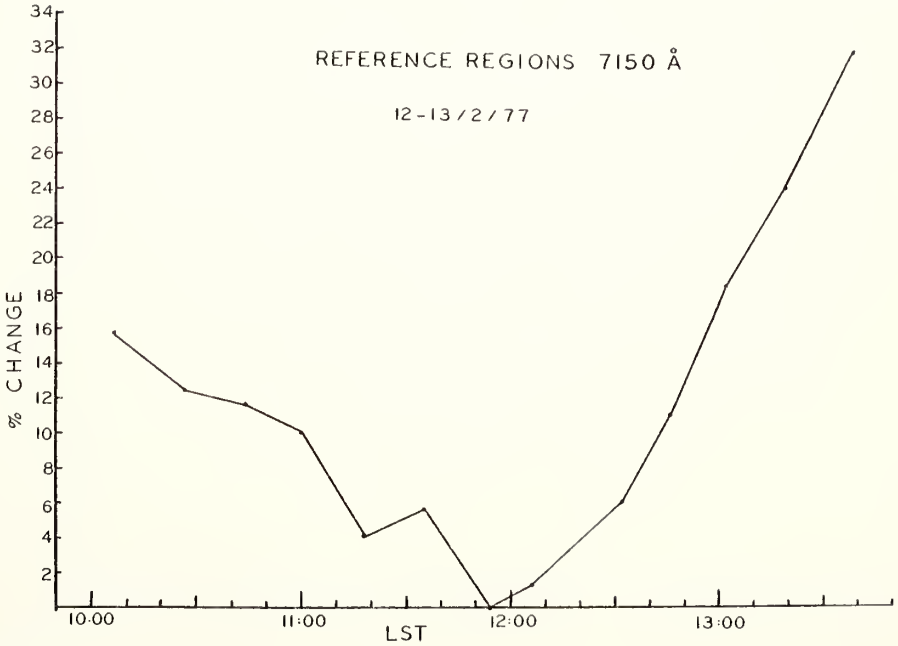
REFERENCE REGIONS 7150 Å
12-13/2/77
% CHANGE
34
32
30
28
26
24
22
20
18
16
14
12
10
8
6
4
2
10:00
11:00
12:00
13:00
LST

FIGURE 61

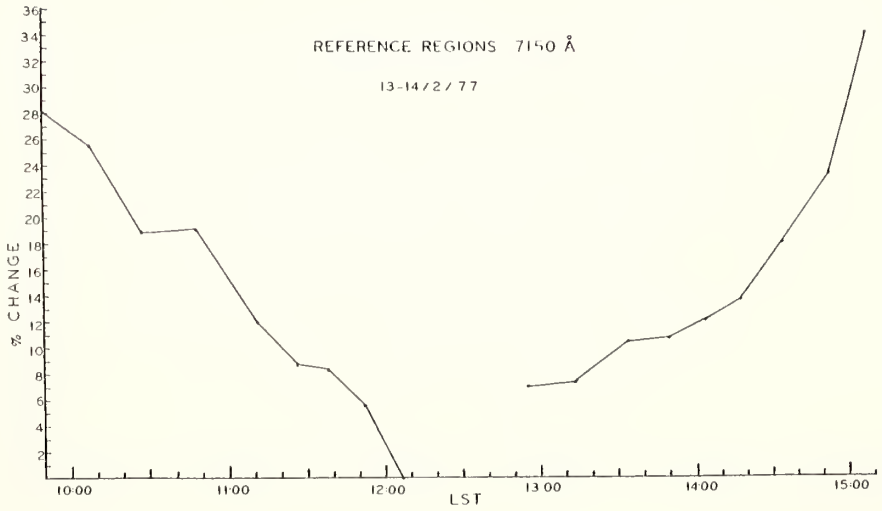
REFERENCE REGIONS 7150 Å
13-14/2/77
% CHANGE
LST
10:00
11:00
12:00
13:00
14:00
15:00

FIGURE 62

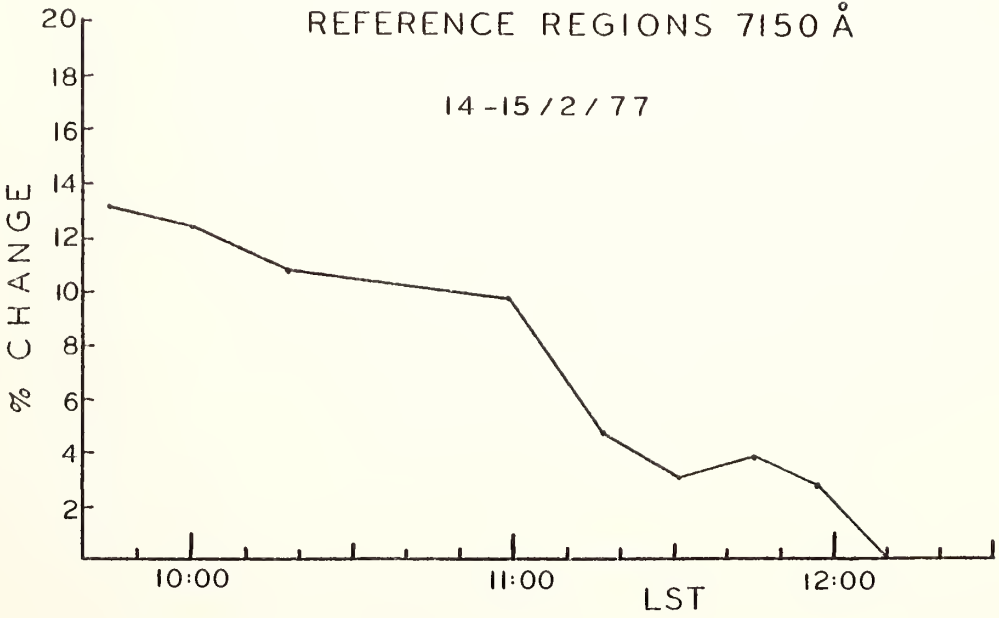
REFERENCE REGIONS 7150 Å
14-15/2/77
% CHANGE
20
18
16
14
12
10
8
6
4
2
10:00
11:00
12:00
LST

FIGURE 63

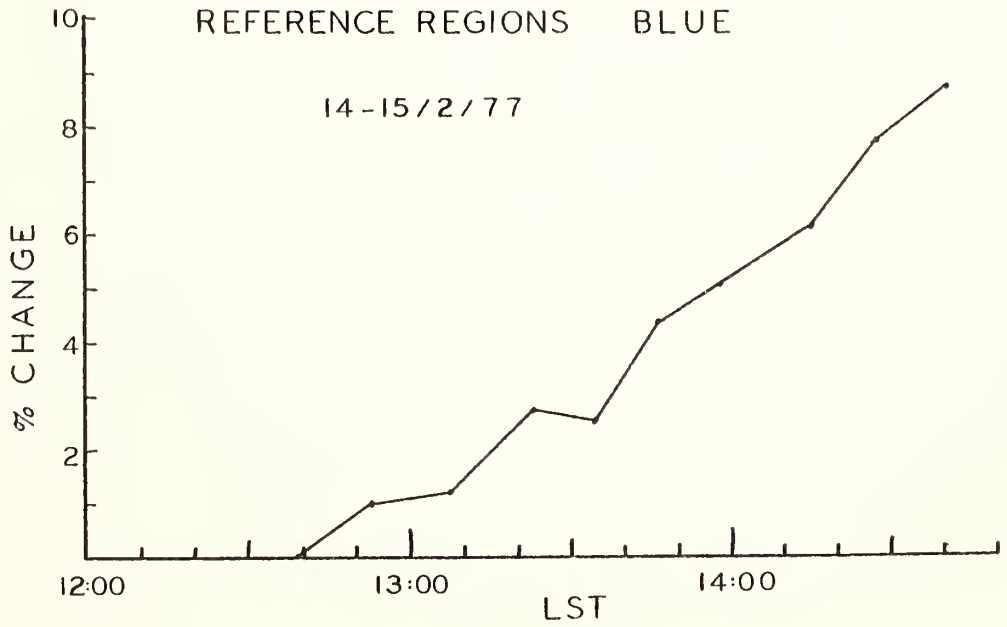
REFERENCE REGIONS BLUE
14-15/2/77
% CHANGE
10
8
6
4
2
12:00
13:00
14:00
LST

FIGURE 64

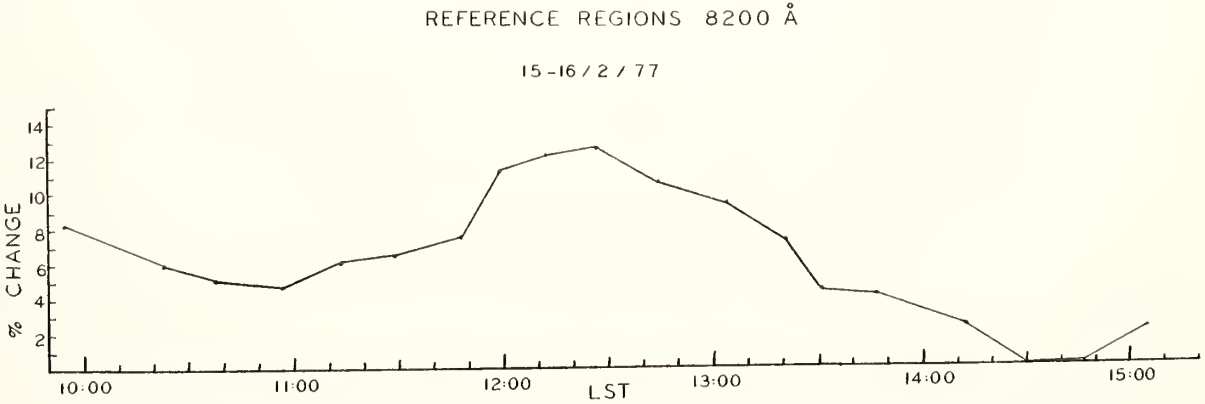
REFERENCE REGIONS 8200 Å
15-16/2/77
% CHANGE
14
12
10
8
6
4
2
10:00
11:00
12:00
LST
13:00
14:00
15:00

FIGURE 65